MODIFICATION OF HOLE TRANSPORT LAYER TO ENHANCE THE PERFORMANCE OF POLYMER SOLAR CELLS

SAQIB RAFIQUE

FACULTY OF SCIENCE
UNIVERSITY OF MALAYA
KUALA LUMPUR

2017

MODIFICATION OF HOLE TRANSPORT LAYER TO ENHANCE THE PERFORMANCE OF POLYMER SOLAR CELLS

SAQIB RAFIQUE

THESIS SUBMITTED IN FULFILMENT OF THE REQUIREMENTS FOR THE DEGREE OF DOCTOR OF PHILOSOPHY

FACULTY OF SCIENCE
UNIVERSITY OF MALAYA
KUALA LUMPUR

2017

UNIVERSITY OF MALAYA

ORIGINAL LITERARY WORK DECLARATION

Name of Candidate: **SAQIB RAFIQUE**

Registration/Matric No: **SHC 140123**

Name of Degree: **DOCTOR OF PHILOSOPHY**

Title of Project: Thesis

MODIFICATION OF HOLE TRANSPORT LAYER TO ENHANCE THE PERFORMANCE OF POLYMER SOLAR CELLS

Field of Study: **EXPERIMENTAL PHYSICS**

I do solemnly and sincerely declare that:

(1) I am the sole author/writer of this Work;
(2) This Work is original;
(3) Any use of any work in which copyright exists was done by way of fair dealing and for permitted purposes and any excerpt or extract from, or reference to or reproduction of any copyright work has been disclosed expressly and sufficiently and the title of the Work and its authorship have been acknowledged in this Work;
(4) I do not have any actual knowledge nor do I ought reasonably to know that the making of this work constitutes an infringement of any copyright work;
(5) I hereby assign all and every rights in the copyright to this Work to the University of Malaya ("UM"), who henceforth shall be owner of the copyright in this Work and that any reproduction or use in any form or by any means whatsoever is prohibited without the written consent of UM having been first had and obtained;
(6) I am fully aware that if in the course of making this Work I have infringed any copyright whether intentionally or otherwise, I may be subject to legal action or any other action as may be determined by UM.

Candidate's Signature Date:

Subscribed and solemnly declared before,

Witness's Signature Date:

Name: KHAULAH SULAIMAN (Ph.D.)

Designation: ASSOCIATE PROFESSOR

Associate Prof Dr Khaulah Sulaiman
Low Dimensional Materials Research Center
(LDMRC), Department of Physics
Faculty of Science, University of Malaya
50603 Kuala Lumpur, Malaysia

ABSTRACT

Despite the fact that development of organic solar cells (OSCs) is rapidly accelerating as the new need of green energy sources, they continue taking backstage roll in growing markets of various photovoltaic technologies due to their limited efficiency and stability. One of the challenges in obtaining the high performance of OSCs is an inefficient charge extraction and transportation to the electrodes, in particular, inability of new generation of donor polymers to obtain Ohmic contacts between the electrodes and the photo-active layer. Poly (3, 4-ethylenedioxythiophene) polystyrene sulfonate (PEDOT:PSS) is the current state of the art interfacial material used to reduce these contact barriers between the photo-active layer and indium tin oxide (ITO) electrode. However, PEDOT:PSS as a hole transport layer (HTL) also favors device degradation due to its hygroscopic and acidic nature, resulting in severe device instability. Combination of metal oxides and/or graphene oxide (GO) along with PEDOT:PSS to form a composite HTL is expected to compliment the drawbacks of any of the individual materials. This dissertation is primarily focused on identifying and addressing the stability and degradation issues associated with bulk heterojunction (BHJ) solar cells. In particular, vanadium pentaoxide (V_2O_5), and/or graphene oxide (GO) along with the PEDOT:PSS were studied and device based on organic-inorganic hybrid HTL were fabricated and characterised. The first part of the work is devoted to the stability and degradation issues. Layer by layer degradation study of BHJ OSCs with pristine PEDOT:PSS HTL was performed to identify the factors affecting device efficiency and stability. It was demonstrated that indium diffusion from ITO anode and oxygen ingress from atmosphere are some of the major causes of device instability, which affect the morphological, optical, compositional and photovoltaic characteristics of the OSCs. Another task of this work was to fabricate and study the normal

architecture BHJ OSCs based on hybrid HTL consisting of PEDOT:PSS along with V_2O_5, and/or GO, and compare the device performance with that of pristine PEDOT:PSS. In this context, applicability of V_2O_5 incorporated in PEDOT:PSS aqueous suspension to form organic-inorganic HTL in BHJ OSCs was shown. The resultant devices were tested on merits of their efficiency and operational stability. Our results indicate that V_2O_5 could be a simple addition into the PEDOT:PSS layer to overcome its stability and degradation issues leading to an effective HTL in BHJ OSCs. The last part of the work demonstrates the applicability of GO as an HTL material and further challenges were discussed. Firstly, the GO concentration was optimised, thereafter, optimised concentration of GO was used along with PEDOT:PSS in GO/PEDOT:PSS double decked HTL structure. The devices were tested on merits of their power conversion efficiency (PCE), reproducibility, stability and compared with the devices with individual GO or PEDOT:PSS HTLs. It was shown that performance of the device with GO/PEDOT:PSS HTL is significantly improved than that of devices with individual PEDOT:PSS or GO HTLs. The current work is based on highly reproducible, solution processable and cost effective fabrication techniques.

ABSTRAK

Walaupun perkembangan sel suria organik (OSCs) kian meningkat dengan permintaan sumber tenaga hijau, ia masih lagi tidak mampu menembusi pasaran teknologi foto-voltan kerana masalah lazim yang kekurangan kecekapan dan kestabilan peranti jenis ini. Salah satu cabaran dalam mencapai prestasi lebih tinggi bagi OSCs adalah ketidak-cekapan pengekstrakan cas dan masalah angkutan cas ke elektrod. Ini ditambah dengan ketidak-upayaan polimer penderma yang baharu dalam mencapai sentuhan Ohmic antara elektrod dan lapisan foto-aktif. Poly (3, 4-ethylenedioxythiophene) polystyrene sulfonate (PEDOT:PSS) adalah bahan antara-muka yang terbaru digunakan untuk mengurangkan sentuhan halangan antara lapisan foto-aktif dan elektrod indium timah oksida (ITO). Walau bagaimanapun, PEDOT:PSS sebagai lapisan angkutan holong (HTL) juga menyumbang degradasi peranti ini kerana sifat semulajadinya yang higroskopik dam berasid boleh menyebabkan ketidakstabilan peranti yang teruk. Gabungan oxida logam dan grafin oksida (GO) bersama-sama PEDOT:PSS dalam membentuk komposit HTL dijangka akan melengkapkan kekurangan bahan-bahan berkenaan yang digunakan secara individu. Disertasi ini memberi fokus utama kepada langkah mengenal pasti dan menangani masalah kestabilan dan degradasi yang berkait rapat dengan sel suria hetero-simpang pukal (BHJ). Secara khusus, vanadium pentaosida (V_2O_5), dan/atau grafin oxida (GO) bersama-sama PEDOT:PSS dikaji dan peranti berasaskan HTL hibrid organic-tak organik difabrikasi dan dicirikan. Pada bahagian pertama, keutamaan diberikan kepada masalah kestabilan dan degradasi. Kajian degradasi lapisan demi lapisan bagi BHJ OSCs dilakukan dengan menggunakan PEDOT:PSS tulen sebagai HTL dalam mengenal pasti faktor-faktor yang memberi kesan kepada kecekapan dan kestabilan peranti ini. Ia menunjukkan bahawa penyebaran indium dari anod ITO dan kemasukan

oksigen dari atmosfera adalah penyebab utama ketidakstabilan peranti, yang juga memberi kesan kepada ciri-ciri morfologi, optikal, komposisis dan foto-voltan bagi OSCs berkenaan. Tugas seterusnya adalah memfabrikasi dan mengkaji struktur asas BHJ OSCs berasaskan HTL hidrid yang mengandungi PEDOT:PSS bersama-sama V_2O_5, dan/atau GO, dan kemudiannya prestasi peranti ini dibandingkan dengan peranti piawai yang hanya terdiri dari PEDOT:PSS tulen. Dalam konteks ini, keserasian V_2O_5 yang digabungkan dengan PEDOT:PSS membentuk HTL organik-tak organik dalam BHJ OSCs ditunjukkan. Peranti berkenaan diuji bagi menentukan kecekapan dan kestabilannya dalam jangka masa panjang. Keputusan kami mendapati bahawa V_2O_5 mampu menjadi komponen penambahan yang ringkas kepada lapisan PEDOT:PSS dalam menangani masalah kestabilan dan degradasi, sekaligus menjadikannya HTL yang berkesan dalam BHJ OSCs. Tugas terakhir adalah membuktikan keserasian GO sebagai bahan HTL dan cabarannya dibincangkan. Pertama, kepekatan GO dioptimimkan lalu ia digunakan bersama PEDOT:PSS di dalam GO/PEDOT:PSS dengan struktur HTL yang bertingkat. Peranti ini diuji bagi mengenal pasti prestasinya termasuklah kecekapan, keboleh ulangan, kestabilan, dan dibandingkan dengan peranti yang mengandungi HTL GO atau PEDOT:PSS sahaja. Peranti yang mempunyai HTL GO/PEDOT:PSS ini telah menunjukkan peningkatan prestasi yang ketara berbanding dengan peranti yang menggunakan PEDOT:PSS dan GO sahaja sebagai HTL. Kerja terbaru ini adalah berasaskan teknik fabrikasi yang menjimatkan, keboleh prosesan secara larutan dan keboleh ulangan yang tinggi.

ACKNOWLEDGEMENTS

"Limitless is Allah in his glory and all praise is due to him alone (سبحان الله و بحمده سبحان الله العظيم)**."** First of all, I am grateful to Allah Almighty the most Merciful and the most Beneficent. I humbly offer salutations upon all Prophets, the source of guidance and knowledge to all mankind.

Above all, I want to express my special gratitude to my supervisor Associate Professor Dr. Khaulah Sulaiman; for being a tremendous mentor for me. I am genuinely grateful to her for encouraging my research and for her contribution of time, ideas and funding to make my PhD. I would also like to thank my co-advisor Dr. Shahino Mah Abdullah for his continuous positive and encouraging attitude and I thank him for always being a great mentor to look up to. The joy and spirit he has for his research was contagious and inspiring for me who taught me how to work during tough times in my Ph.D.

I would extend my gratitude to Dr. Omaish Ansari and Dr. M. Aslam for valuable scientific discussions and advices, for always willingly helping me out with any scientific problems. They are greatly acknowledged for comments on my reports, dissertation and manuscripts. I would especially like to thank the group members of Solar/Photovoltaic Materials Research Group and LDMRC at UM, particularly, Dr. Mansoor Ani Najeeb, Numan Arshid, Muhammad Mehmood Shahid, Mohamad Izzat Azmer, Muhammad Saipul Fakhir and Dr. Karwan Wasman Qadir for being such a wonderful fellows. It's been a real pleasure to experience their company and support both in working area and in social life.

In regard to the characterizations at Center of Nanotechnology, King Abdulaziz University, Jeddah, Saudi Arabia, I am grateful to Mohammad Shahnawaze Ansari for

carrying out FESEM analysis, Asim Jilani for helping me in XPS measurements, Sajith Vattam Kandathil for AFM morphological analysis and Akhalakur Rahman Ansari for helping in UV-Vis analysis.

Finally, a deepest gratitude goes to my family. I cannot express how grateful I am to my parents, my wife, and my kids for all of the sacrifices that they've made on my behalf. Their prayer for me was what sustained me thus far. I would like express appreciation to my beloved wife Zara Jehangir who spent sleepless nights with and was always my support in the moments when there was no one around to care for me. I feel sorry and touched for my kids, Huzaifa and Abdulhadi because I took their time and invested in my studies.

SAQIB RAFIQUE

April, 2017

TABLE OF CONTENTS

LIST OF FIGURES

LIST OF TABLES

LIST OF SYMBOLS AND ABBREVIATIONS

AFM	:	Atomic force microscopy
Al	:	Aluminium
BHJ	:	Bulk heterojunction
EDS	:	Energy dispersive spectra
ETL	:	Electron transport layer
FESEM	:	Field emission scanning electron microscopy
FF	:	Fill factor
GO	:	Graphene oxide
HOMO	:	Higher occupied molecular orbital
HTL	:	Hole transport layer
ITO	:	Indium tin oxide
I-V	:	Current-Voltage
J_{sc}	:	Short circuit current density
J-V	:	Current density-Voltage
LUMO	:	Lower unoccupied molecular orbital
OPV	:	Organic photovoltaic
OSC	:	Organic solar cells
$PC_{71}BM$	:	(6,6)-phenyl C_{71} butyric acid methyl ester
PCDTBT	:	poly[N-90-heptadecanyl-2,7-carbazole-alt-5,5-(40,70-di-2-thienyl-20,10,30 benzothiadiazole)]
PCE	:	Power conversion efficiency
PEDOT:PSS	:	Poly(3,4-ethylenedioxythiophene) polystyrene sulfonate
PV	:	Photovoltaic
R2R	:	Roll to roll

RMS	:	Root mean square
RR	:	Rectification ratio
R_s	:	Series resistance
R_{sh}	:	Shunt resistant
TMO	:	Transition metal oxide
UV-Vis	:	Ultraviolet-Visible
V_2O_5	:	Vanadium Pentaoxide
V_{oc}	:	Open circuit voltage
WF	:	Work function
XPS	:	X-ray photoelectron spectroscopy
XRD	:	X-ray diffraction

CHAPTER 1: INTRODUCTION

1.1 Background

In today's world, the energy regimen is largely reliant on non-renewable and polluting energy sources, consequently, the global temperature is expected to rise about 1 to 6 °C during the 21st century (Ameri et al., 2009). Conventional energy harvesting is based on fossil fuels such as oil, gas, and coal which have unsustainable consequences for environmental, economical, geopolitical and societal issues. Carbon dioxide (CO_2) concentration is expected to rise between 540 to 970 parts per million until 2100 that is sufficient to cause substantial and irreversible modifications in the global climate (Ameri et al., 2009; Karl & Trenberth, 2003). Moreover, the energy consumption in many developed nations is still not at its peak plus there is an increasing demand of electricity utilization from the developing countries (Conti et al., 2011). According to the International Energy Outlook 2016, projected increases in world energy consumption is estimated to reach at 815 quadrillion Btu in 2040 which was 549 quadrillion Btu in 2012, an increase of 48 %. Consequently, a rise in energy consumption, the depletion of these non-renewable sources and global warming are causing a severe threat to the balance of human life. Therefore, great attention was driven towards the clean and renewable energy sources of which solar energy is believed to have highest potential among other alternative energy resources such as hydroelectric, biomass and wind energy. There are several reasons of choosing solar energy as one of the most promising renewable energy resources to fulfill energy demands of the world. Many areas of developing countries lack grid infrastructures for transmission of electricity generation. This makes locally generated power potentially better suited to meet energy demands of these countries. In addition, sun is the most abundant source of energy on earth and the annual amount of energy received from the

sun is enormous; 3.9×10^{20} joules which is enough to meet world energy demand in less than an hour (Anderson et al., 2004).

Despite of the fact that earth receives abundant solar power, the photovoltaic (PV) technology is still cost intensive to become a primary energy source. Therefore, the development of highly efficient, cost effective and industrial scale technology is required to ensure a bright future of PV products.

1.2 Solar Cell Generations

Solar cells are manufactured through range of technologies including wafer based and variety of thin film technologies. These technologies are traditionally grouped into first, second and third generations. Below, a brief description of each generation is presented.

First Generation (IG): First generation (1G) solar cells are produced on silicon wafers including single crystal (c-Si) and multi-crystalline silicon (mc-Si) (Bagnall & Boreland, 2008). Current photovoltaic market is dominated by this generation due to their high efficiencies typically in the range of 15-25 % (Bagnall & Boreland, 2008; Green et al., 2015). However, the production of these solar cells require high quality silicon, state of the art high temperature processing and complex engineering, and are therefore not a cost effective energy source (Sun & Sariciftci, 2005). In addition, these solar cells are rigid with less mechanical flexibility.

Second Generation (2G): One of the key challenges in the production of IG solar cells is their high production cost. Therefore, the second generation (2G) solar cells were designed with the aim to remove unnecessary material from the cost equation by using single-junction devices based on thin film technology (Badawy, 2015), while maintaining the high efficiencies comparable with the 1G solar cells. These 2G devices

are fabricated on low cost substrates by using less material based on amorphous silicon (a-Si), cadmium telluride/sulfide (CdTe/CdS), copper Indium (Gallium) diselenide (CIS, CIGS) or polycrystalline-Si (p-Si), thereby reducing the overall cost in the manufacturing process (Green et al., 2006).

Third Generation (3G): The third generation (3G) solar cells are based on organic small molecules or polymers and designed to complement the advantages of both 1G and 2G devices (Brown & Wu, 2009). The concept aims to reduce the cost per watt peak, by maintaining high efficiencies, and economic and environmental cost advantages of thin-film deposition techniques (Conibeer, 2007). 3G technologies introduce the idea of multiple stacking of solar cells, which can significantly increase the efficiency by improving the harvesting of photons and even overcome the theoretical limit of 30 % (Karam et al., 1999; Zweibel, 2010).

The 3G exhibits an entirely new concept of device architecture and materials *i.e.* organic solar cells (OSCs), dye sensitized solar cells (DSSCs) and perovskite solar cells etc. (Sharma et al., 2015). The polymer solar cells including organic/inorganic hybrid are fundamentally new types of devices which offer several advantages over their 1G and 2G counterparts such as their tunable properties, low manufacturing cost, roll to roll (R2R) production compatibility, solution processed and light weight (Chen et al., 2013; Sun et al., 2010; Synooka et al., 2014). However, they exhibit significant instability when exposed to air, mainly due to oxygen and moisture ingress from air, and diffusion of indium from indium tin oxide (ITO) anode (Krebs et al., 2008; Kawano et al., 2006). Further improvement in the stability of OSCs is however, essential for most of the technological applications (Kawano et al., 2006).

This thesis purely focused on modification of hole transport layer (HTL) in the bulk heterojunction (BHJ) OSCs with polymer-fullerene photoactive layer to improve

the stability as well as efficiency of devices. The basic working principle of BHJ OSCs, device architecture, typical materials, role of interfacial layers and stability/degradation of OSCs will be discussed briefly in the following sections.

1.3 Bulk-Heterojunction Organic Solar Cells

Since the production of organic photovoltaic materials in mid 1980s, solution processable OSCs based on thin film technologies have attracted immense attraction as a possible alternative to their inorganic counterparts (Bulavko & Ishchenko, 2014). Potential for cost effective and fast R2R production as well as their light weight and fabrication on flexible substrates could give them an edge over traditional inorganic solar cells (Scharber & Sariciftci, 2013; Shivanna et al., 2014).

Thanks to the discovery of an ultrafast charge transfer which opened the great but simple field of so-called BHJ OSCs. To date, remarkable progress in the BHJ OSCs has been recorded and power conversion efficiencies (PCEs) of more than 10% have been successfully demonstrated (Li et al., 2012; Trost et al., 2015). The photoactive layer of a BHJ-OSC is made of a bi-continuous composite of electron-donor and electron-acceptor modules sandwiched between the cathode and anode (Huang et al., 2014). The basic structure , operational principal, device geometries and materials have been briefly discussed below, whereby schematic illustration of BHJ OSCs and corresponding energy-bands is illustrated in Figure 1.1.

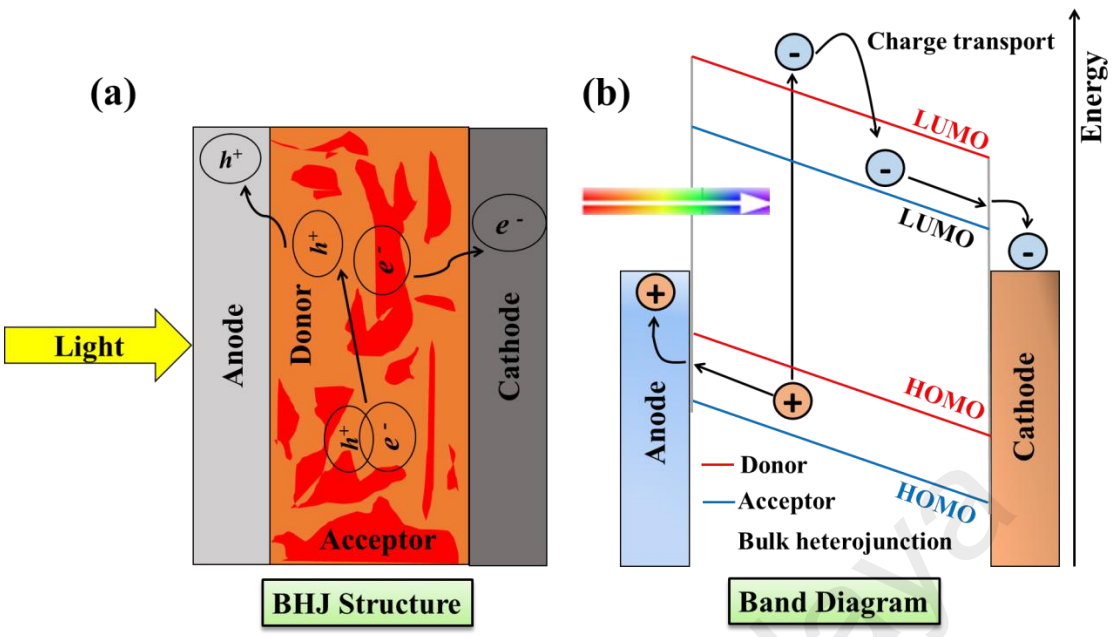

Figure 1.1: (a) Schematic illustration of photocurrent generation steps e.g. from light absorption to charge carriers collection and (b) band diagram of the photocurrent generation mechanism in a BHJ solar cell.

1.3.1 Device Structure and Materials

A BHJ OSC is essentially consisted of multilayer structure in which each layer in the device architecture could be deposited by an individual fabrication technique. The device is illuminated through the transparent substrate, a glass or flexible (plastic) substrate in most cases, coated with high work function (WF) indium tin oxide (ITO), the transparent anode that provides the extraction and collection of positive charge carriers (Huang & Huang, 2014). The cathode is usually made of a low WF opaque metal such as aluminum (Al) or calcium (Ca) (Po et al., 2011), whereas, the absorber layer is comprises of two constituents; A donor material is usually a conjugated polymer, conjugated pigments or oligomers, and for an acceptor material often fullerene derivatives are applied. The photoactive layer is sandwiched between the anode and top low WF cathode. In order to improve the performance and stability of the BHJ OSCs, often interfacial layers namely HTL and electron transport layer (ETL) are inserted between the anode-photoactive and cathode-photoactive interfaces (Facchetti,

2013). Over the years, inverted device architecture has also been established for BHJ OSCs. In an inverted device, the bottom transparent electrode serves as the cathode while the top electrode is anode. The performance of inverted devices is comparable with the normal architecture solar cells; in addition, they also exhibit relatively higher environmental stability. Typical device architecture for normal and inverted solar cells is illustrated in Figure 1.2.

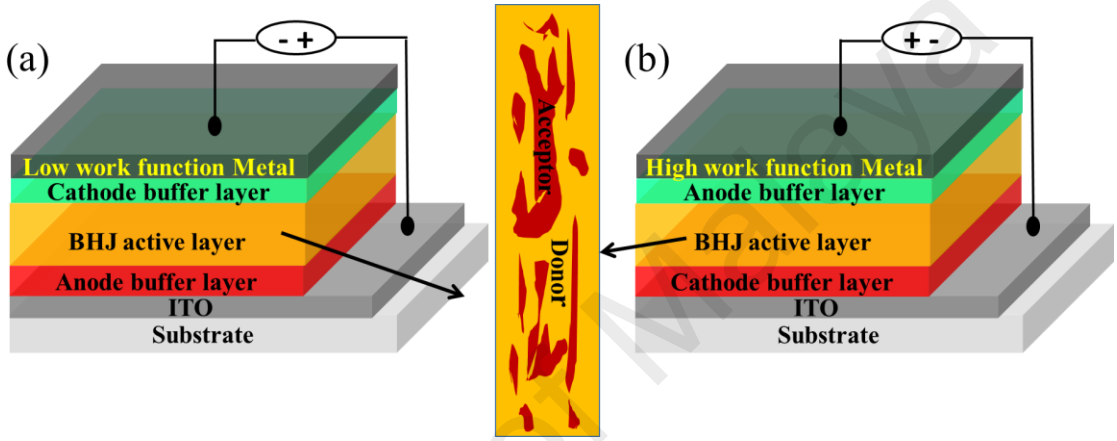

Figure 1.2: Device architecture of the (a) normal and (b) inverted BHJ OSCs.

1.3.2 BHJ OSCs Working Principle

The simplified working principle of BHJ OSC device can be described in at least four fundamental steps namely (i) Photons absorption and exciton formation, (ii) exciton diffusion and splitting, (iii) charge transportation and (iv) charge collection (Deibel & Dyakonov, 2010; Dou et al., 2013; Facchetti, 2013).

In a BHJ OSC device, light is usually absorbed in the donor material *e.g.* a conjugated polymer. Upon absorption of photons, an electron is excited from the highest occupied molecular orbital (HOMO) to the lowest unoccupied molecular orbital (LUMO). The offset between donor (LUMO) and acceptor (LUMO) must be in the range of 0.1-1.4 eV to generate the electron-hole pairs also known as the excitons. The

excitons must diffuse to the donor-acceptor interface where there is sufficient chemical potential energy drop to split these excitons into the free charge carriers i.e. the electrons and the holes (Mayer et al., 2007). After splitting into free charge carriers, each carrier must be transported to the respective electrode through the bi-continuous interpenetrating pathway while avoiding recombination and trapping of charges. Some limitations and losses could occur during these steps such as absorption loss due to spectral mismatch, thermalization loss, insufficient energy required for exciton splitting, and charge recombination etc. (Siddiki et al., 2010).

Three important parameters determine the PCE of a solar cell: The current that reaches to the electrodes without any applied field is termed as the short circuit current (J_{sc}) whereas open circuit voltage (V_{oc}) is the maximum potential generated by the device. In order for the current to do work, it must be generated with some potential. The ratio of maximum obtained power to the product of J_{sc} and V_{oc} is known as fill factor (FF) and it defines the quality of the device. PCE is defined as product of these three parameters divided by input power (P_{in}) and denoted by sign (η). Mathematically;

$$\eta = \frac{P_{out}}{P_{in}} = \frac{FF(V_{oc} \times J_{sc})}{P_{in}} \qquad (1.1)$$

$$FF = \frac{V_{mpp} \times I_{mpp}}{V_{oc} \times J_{sc}} \qquad (1.2)$$

Where, V_{mpp} and J_{mpp} (eq.1.2) are the voltage and current density at the maximum output power, respectively. The schematic illustration of the basic structure and working principle of BHJ OSCs is presented in the Figure 1.3.

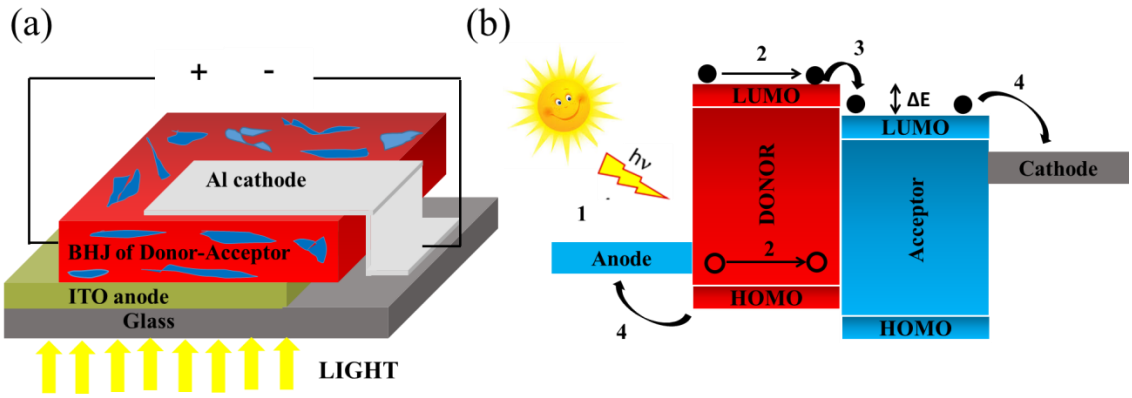

Figure 1.3: (a) BHJ OSC structure and (b) operation principle of BHJ OSC devices**.**

1.3.3 Role of Interfacial Layers in OSCs

In BHJ OSCs, each layer of the solar cell architecture significantly influences the device performance and optimization of every layer is essential to achieve the best optimum performance. As discussed earlier, in the basic device structure the photoactive layer is sandwiched between the ITO anode and a low WF metal cathode. In order to ensure the efficient charge extraction at the respective electrodes, the energy level structure at the electrodes and photoactive layer interface plays an essential role (Po et al., 2011; Zheng et al., 2016). The electrodes- active layer interface affects the phase separation, energy level alignment, and a proper interfacial engineering (insertion of optimized ETL and HTL between photoactive layer and respective electrodes) provides good ohmic contacts with minimum resistance and higher charge selectivity to prevent carriers from reaching to the opposite electrodes (Lian et al., 2014; Steim et al., 2010). In addition it helps in adjusting the surface energetics and WF, and affects the formation of gradients within the BHJ (Chueh et al., 2015; Zeng et al., 2015). A detailed discussion on the developmental history of BHJ OSCs, materials and design parameters, role of interfacial layers in BHJ OSCs, in particular the HTL in context of this thesis, device physics, performance characteristics, stability/degradation mechanisms and strategies to improve device performance will be presented in Chapter 2.

1.4 Stability/Degradation of the OSCs

During the recent years, OSCs have evolved in terms of efficiency as well as stability. Stability of the OSCs is one of the major bottlenecks in their long term performance. Although, the stability of OSCs has remarkably improved and it was measured in minutes in earlier days which can sustain now for several thousands of hours under favorable circumstances. However, still a lot of improvement is needed to address the factors limiting the stability of OSCs (Jørgensen et al., 2012). Degradation process comprises a range of complex phenomenon simultaneously in play, of which many of them are not completely understood yet. The multilayers structure and interfaces of metal/organic, organic/organic materials significantly influences the overall performance (Bao et al., 2014). Recent reports on the lifetime stability of OSCs highlighted two major problems regarding the device stability. Firstly, the extrinsic stability which requires proper encapsulation of devices to prevent the environmentally induced degradation mainly caused by oxygen and moisture present in the air (Ecker et al., 2011; Udum et al., 2014). Secondly, the intrinsic stability which is related to the materials and interfaces present in the OSCs (Jørgensen et al., 2008; Zeng et al., 2015). Some of the known factors affecting the device stability are surface morphology of different layers, diffusion of oxygen from atmosphere, corrosion and diffusion of indium and tin (from ITO anode), mechanical stress and photo-degradation etc. (Cheng & Zhan, 2016). Several processes and strategies have been employed in recent years to address stability issues such as optimization of active layer morphology, interfacial engineering and utilization of hybrid buffered layers, employing inverted geometry, using stable electrodes and proper device encapsulation. A detailed overview of the each of the factors limiting the device stability and possible strategies to increase the stability of OSCs is presented in Chapter 2.

1.5 Project Motivation

During the past few years, significant progress has been recorded in BHJ OSCs by virtue of their low cost, solution processed and environmental friendly fabrication processes (Deibel & Dyakonov, 2010; Jagadamma et al., 2014). Considerable improvement in the device performance has pushed the device efficiency towards the efficient 10% regime (Dennler et al., 2009; Nelson, 2011). Although, a lot of research has been carried out on OSCs for their widespread commercialization and large scale production, but they still have many constraints that prevent them to move beyond the laboratory. Most of the limiting factors are environmentally induced degradations caused by oxygen, humidity and intrinsic instability of OSCs materials and interfaces (Choi et al., 2012; Jong et al., 2000). Since chemical, physical, mechanical and structural properties of organic semiconductors are very sensitive towards ambient atmosphere, therefore, the photovoltaic properties of OSCs are quite susceptible to degradation in ambient environmental conditions (Bekci & Ela, 2012; Jørgensen et al., 2008). Although, the lifetime of OSCs can be improved by adopting various encapsulation techniques but this approach would significantly increase the production cost (Udum et al., 2014). Most of the OSCs which are being fabricated today are tested under controlled environment without even being exposed to ambient air containing natural humidity. Hence, for the successful widespread commercialization and large scale production of OSCs, the stability of OSCs also needs to be improved along with their efficiency (Savagatrup et al., 2015).

Poly (3.4-ethylenedioxythiophene):Poly (styrenesulfonate) (PEDOT:PSS) is the most commonly applied HTL in OSCs. However it limits the device performance due to its highly hygroscopic and acidic nature which causes reliability issues while reducing the cell life drastically (Schulz et al., 2014). There are several pathways that have been adopted in order to improve the stability of the interface between photoactive layer and

the ITO anode. One of the most reliable methods is to optimize the HTL by introducing favorable materials along with PEDOT:PSS or to replace it with suitable alternatives. Materials such as metal oxides and/or graphene oxide (GO) along with PEDOT:PSS to form an organic-inorganic hybrid HTL are expected to address the stability issues associated with PEDOT:PSS and compliment the drawbacks of any of the individual materials. The aim to improve the stability and efficiency of BHJ OSCs by utilizing the aforementioned hybrid HTLs has become the main motivation of this work.

1.6 Project Goals and Outlines

The title of this dissertation is rather broader and involved a couple of different tasks that have been accomplished during this work. The work is based on results; some of which have already been published. The articles comprises of projects of different but interlinked character with the aim to identify the degradation factors limiting the device stability in general, particularly, in the context of HTL. Further, to optimize the HTL by using metal oxides such as vanadium pentaoxide (V_2O_5), and/or GO along with the PEDOT:PSS in order to address the reliability issues associated with pristine PEDOT:PSS HTL and enhance the stability of the device while addressing these factors. In this context, the attempt to group these tasks in different sections, led to generation of four chapters (Chapter 3-6) that are presented after introduction and literature review chapters. In particular, **Chapter 3** discusses the stability/ degradation issues involves in deterioration of device performance. It presents layer by layer identification of degradation factors affecting the device performance. Several characterization techniques have been employed in order to record the compositional, morphological, chemical, optical and photovoltaic decay as a function of aging time in ambient air. **Chapter 4** addresses some of the reliability issues associated with the instability of the HTL by incorporating V_2O_5 into the PEDOT:PSS HTL. The resultant device showed enhanced stability and efficiency as compared to pristine PEDOT:PSS

HTL. **Chapter 5 and 6** present two small projects that involve the utilization of GO as an HTL. At first, **Chapter 5** describes the optimization of GO concentration to replace PEDOT:PSS as an HTL. It also identifies the limitation brought by GO as a single HTL material and suggests the possible improvement which could be brought in the device performance by using GO along with PEDOT:PSS in a bi-layer structure. Further, **Chapter 6** suggests a novel approach to use GO/PEDOT:PSS HTL in the poly[N-90-heptadecanyl-2,7-carbazole-alt-5,5-(40,70-di-2-thienyl-20,10,30 benzothiadiazole)] (PCDTBT), and (6,6)-phenyl C_{71} butyric acid methyl ester ($PC_{71}BM$) based device structure. A set of characterizations confirm the efficacy of this approach and a detailed study on reproducibility and stability of the resultant device has been presented. Finally, the conclusion of this work is reported in **Chapter 7**. Along with presenting the summary of the project this chapter also includes the future challenges and research directions.

Four goals have been extracted from the current work that describes the aims of the present study:

1. To optimize the fabrication parameters in order to develop a facile, solution processable and cost effective fabrication technique of the polymer solar cells.
2. To identify the degradation factors and stability concerns particularly related to HTL in the ITO/PEDOT:PSS/ PCDTBT:$PC_{71}BM$/ Al device structure.
3. To evaluate the V_2O_5 and/or GO along with the PEDOT:PSS as a hybrid HTL in order to address the reliability issues associated with pristine PEDOT:PSS HTL.

4. To evaluate and improve the operational stability of the fabricated devices with hybrid HTL.

CHAPTER 2: LITERATURE REVIEW[1]

2.1 Development in BHJ OSCs

Tang in 1986, reported the first successful organic photovoltaic device yielding a PCE of 1% but with a high FF of 65% in a bi-layer device architecture (Tang, 1986). Both donor and acceptor materials were deposited by sequential thermal vacuum sublimation of two small molecules. Six years later in 1992, Sariciftci et al. reported the ultrafast electron transfer from the donor polymer poly[2-methoxy-5-(2-ethylhexyloxy)]-1,4-phenylenevinylene (MEH-PPV) to the fullerene (C_{60}), which for the first time suggested the use of conjugated polymers as donor materials and fullerene derivatives as acceptor material (Kraabel et al., 1993; Sariciftci et al., 1992). Later, the concept of BHJ comprises of donor and acceptor materials was introduced to address the performance constraints associated with the shorter diffusion length in OSCs (Halls et al., 1995; Yu et al., 1995). BHJ is an intimate blend of donor and acceptor materials within the photoactive layer with large interfacial areas for efficient charge separation (Zheng, et al., 2015; Rafique et al., 2016). Due to tremendous progress in optimization of materials and devices, the BHJ architecture is considered as standard for OSCs.

PCEs of more than 10% have been reported recently, however, this value is still significantly less than what is required for daily applications (Liu et al., 2015). The development of BHJ OSCs is rapidly accelerating as a potential green solar energy technology. OSCs are attractive mainly because of the modifiable structures of their

[1] **The review presented in this Chapter has been submitted to Elsevier: "Renewable & Sustainable Energy Reviews" as;**

Rafique et al. Fundamentals of Bulk Heterojunction Organic Solar Cells: An overview of design parameters, device physics, performance characteristics, stability/degradation factors and strategies for improvement. *Renewable & Sustainable Energy Reviews.* **(Manuscript Submitted)**

organic constituents, flexibility, and compatibility with R2R production (Cao et al., 2014). Most of the work is focused on improving the device efficiency; however, some visionary scientists have already paid attention to the stability constraints of the BHJ OSCs (Cao et al., 2014; Jørgensen et al., 2012; Katz et al., 2006). This literature review chapter does not cover a huge body of literature on this subject during last few years; instead, it focuses fundamental concept of BHJ OSCs including device physics of BHJ OSCs, performance characteristics, working principle, materials, limitations and possible routes of improving the performance.

2.2 OSCs Materials: Ideal Design Properties

The choice of materials used in OSCs is crucial to the overall performance in terms of efficiency and stability. This section presents a detailed overview of the material choice and properties, limitations and possibilities for improvement. Further, it surveys the materials which have been investigated in recent years and analyses the specific material (PCDTBT:$PC_{71}BM$) with reference to the aforementioned desired properties and also discusses the potential advantages and major limitations of these materials.

BHJ OSCs employing organic donor and acceptor materials should comply with several performance characteristics for an efficient photocurrent and photovoltage generation and are thus as follows (Zheng, et al., 2015; Nelson, 2011):

- Optimized absorption features of the OSCs by fine tuning the absorption characteristics to maximize the visible light absorption.
- The width of domains of pure donor or acceptor material should be shorter than the diffusion length of (< ~10 nm) an exciton, in order for most photo-generated excitons to dissociate, *i.e.*, the two components should be sufficiently well mixed.

- Both phases should form continuous percolating networks that connect the bulk of the film to the anode and cathode.
- The electrodes should be chosen to ensure the high selectivity of charge carrier extraction and collection *i.e.* electrons must be collected at one and holes at the other electrode, in order to provide a direction for the photocurrent. Such selectivity can be achieved using one high and one low work function electrode.

2.2.1 Donor and Acceptor Polymers

Several factors determine the efficacy of donor and acceptor materials in BHJ solar cells architecture. While choosing a donor material, it is important to consider HOMO and LUMO levels with respect to the acceptor material. Moreover, absorption range can be broaden by lowering the bandgap, thus polymer can absorb more photons which will consequently increase the J_{sc} (Scharber et al., 2006; Su et al., 2012). Most of the semiconductor polymers are hole conductor and named as electron donor polymers (Cai et al., 2010). The progress of donor polymers has gone through several phases of research; as a result four prominent names emerged, namely (i) poly (phenylenevinylene) (PPV) derivatives such as MEH-PPV (Hou & Guo, 2013; Zhou et al., 2004), (ii) MDMO-PPV (Zheng, et al., 2015), (iii) poly- (thiophene) derivatives, mainly P3HT (Wright & Uddin, 2012) and (iv) polyfluorene derivatives like PFDTBT and PCDTBT (Blouin et al., 2007; Cai et al., 2010). Figure 2.1 shows the structure of these donor polymers. In addition, the full names of these polymers are:

MEH-PPV: Poly [2-methoxy-5-(2'-ethyl-hexyloxy)-1,4-phenylene vinylene]

P3HT: Poly (3-hexylthiophene-2, 5-diyl).

MDMO-PPV: Poly [2-methoxy-5-(3′, 7′-dimethyloctyloxy)-1, phenylenevinylene]

PFDTBT: Poly {[2, 7-(9, 9-bis-(2-octyl)-fluorene)]-alt- [5, 5-(4, 7-di-20-thienyl-2, 1, 3-benzothiadiazole)]}.

PCDTBT: Poly [N-9'-hepta-decanyl-2,7-carbazole-alt-5,5-(4',7'-di-thienyl-2'1',3'-b3nzothiadizaole).

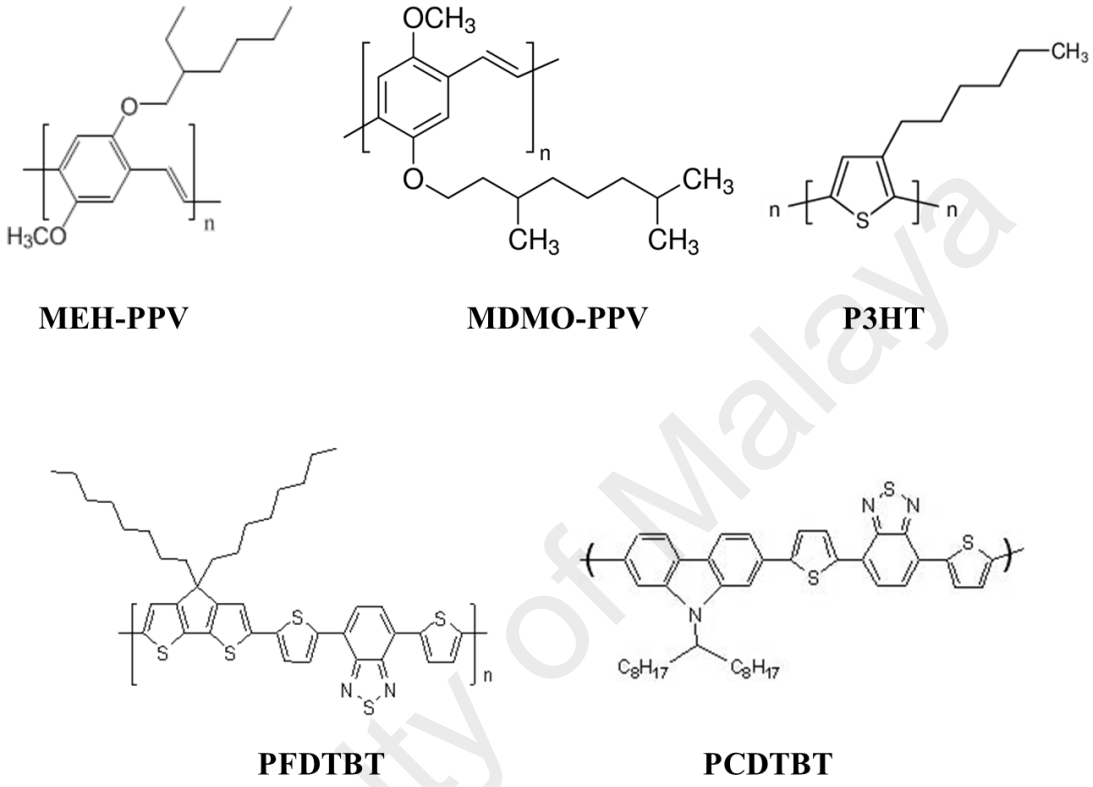

Figure 2.1: Chemical structure for materials typically used as polymer donor materials including MEH-PPV, MDMO-PPV, P3HT, PDFTBT and PCDTBT.

Since last one decade, P3HT emerged as a prominent semiconductor polymer due to its self-assembling tendency, improved absorption, higher hole mobility (Schilinsky et al., 2002; Wright & Uddin, 2012) and its ability to crystallize which means that the final morphology is controllable by varying process conditions or subsequent treatments (Quiles et al., 2008). P3HT exhibits a bandgap of ~ 1.9eV which can be further reduced by enhancing the quinoidal character in the polymer (Roncali, 2007). However, in past few years, PCDTBT emerged as a superior donor polymer as compared to P3HT due its ultrafast charge carrier generation ability and different charge

carrier recombination dynamics (Synooka et al., 2014). Section 2.2.2 presents a brief description of PCDTBT as a prominent donor polymer.

The conventional OSCs mostly use fullerene derivatives as the electron acceptor material. The unsubstituted fullerene shows poor solubility which limits its applicability in the device fabrication; therefore a number of substituents were introduced onto fullerene to overcome the solubility issues (Hou & Guo, 2013). In this context, Hummelen et al. demonstrated a feasible approach to synthesize PCBM ([6,6]-phenyl-C61-butyric acid methyl ester), which have been broadly used as one of the most successful electron acceptor materials due its excellent photovoltaic properties (Hummelen et al., 1995). Thereafter, the soluble derivatives of C_{60} have been successfully utilized as fullerene derivatives to act as electron acceptor materials. These so-called fullerene derivatives offer several advantages such as ultrafast charge transfer mechanism between donor polymers and acceptor fullerenes, high electron mobility and better phase segregation in the polymer-fullerene blend (Cai et al., 2010). Chemical structures of some of the famous fullerene based electron acceptor materials are shown in Figure 2.2.

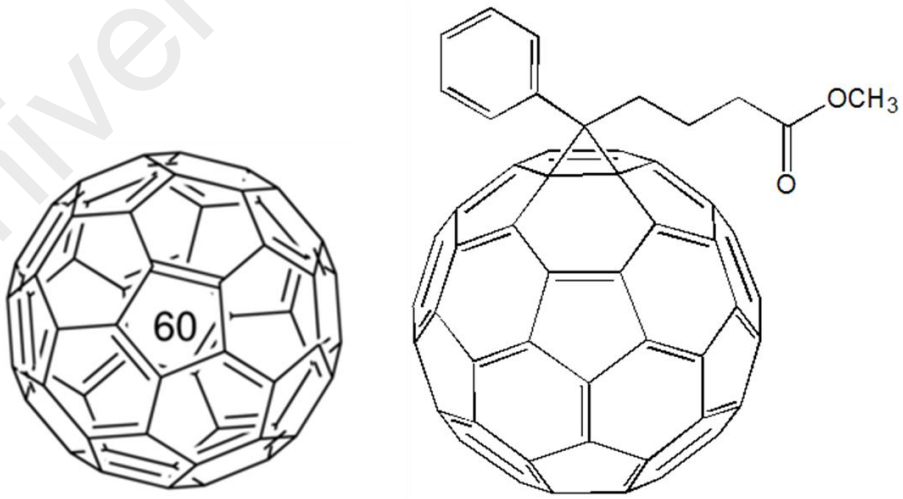

C60 **$PC_{60}BM$**

Figure 2.2: Examples of the fullerene based electron acceptor materials used in OSCs.

In recent years, all polymer solar cells which employ polymer donor and polymer acceptor materials as photoactive layer has received great attention (Facchetti, 2013; Kim et al., 2015) due to their enhanced photo-absorption in the visible range as compared to fullerene. Consequently, it improves the light harvesting and enables higher PCEs (Lee et al., 2015; Long et al., 2016; Zhou et al., 2016). Recently, Gao et al. (Gao et al., 2015) demonstrated the all-polymer solar cells with a PCE of 8.27%. This shows that polymer donor and polymer acceptor based active layer could dominate the OSCs field in future.

2.2.2 PCDTBT:$PC_{71}BM$ Blend

Leclerc and co-workers in 2007, synthesized the PCDTBT donor polymer for the first time (Blouin et al., 2007). Since then PCDTBT is regarded as one of the most extensively studied donor-acceptor copolymers due to its excellent properties (Synooka et al., 2014). PCDTBT shows nearly perfect quantum efficiency (Park et al., 2009), high solubility (Blouin et al., 2007), significantly higher PCEs (Wang et al., 2016), excellent thermal stability (Cho et al., 2010) and longer operational stability of several thousand hours (Roesch et al., 2013; Zhang et al., 2016).

Recently, Wang et al. (Wang et al., 2016) reported a PCE of 7.13% by employing co-additives in PCDTBT:$PC_{71}BM$ based BHJ OSCs. PCDTBT:$PC_{71}BM$ blend also shows excellent operational stability along with high PCEs. Zhang et al. demonstrated outdoor stability of PCDTBT:$PC_{71}BM$ based BHJ OSCs for over the course of an year (Zhang et al., 2016). It was concluded that PCDTBT:$PC_{71}BM$ based solar cells show relatively good stability in the real operational conditions. Contrary to P3HT-PCBM based blend, where we need post fabrication annealing for the higher efficiencies, the PCDTBT based OSCs exhibit best performance with un-annealed state, thus reducing processing steps as compared to P3HT based devices (Synooka et al., 2014).

The main focus of this thesis is to optimize the HTL by using metal oxides (V_2O_5) and GO along with PEDOT:PSS to address the stability issues associated with conventional PEDOT:PSS while maintaining the efficiencies comparable with the device containing pristine PEDOT:PSS, therefore section 2.2.3 below presents a brief description of it.

2.2.3 The Buffered Layers

A typical OSC architecture consists of a BHJ photoactive layer sandwiched between the two electrodes. However, this basic architecture possesses several performance constraints including lack of ohmic contacts, inefficient charge extraction and transportation, lack of selectivity in charge collection and mismatch of *WF* etc. (Chen et al., 2012). To overcome these issues, OSCs usually include functional layers (namely HTL and ETL) at the active layer/electrodes interface (Po et al., 2011). The buffered layers are considered to be critically essential part of the device architecture for achieving high efficiency and stability in OSCs and can no more be considered as "optional". These layers can be used to "engineer" the interface between the photoactive layer and electrodes which strongly affect this interface by inducing geometry modifications, chemical reactions and charge redistribution etc. (Ma et al., 2010). These layers are mainly selected on the merits of their charge transport properties, their energy levels and offer several potential advantages such as (Cao et al., 2016; Steim et al., 2010);

i. Buffered layers enable the high selectivity of charge carriers from the photoactive layer towards the electrodes.
ii. In some cases, they enhance the light absorption leading to higher PCEs, thus playing the role of an "optical spacer"
iii. Limit the reaction between the photoactive layer and the electrodes.

iv. Reduce the energy barriers due to mismatch in the energy levels of photoactive layer and electrodes.

Anode buffered layer: Since the discussion of ETL is out of this thesis scope, therefore, a brief description of HTL would only be presented here. The primary role of HTL is to improve the collection and extraction of positive charge carriers. In addition, it should block the negative charge carriers to the anode, thus needing a high WF material. ITO is the most commonly used anode electrode and its WF (~ 4.7 eV) does not match either with the HOMO level of most of the donor polymers or with the LUMO of fullerene based acceptor, thus, leading to a large band offset which results in recombination of charge carriers at the interface (Kettle et al., 2012). Therefore, use of PEDOT:PSS as state of the art HTL enables the high WF and planarize the electrode/active layer interface (Bailo et al., 2012). In addition, it also offers high conductivity and transparency and helps in adjusting surface defects passivation (Ameen et al., 2015). On the other hand, it is also true that PEDOT:PSS favors the device degradation due to its highly acidic and hygroscopic properties, leading to indium corrosion and oxygen ingress, respectively Shrotriya et al., 2006).

To date, the known HTL materials are transition metal oxides (TMOs) (Chen et al., 2012; Shrotriya et al., 2006), conjugated or non-conjugated polymers (He et al., 2014), small molecule organic materials, self-assembled monolayers (Zhao et al., 2015) and GO (Jeon et al., 2014; Liu et al., 2013). These materials have been reported to either replace PEDOT:PSS or used along with PEDOT:PSS to overcome stability issues associated with pristine PEDOT:PSS HTL. Among the HTL materials used in OSCs, TMOs are promising candidates due to their better environmental stability, high transparency and comparable device performance with that of PEDOT:PSS (Chen et al., 2012; Choi et al., 2015).

The very first use of TMOs in the field of organic electronics can be traced back in 1996 when Tokito et al. used vanadium oxide (VO_x), molybdenum oxide (MoO_x) and ruthenium oxide (RuO_x) as HTLs in organic light emitting diodes (OLEDs) (Tokito et al., 1996). In the pursuit for overcoming the stability concerns pertaining to PEDOT:PSS, researchers have identified several TMOs such as V_2O_5 (Chen et al., 2011; Cho et al., 2015), tungsten oxide (WO_3) (Li et al., 2012; Stubhan et al., 2012), molybdenum oxide (MoO_3) (Lee et al., 2012; Murase & Yang, 2012) and nickel oxide (NiO_x) (Hsu et al., 2015; Manders et al., 2013) to serve as HTLs in OSCs. It has been reported that certain metal oxides can act as an optical spacer (Gershon, 2011), moreover, TMOs are chemically and mechanically stable during their interaction with the organic photoactive layer, thus minimizing any undesired chemical reactions and increasing device life time (Ma et al., 2010). In addition, these metal oxides have high WFs so their Fermi levels match well with the HOMO level of photoactive polymer and they help to decrease the energy level offset between the photoactive layer and the ITO anode.

In the current work, V_2O_5 and GO have been employed as an HTL material along with the PEDOT:PSS to form a hybrid HTL in the PCDTBT:PC_{71}BM normal architecture solar cells. Therefore, a short description of each of these two materials is presented below.

2.2.3.1 V_2O_5 as an HTL Material

Metal oxide V_2O_5 has been widely explored as an HTL in BHJ OSCs. It can form an efficient HTL junction with the photoactive layer due to its much higher conduction level than the lowest occupied molecular orbital (LOMO) of the organic photoactive layer which can effectively block the undesired transportation of electrons towards the electrodes and thus, performance of the device can be significantly enhanced (Pan et al.,

2016). In addition, it shows very good transparency in visible region, wide optical bandgap, good interfacial adhesion and better environmental stability (Meyer et al., 2011; Rafique et al., 2016; Zilberberg et al., 2011). At initial stage of TMO based OSCs, metal oxides were usually deposited by cost intensive vacuum based processes (Kyaw et al., 2008). However, in recent years several reports confirm the efficacy of solution processable V_2O_5 HTL in BHJ OSCs device architecture showing high stability and efficiency (Rafique et al., 2016; Escobar et al., 2013; Wang et al., 2012). The reported work related to V_2O_5 as an HTL can be classified into two categories: one is using V_2O_5 as an HTL to replace PEDOT:PSS; the other is to use V_2O_5 along with PEDOT:PSS to form an organic-inorganic hybrid HTL. The latter option has been adopted to compliment the best features of both of the materials while overcoming their disadvantages. In this context, J. Pan et al. recently reported PEDOT:PSS/V_2O_5 double decked HTL by depositing V_2O_5 nanowires on top of the PEDOT:PSS layer (Pan et al., 2016). The resultant device outperformed the devices fabricated with either of individual materials on merits of their performance. In our recently reported work, V_2O_5 nanoparticles were dispersed in PEDOT:PSS aqueous suspension and the resultant device showed enhanced stability as compared to the device with that of pristine PEDOT:PSS (Rafique et al., 2016). It is thus concluded that solution processable V_2O_5 based HTL could be a simple and facile route to fabricate BHJ OSCs with high efficiency and stability.

2.2.3.2 GO as an HTL Material

It is obvious that development of facile, solution processable and low cost HTL material compatible with OSC materials is urgently demanded in recent years. In this context, solution processed GO derivatives have emerged as an efficient HTL material for OSCs with long term stability (Li et al., 2010; Liu et al., 2012). In particular, spin coated GO is regarded as a promising alternative to pristine PEDOT:PSS HTL due to its

easy fabrication approach, excellent transparency, mechanical flexibility and R2R production compatibility (Kim et al., 2013; Stratakis et al., 2014; Stratakis et al., 2013). GO is a derivative of graphene, consisting of one atomic layer thick graphene sheet functionalized with hydroxyl (OH) and epoxy groups on the basal planes and carboxylic groups (COOH) at the edge (Cheng et al., 2015; Ding et al., 2015). It contains a mix of sp^2 and sp^3 hybridized carbon atoms and, especially, sp^2 hybridized domain of GO provides opportunities to tailor its optoelectronics characteristics (Li et al., 2010; Yang et al., 2012). Although, GO possesses insulating properties, however, it still can facilitate the transportation of holes via hoping (Dehsari et al., 2014). Moreover, the GO based device possess excellent device stability as compared to the one with PEDOT:PSS HTL (Yusoff et al., 2014). GO is water soluble and could be combined with different organic and inorganic materials. It also retains the high transparency and its WF (4.9 eV, lower than PEDOT:PSS which is 5.1 eV) is comparable to PEDOT:PSS (Smith et al., 2014). However, GO as an HTL material also possesses some drawbacks including its insulating properties leading to poor Ohmic contacts, poor film uniformity and relatively low WF as compared to PEDOT:PSS (Ding et al., 2015). Therefore, a GO/PEDOT;PSS composite layer is expected to overcome these issues associated with either of the single material. It is reported that an ultrathin layer of GO underneath the PEDOT:PSS could act as a barrier against the ITO diffusion and acid corrosion, and also facilitates the extraction of holes via hoping due to well matched WF between GO and PEDOT:PSS as well as GO can effectively block the undesired flow of electrons due its large bandgap (~ 3.6 eV) (Dehsari et al., 2014). Moreover, the GO/PEDOT:PSS composite HTL shows better electrical conductivity, higher PCEs and enhanced stability (Yu et al., 2014).

2.3 Device Physics of BHJ OSCs

Since the development of BHJ device structure based on conjugated polymers-fullerene based intimated blend, this material combination has led to several breakthroughs in efficiencies with PCEs approaching above 10% regime (Chen et al., 2014). In addition, the stability of the OSCs has also substantially enhanced while device life of several thousand years has already been reported in real operational conditions (Zhang et al., 2016). This section reviews the process and performance characteristics that govern device operation of polymer-fullerene BHJ OSCs. The schematic representation of operating principle of OSCs is illustrated in Figure 2.3.

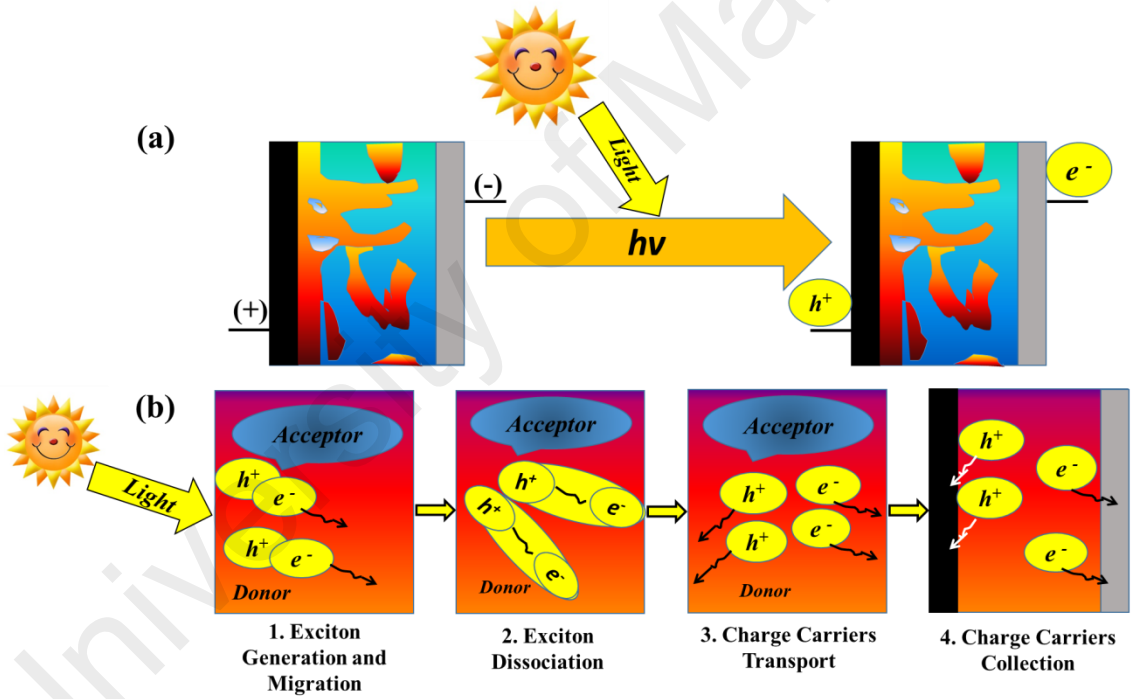

Figure 2.3: (a) Photogeneration in BHJ OSCs upon illumination and (b) Steps involved in energy production upon illumination (From exciton generation until charge carriers collection)

2.3.1 Light Absorption and Exciton Generation

To achieve the high efficiency, the photoactive layer must absorb the maximum of the incoming sunlight. Light is usually absorbed by donor fraction of the BHJ

photoactive layer. Due to high absorption co-efficient of conjugated polymers (10^7 m^{-1}) , they can effectively absorb light at maximum of their absorption spectrum (Blom et al., 2007) with very low thickness of the photoactive (100-200 nm) layer as compared to their in-organic silicon (an indirect semiconductor) based counterparts where thicknesses of hundreds of micrometers are required. Thus, the OSCs employing conjugated polymers significantly lower the amount of material. Unfortunately, owing to the narrow band of conjugated polymers as compared to inorganic semiconductor, they typically cover the small region of the solar spectrum only, thus, showing poor performance than inorganic solar cells (Hoppe et al., 2003; Lioudakis et al., 2007; Peet et al., 2007). Moreover, the thickness of polymer based photoactive layer is also limited to 100 nm due to low charge-carrier mobilities in most of the polymers which leads to an absorption of only 60% of the incident light at the absorption maximum (excluding back reflection of the electrode) (Blom et al., 2007). In contrast, the inorganic semiconductors can effectively absorb the whole visible solar spectrum (Blom et al., 2007; Deibel & Dyakonov, 2010). Thus, low absorption in conjugated polymers leads to low photocurrent generation. Interestingly, the absorption of light can be enhanced by lowering the bandgap of donor polymers which results in absorption of maximum number of photons that lead to higher PCEs (Brabec et al., 2002; Yeh & Yeh, 2013). Therefore, materials with lower bandgap are necessary to optimize the photon harvesting. Generally, a material with bandgap lower than 2 eV is considered as a low bandgap material that lead to the possibilities of improving the efficiency of OSCs due to a better overlap with the solar spectrum. For example, a bandgap of 1.1 eV can cover 77% of the AM 1.5 solar photon flux as compared to bandgap of 1.9 eV that can hardly cover 30 % of the AM1.5 photon flux (Yeh & Yeh, 2013). Thus, a low bandgap material can significantly improve the photocurrent generation.

Luckily, the bandgap of conjugated polymers can be lowered down to even 0.5 eV through numerous manipulations and modifications of their chemical structures (Jean Roncali, 1997). A simple rule of thumb to lower the bandgap is to either raise the LUMO or lower the HOMO levels of the polymer or bring them together simultaneously (Cheng et al., 2009). Several methods have been adopted to enhance the absorption range of donor polymers such as extending the conjugation length of the π-conjugated segments (Mühlbacher et al., 2006). In general, conjugation length is in inverse proportion to the difference between the HOMO and LUMO of the conjugated polymers. However, after certain extension in conjugated length it reaches to a saturation point and the bandgap starts to level off. Thus, an unlimited extension of the conjugation length results only in a limited reduction of the bandgap (Cheng et al., 2009). Another widely used approach is to combine electron rich and electron poor units in the polymer backbone in a 'push-pull' structure *i.e.* combining the thiophene containing (electron rich) and benzothiadiazole [BT] (electron poor). In this approach, the HOMO of the copolymer is dominated by the HOMO of the electron deficient unit and the LUMO by that of the electron rich unit. A remarkable improvement in the PCEs of OSCs has been made by using the so-called push-pull copolymers (Bronstein et al., 2011; Mühlbacher et al., 2006; Peet et al., 2007).

Light is illuminated from the transparent electrode side, and on absorption of photon; an electron is excited from the HOMO to the LUMO. It is similar to inorganic semiconductors where electron is excited from valence band to the conduction band. As a result an electron-hole pair (exciton) with binding energy typically in the range of 0.1–1.4 eV is generated (Mayer et al., 2007). Contrary to inorganic semiconductors, higher binding energy in organic materials is due to strong coulomb's attractions between the electron–hole pairs. The excitons are then migrated to donor-acceptor interface. A schematic representation of steps in energy production is shown in Figure 2.3.

2.3.2 Exciton Diffusion and Charge Dissociation

Singlet excitons in organic semiconductor materials migrate between conjugated segments through Förster energy transfer (Scheidler et al., 1996). Owing to the disordered nature of the polymers such hopping is referred as diffusion (Mikhnenko et al., 2014). These coulombically bound electron−hole pairs cannot generate photocurrent and for photovoltaic applications, BHJ of electron donor and electron acceptor is used to generate charge carriers. Further, the energy offset in LUMO between donor and acceptor materials breaks the Coulomb attraction which ultimately causes the excitons to dissociate (Dimitrov & Durrant, 2013; Gao & Inganäs, 2014; Ohkita & Ito, 2013). Therefore, excitons must diffuse into the donor-acceptor interface to dissociate into charge carriers before deactivating to the ground state (Tamai et al., 2015). However, the thermal energy at room temperature which is required to dissociate an exciton into free charge carriers is not enough due to the high exciton binding energy in conjugated polymers (Blom et al., 2007).

As most of the conjugated polymers exhibit shorter lifetime of the excitons, the diffusion lengths are limited to a few nanometers (less than 20 nm), which is much shorter than the optical absorption pass length (∼100−200 nm). As a result, the PCE of a bi-layer cell is limited by the low number of photons that can be absorbed within the effective exciton range (Markov et al., 2005). To circumvent this issue, the BHJ structure has been widely adopted to maximize the harvesting of excitons at the interface (Kang et al., 2016; Yu & Heeger, 1995). However, it is the prerequisite that excitons must be generated within their diffusion length (L_D) for efficient charge generation (Scharber & Sariciftci, 2013). Exciton diffusion length is defined as the distance travelled by an exciton before recombination (Fung & Choy, 2013). The reported excitons diffusion length for various conjugated polymers significantly varies ranging from 5 to 20 nm (Halls et al., 1996; Haugeneder et al., 1999; Stübinger &

Brütting, 2001). Thus, the thickness of the photoactive layer is very much critical for an efficient charge generation. However, a thin layer of photoactive BHJ material has to compromise on low absorption efficiency. Therefore, large interface area for exciton splitting and optimum phase separation is highly desirable which results in efficient exciton dissociation (Fung & Choy, 2013).

In organic semiconductors, photogenerated holes and electrons at the donor/acceptor interface experience a strong Coulomb binding energy (Clarke & Durrant, 2010; Deibel et al., 2010). These Coulomb bound electron–hole pairs have to be dissociated to get free charge carriers. However, they either recombine or dissociate into free charge carriers upon escaping their mutual Coulomb attraction (Blom et al., 2007; Deibel & Dyakonov, 2010). Efficient charge transportation requires efficient dissociation of excitons at the interface. The difference in HOMO and LUMO between donor and acceptor layers creates electrostatic forces at the interface. When materials choice is proper, such differences generate electric field that leads to the efficient break up of excitons into electrons and holes (Yeh & Yeh, 2013). Further, the free electrons are then accepted by the material with higher LUMO level and holes by the material with lower HOMO. Unfortunately, these free charge carriers can lead to recombination or trapping in a disordered interpenetrating organic material while travelling towards the electrodes.

2.3.3 Free Charge Carrier Transport

After the exciton dissociation into free charge carriers, the charges should be transported towards the respective electrodes as shown in Figure 2.3. The transportation of charge carriers in organic semiconductors mostly takes place by hopping from one localized state to the next (Baranovskii et al., 2000; Pivrikas et al., 2007). Moreover, in the BHJ of donor- acceptor materials, the donor is generally a hole conductor and an

acceptor transports the electrons. Transportation of free charges towards their respective electrodes is driven by an internal electric field occurred due to the Fermi level difference of the electrodes (Zhou et al., 2010). In general, a high WF anode and a low WF cathode create an internal electric field that determines the V_{oc} of the cell (Fung & Choy, 2013). Transportation of free charge carriers is either driven by the carrier diffusion or electric field induced drift.

The main bottleneck to the efficient transportation of free charge carriers towards the anode and cathode is their recombination before reaching to their respective electrodes. The charge carrier mobility in the photoactive layer governs both the carrier transportation as well as the losses caused due to carrier recombination (Mandoc et al., 2007). In the case of low mobility materials, electrons and holes remain bound by the Coulomb potential, as a result they cannot overcome their mutual attraction and finally recombine prior to charge collection at the electrodes (Pivrikas et al., 2007). Consequently, the solar cell experiences a significant loss in terms of photogenerated current. As discussed earlier, because of low carrier mobility in BHJ materials, the thickness of the photoactive layer is restricted to less than 100 nm for an optimized performance (Park et al., 2009). The path length of photogenerated electrons and holes is in direct proportion to the thickness of the photoactive layer (Cowan et al., 2012). Charge carrier recombination increases as the photoactive layer gets thicker, resulting in a substantial loss in the device performance (Lenes et al., 2006). Thus, competition between carrier sweep-out by the internal field and the loss of photogenerated carriers by recombination are the important issues to overcome for high efficiency devices (Cowan et al., 2012).

2.3.4 Collection of the Charge Carriers at the Electrodes

Photogenerated charge carriers that do not recombine are finally extracted from the photoactive layer to the respective electrodes. The potential barrier at the photoactive layer/ electrodes interface must be reduced to maximize the extraction of charges (Deibel & Dyakonov, 2010). Therefore, the WF of the anode should match with the HOMO of the donor material, while the WF of the cathode must match with the LUMO of the acceptor material (Fung & Choy, 2013). If the WF matches well as described then the contacts are said to be Ohmic contacts. Contrary to this, if there is a mismatch between the anode and cathode with that of donor HOMO or acceptor LUMO, respectively, then no Ohmic contacts would be established. Ultimately, the performance of the solar cells will decrease (Blom et al., 2007).

The charge collection at the respective electrodes concludes the steps from absorption of light to generation of photocurrent as show in Figure 2.3. The PV performance characteristics such as J_{sc}, V_{oc} and *FF* etc. are reliant on the photocurrent generation. Therefore, a brief discussion on the performance characteristics of an OSC is presented in section 2.3.5.

2.3.5 Performance Characteristics

At present, BHJ OSCs are one of the most successful device architectures in OSCs, which employ an intimate blend of donor and acceptor materials incorporated in photoactive layer. In addition, OSCs have the lowest energy payback time (~ 0.4 years) than silicon (~2.4 years for c-Si) and CdTe (~ 0.7 years) (Peet et al., 2007). To achieve an optimum performance, a basic understanding of the performance characteristics that govern the operation of solar cells is necessary that can serve as a guideline to identify and develop new materials for highly efficient devices.

As discussed briefly in Chapter 1, the *PCE* of an OSC is reliant on the V_{oc}, J_{sc}, *FF*, and P_{in} defined by the equation 1.1 in Chapter 1. Figure 2.4 shows a typical Current density - Voltage (*JV*) curve for a solar cell. It illustrates the critical parameters which determine the PCE of an OSC. These include the V_{oc}, J_{sc}, *FF*, and the values for J_{Mpp} and V_{Mpp} (J_{Mpp} and V_{Mpp} are the points on the *J-V* curve where maximum power is produced). The outlined shaded area in the graph indicates the FF whereas, the product of current and voltage has the highest yield at the maximum power point (M_{PP}) (Hoppea & Sariciftci, 2004).

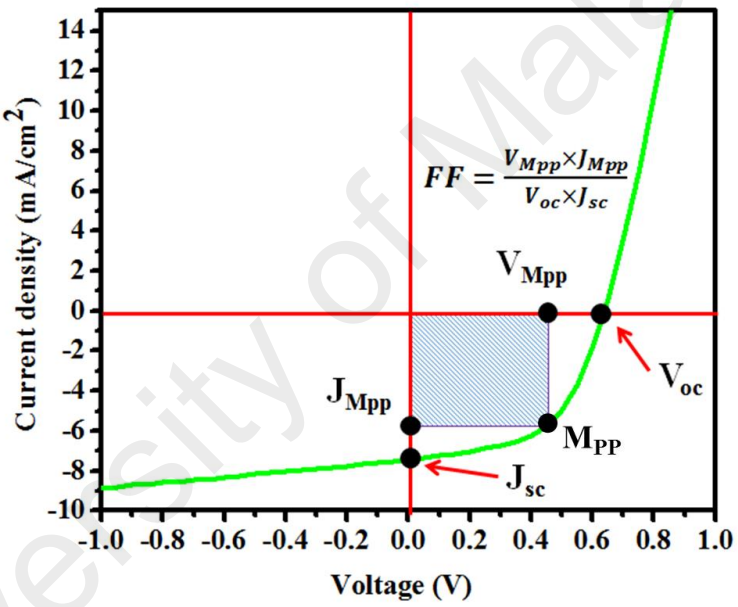

Figure 2.4: Typical Current density- Voltage (*J-V*) curves of an OSC.

Rigorous research has been carried out to optimize these parameters in order to enhance PCEs of OSCs. Below, a brief description for each of them is presented.

2.3.5.1 Short Circuit Current Density (J_{sc})

The J_{sc} is the maximum photocurrent density generated at zero applied potential (*e.g.* short circuit conditions when V_{oc} = 0) (Troshin et al., 2008). Although, there is no power produced at this point, however, the J_{sc} marks the onset of the power generation.

It is essential parameter which can be affected due to several factors such as locally enhanced surface recombination, due to regions of low charge carrier lifetimes, inhomogeneous optical characteristics as well as distances to the metal contacts during the production process (Padilla et al., 2014). J_{sc} represents the number of charge carriers generated and finally collected at the respective electrodes at zero applied potential (Fung & Choy, 2013). Although it is technically a negative number, but conventionally its magnitude is considered and treated as a positive number, *e.g.* a higher J_{sc} is desired for higher efficiency.

The performance of an OSC is largely governed by the incident photon to converted electron (IPCE) efficiency, defined as the externally measured number of collected charge carriers verses the number of incident photons, and also referred as external quantum efficiency (EQE) (Armin et al., 2014; Chen et al., 2013). The J_{sc} is directly related to the EQE and the relationship between the J_{sc} and EQE is expressed as (Wright & Uddin, 2012):

$$J_{sc} = \frac{q}{hc}\int_{\lambda_{min}}^{\lambda_{max}} EQE \times P_{in}(\lambda)\lambda \times d\lambda \quad \text{..... (2.1)}$$

Where, q is the charge of electron, λ [nm] is the wavelength of incident photons and P_{in} [W/m^2] is the incident power. Moreover, IPCE can also be understood as how efficiently the device converts the incident light into electrical energy at a certain wavelength (Günes et al., 2007). Mathematically the IPCE it expressed as:

$$IPCE = \frac{1240 I_{sc}}{\lambda P_{in}} \quad \text{..... (2.2)}$$

Where, I_{sc} is the photo-current [µA/cm^2], λ [nm] is the wavelength of incident photons and P_{in} [W/m^2] is the incident power.

2.3.5.2 Open Circuit Voltage (V_{oc})

One of the most important factors determining the device efficiency is V_{oc} which is determined when $J = 0$ or it is being open circuited (Chandrasekaran et al., 2011). It is the measure of the maximum of voltage that a solar cell can extract for an external circuit (Elumalai & Uddin, 2016; Qi & Wang, 2012). Although, a generally acceptable view is that V_{oc} in the BHJ OSCs originates from the energy offset between the HOMO of the donor and LUMO of the acceptor material (Ke et al., 2015), however, early studies reveals that the V_{oc} is determined by the difference in the WFs of the two electrodes (Lo et al., 2010), the so called metal-insulator-metal (MIM) model (Günes et al., 2007; Mihailetchi et al., 2003). Brabec et al. fabricated series of devices with several fullerenes of varied LUMO level and commonly used donor materials, and reported that V_{oc} is directly related to the acceptor strength of the fullerenes. Moreover, their results fully support the view that V_{oc} is reliant on offset between the HOMO level of the donor and the LUMO level of the acceptor components (Brabec et al., 2001). Scharber et al. reported in their work that MIM model is not valid for BHJ OSCs and V_{oc} of a BHJ OSC linearly changes with the energy level offset between the HOMO of donor and LUMO of the acceptor (Scharber et al., 2006). From their analysis, a simple empirical equation was proposed to express V_{oc} as:

$$V_{oc} = (1/q)\left(\left|E_{HOMO,D}\right| - \left|E_{LUMO,A}\right|\right) - 0.3V \quad \text{..... (2.3)}$$

Here q is the elementary charge, ($E_{HOMO,\,D}$) and ($E_{LUMO,\,A}$) are the energy levels of donor HOMO and acceptor LUMO, respectively. It is noteworthy that 0.3V loss is empirical, and could be less or more (Qi & Wang, 2012). However, the origin of V_{oc} is not clear and its variations cannot be fully included from the above rules, thus, indicating that its origin still needs to be further investigated for better understanding on OSCs.

It is discussed by Widmer et al. (Widmer et al., 2013) in their recent study on V_{oc} of an OSC that V_{oc} of an OSC is also restricted by the donor-acceptor material system. Moreover, the nano-morphology of the BHJ photoactive layer also affects the device performance (Liu et al., 2001). In addition, charge carrier recombination (generally non-geminate recombination in OSCs) (Groves & Greenham, 2008; Shuttle et al., 2008)) potentially brings the significant loss in the V_{oc} of a device (Qi & Wang, 2012). There are several factors which can potentially reduce the V_{oc} of an OSC such as temperature, light intensity, WF of electrodes and material microstructure etc. (Qi & Wang, 2012). The V_{oc} of the device can potentially be improved by employing interfacial engineering at the active layer/ electrodes interface such as introducing HTLs and ETLs in the device structure (Lieuwma et al., 2003). The HTLs and ETLs can effectively reduce the surface recombination at the electrode/photoactive layer interface (Qi & Wang, 2012). The V_{oc} is proportional to the built-in potential of an OSC, and by enhancing it will obviously increase the V_{oc}.

2.3.5.3 Fill Factor *(FF)*

The *FF* is an important parameter that determines the *PCE* of an OSC. The PCE of an OSC is calculated from its *J-V* characteristics as a product of J_{sc}, V_{oc} and *FF*. Moreover, the shape of the *J-V* characteristics of an OSC is characterized by the *FF* that is the ratio of the maximum output power to the product of I_{sc} and V_{oc} (Trukhanov et al., 2015). The shape of the *J-V* curve determines how ‘‘difficult’’ or how ‘‘easy’’ the photogenerated carriers can be extracted out of a solar cell device and ideally *FF* should be 100% when the *J-V* curve is exactly a rectangle (Qi & Wang, 2013). In the Figure 2.4, the shaded area represents the *FF* whereas the representative equation to express FF has been presented in equation 1.2 of Chapter 1.

It is noteworthy that *FF* is more sensitive parameters as compared to V_{oc} and J_{sc} and depends upon several factors such as charge carrier mobility, thickness of the photoactive layer, morphology of cathode/photoactive layer interface and bulk material properties (Gupta et al., 2010). Moreover, series resistance R_s is one of the most important factors affecting *FF* of an OSC (Kim et al., 2009). In general, a low R_s is highly desirable that can be achieved with optimized surface morphology, and consequently a much higher *FF* is possible to achieve (Kim et al., 2009; Street et al., 2011). A fraction of increase in R_s can reduce high percentage of *FF e.g.* for every 0.1Ω increase in R_s value can reduce 2.5% of *FF* (Lindmayer & Allison, 1990). The R_s (often referred as the internal resistance) is comprises of several factors such as active layer resistance, interfacial layer resistance, electrode resistance, contact resistance of every interface in the device and probe resistance. Consequently, all these factors have adverse effects on the *FF* of a solar cell device (Servaites et al., 2010).

Shunt resistant (R_{sh}) represents the current leakages in a solar cell including leakage from edges, pinholes, traps and films etc. An ideal device should not have any current leakage which implies that ideally R_{sh} should approach to infinity. Several factors influence the R_{sh} of a device and ultimately lower the *FF*. Kim et al. reported effective design variables to control *FF*; their study concluded that most prominent factors affecting R_{sh} of a device are the electrode/photoactive layer interface, illumination intensity and thickness of the blend layer and ultimately, lower the *FF* (Kim et al., 2009). By optimizing the aforementioned characteristics of an OSC including film morphology, interfacial optimization, lower R_s and high R_{sh} etc., higher *FF* values are possible to achieve.

2.3.5.4 Power Conversion Efficiency (*PCE*)

Finally, the most discussed performance parameter of a solar cell device is its PCE. It is defined as the percentage of input irradiation (P_{in}) that is converted into the output power and expressed as the product of V_{oc}, J_{sc}, and FF divided by the input power (P_{in}).

In summary, these key performance parameters of OSCs play an important role in determining and optimizing the performance of solar cells. To achieve the best optimum performance, every single factor contributing towards the efficiency of the device has to be enhanced by improving electrodes, BHJ material, every layer and interfaces etc.

2.4 Stability of OSCs/Degradation Factors Limiting the Device Stability

OSCs have exponentially evolved in terms of efficiency and stability. While, the PCE has been increased by almost a factor of ten exceeding 10%, lifetime of the OSCs has also approached several thousand hours under favorable circumstances (Gevorgyan et al., 2013; Jørgensen et al., 2012). However, stability is still a bottleneck to the widespread commercialization of OSCs. While promising achievements in the PCEs of OSCs, above 10% value only represents the initial performance of the OSCs-how the PCE of the solar cell degrades with time is also of critical importance. The energy output of a solar cell device is the product of its efficiency and lifetime stability, illustrated in Figure 2.5. Therefore device stability is of paramount importance in OSCs and inferior device stability still remains a great challenge to compete the inorganic silicon based solar cells in photovoltaic industry. Moreover, the fabrication techniques must be compatible with the R2R production for the widespread commercialization of OSCs.

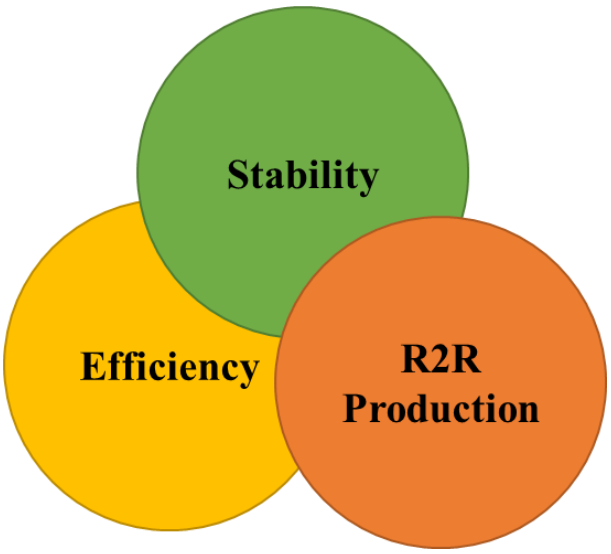

Figure 2.5: Key areas of research pertaining to OSCs

Studying the stability of OSCs helps in understanding how a device degrades during operation. Device instability occurs due to range of complex phenomena that are in play simultaneously of which presumably many have not been identified (Rafique et al., 2017). OSCs are highly sensitive to even small degree of degradations which make degradation factors extremely critical for device operation and thus should be completely removed or at least reduced to improve device lifetime (Krebs et al., 2010).

Obtaining longer operational lifetime in OSCs is generally challenging, even though lifetime of several thousand hours has been reported in certain conditions. Degradation mechanism in OSCs is rather complex and cannot be explained by a single process. It may include factors affecting active layer, the transport layers, the contacts and the interface of every layer with the adjacent layers (Guerrero et al., 2012; Kim et al., 2009). In general, degradation factors in OSCs can be distinguished to be either intrinsic or extrinsic. Among these factors are oxygen and water diffusion (Norrman et al., 2008), electro-migration induced shunts, oxidation and rusting of Al electrode due to moisture (Glen et al., 2015), indium diffusion from anode due to acidic PEDOT:PSS (Ecker et al., 2011), swelling of water-soluble layers as well as corrosion and

delamination of the metal contacts due to oxygen and water ingress (Jørgensen et al., 2008). Moreover, thermal and photo-induced degradation of active layers under illumination in ambient conditions, active layer intrinsic chemical evolution, photo-bleaching and mechanically induced stress also occur in OSCs (Bao et al., 2014; Guerrero et al., 2015; Morse et al., 2015). Both types of degradation are mass-flow (diffusion) processes. This section briefly covers some of the most pronounced degradation effects, while schematic representation of some of the degradation factors limiting the device stability is shown in Figure 2.6.

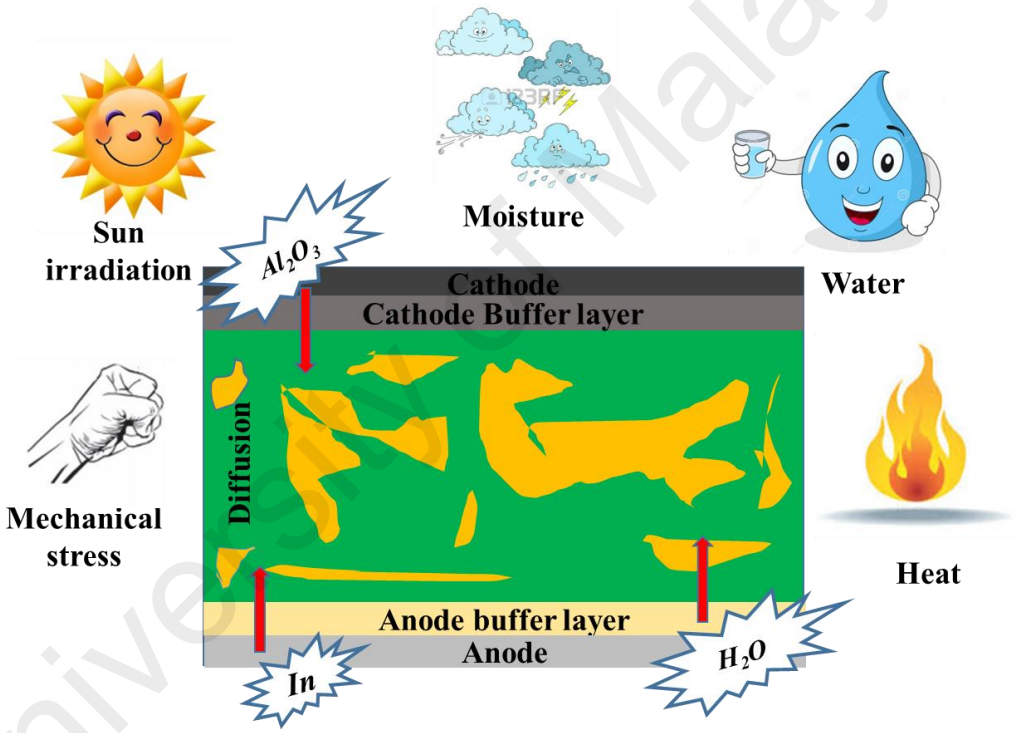

Figure 2.6: Degradation factors affecting device stability.

2.4.1 Intrinsic Degradation

OSCs are currently the ultimate in terms of complexity and they exhibit the most uncontrollable situation in terms of stability. So far, most of the research is focused on effects of extrinsic degradation factors such as temperature, light, oxygen and humidity on photoactive layer, electrodes and interfaces. However, less attention has been given

to the intrinsic degradation mechanisms. In general, the intrinsic degradation arise from thermal diffusion of constituent materials at interfaces of OSCs (Cao et al., 2014). Even after encapsulation (to avoid oxygen and moisture ingress), intrinsic degradation in photoactive layer can occur due to light or by the elevated temperatures due to continued exposure to sunlight (Kesters et al., 2015). It includes inter-diffusion of electrodes (Jeon & Lee, 2012), interfacial layers (Ecker et al., 2011), phase-separation at organic-cathode interface and change in the nanoscale morphology of BHJ constituents (Cao et al., 2014; Motaung et al., 2011). Moreover the thermally activated phase separation, photochemical damages occur in the BHJ films (Savagatrup et al., 2015) which can cause further deterioration of mechanical properties such as brittleness and stiffness in the photoactive layer (Connor et al., 2010; Savagatrup et al., 2014).

Photoactive layer is the most important component of OSCs, comprised of donor, acceptor and donor/acceptor mixed phase. Photoactive layer possesses metastable phase separation due to strong mobility of its organic constituents. In order to increase the efficiency, often high boiling point additive solvents are added in the photoactive blend. On the other hand, these additives significantly hamper the device stability (Tournebize et al., 2015; Wang et al., 2014; Zawacka et al., 2014). Some of these additives are highly sensitive to light and can directly saturate the polymer conjugated backbone or be trapped by the fullerene moieties, moreover, they can accelerate the photo-oxidation of the BHJ layer (Kim et al., 2015; Tournebize et al., 2015).

Similar to photoactive layer, electrodes and interfacial layers also possess mobility resulting in severe device instability (Elumalai et al., 2013). Widely used PEDOT:PSS is highly acidic and hygroscopic which upon contact with ITO anode corrodes its surface. This leads to diffusion of indium (*e.g.* dissolution of In_2O_3) into the

active layer which results in trapping of charge carriers (Jong et al., 2000; Gautier et al., 1996; Sharma et al., 2011; Sharma et al., 2011). Al is normally employed as cathode which readily gets oxidized to form Al_2O_3. Water can diffuse through pinholes and voids to the underneath layers that ultimately lowers the device lifetime (Rafique et al., 2017). Moreover, water ingress from the edges through the PEDOT:PSS also oxidizes the cathode and significantly reduces the J_{sc} (Feron et al., 2013; Glen et al., 2015; Voroshazi et al., 2011). Such diffusion of electrodes and interfacial layers can drastically reduce the device lifetime by changing the energy levels of interfacial layers as well as causing charge carrier trapping and recombination (Cheng & Zhan, 2016).

2.4.2 Extrinsic Degradation

An ideal OSC device should possess consistent performance over time when it is exposed to cyclic changes in the environment such as light/dark, hot/cold, dry humid etc. However, the fact is opposite and with the emergence of new photovoltaic technologies such as OSCs, the stability of these devices is compromised as compared to silicon based solar cells where a life time of over 25 years is warranted (Jørgensen et al., 2012; Mateker et al., 2015). The poor long-term stability of OSCs needs to be overcome for their successful commercialization. Most importantly, an unanticipated decay in the device performance during its initial operation, the so called 'burn-in' loss, is one of the root causes for the device shorter lifetime (Kong et al., 2014). A second phase starts after the burn-in phase which shows linear trend in degradation and the slop of this linear trend determines the lifetime of an OSC, which is chosen to be the time over which device efficiency reduced to the 80% (T_{80}) of the post burn-in efficiency (Tipnis et al., 2009). Extrinsic stability can only be ensured with proper encapsulation of the device from the outside environment because un-encapsulated device rapidly degrades in ambient air and the device efficiency plunges down to negligible within few minutes (Roesch et al., 2013).

Oxygen and water, extrinsic to OSCs are some of the known degradation factors affecting device stability (Grossiord et al., 2012; Jørgensen et al., 2012). Typically, the constituents of an OSC are subjected to degradation upon exposure to ambient atmosphere. Molecular oxygen and water cause chemical degradation (photo-oxidation) of the organic layers and interfaces, which consequently will disrupt the delicate electrochemical processes that are vital for the photovoltaic performance (Jørgensen et al., 2012). Moreover, the photo-oxidation of active layer also alters its absorption, energy levels and charge carrier mobilities such as quenching the polymer excited state and a severe impact on electronic properties of fullerene domains (Reese et al., 2010) as well as aggregation of fullerene domains (Parnell et al., 2016), consequently, the device performance can be severely hampered. In addition, hole concentration can be increased due to oxidation of active layer which leads to a decrease in the density of deeper traps for electrons and eventually reduces the *FF* and V_{oc} of a device (Schafferhans et al., 2010; Seemann et al., 2011).

Oxygen and water diffuses through the whole device and equally damage the functionality of each layer (Kawano et al., 2006). The low *WF* metal cathode gets oxidized due to oxygen ingress. Consequently, an insulating metal oxide layer is formed that creates a transport barrier, ultimately an S-shaped *I-V* curve is induced and the performance of the device gets degraded (Glatthaar et al., 2007). Also, formation of pinholes and voids in the metal layer facilitates the diffusion of water and oxygen to the underneath layers (Feron et al., 2013). Moreover, PEDOT:PSS is known to be hygroscopic and the absorbed water can further penetrate into the whole device. The PEDOT:PSS could be phase separated, with the PEDOT rich phase being responsible for most of the interfacial degradation in the presence of water and oxygen (Norrman et al., 2010). In addition, the photo-oxidation of active layer, formation of metal oxide insulating layer and phase separation lead to a reduction in the donor-acceptor

interfaces, which could potentially harm the exciton dissociation, thus the performance of an OSC significantly reduced (Parnell et al., 2016).

Photodegradation upon irradiation is one of the most crucial issues to be addressed because any photovoltaic device is inevitably operated under the light exposure. OSCs are proven to be unstable upon irradiation and severe deterioration of device efficiency during 100 h of light exposure has been reported by recent studies conducted by Yamanari et al. (Yamanari et al., 2010). This is referred as the burn-in photo-degradation and proves to be one of the major barriers in the successful commercialization of OSCs (Tamai et al., 2016). Unfortunately, light irradiation accelerates the degradation of OSCs in number of ways. Firstly, as discussed earlier, continuous illumination elevates the temperature and cause thermally induced degradation which eventually boost the intrinsic degradation of OSCs (Motaung et al., 2011). Secondly, the irradiation also degrades the organic constituents of an OSC and causes the oxidation of photoactive material near Al interface (Norrman et al., 2006). Moreover, excessive illumination also accelerates the diffusion of oxygen and moisture in the bulk of photoactive layer (Eloi et al., 1993; Voroshazi et al., 2011).

Recently, Córcoles et al. studied the influence of varied wavelength of solar cell spectrum on the stability of P3HT:PCBM based OSCs (Córcoles et al., 2015). Their study reveals that certain wavelengths of solar spectrum are more harmful for the device stability. For example, a blue and ultraviolet wavelength accelerates the device degradation. Madsen et al. demonstrated in their recent work that light intensity also influences the stability of an OSC and the degradation rate linearly scales with the light intensity (Madsen et al., 2013). Above all, the key reason of light induced instability is the photo-chemical and photo-physical degradation occur in every layer and interfaces (Cheng & Zhan, 2016). Further in this context, several reports confirm that photo-

oxidation reaction in the active layer is the main reason that hampers the device degradation (Domínguez et al., 2015; Tournebize et al., 2013). The device faces several consequences of these photo-oxidation reactions such as low photo-absorption due to altered donor and acceptor structures which eventually decrease the excitons generations (Deschler et al., 2012). Moreover, these reactions alter the energy levels of donor and acceptor materials as the two components do not get equally affected by these photo-oxidation reactions, consequently, energy level alignment between the donor and acceptor fractions get disrupted (Aygül et al., 2013). Finally, photo induced oligomerization of fullerene component and photolysis of donor fraction in the active layer occurs which cause the instability of OSCs upon irradiation (Burlingame et al., 2015; Rivaton et al., 2010).

In addition to chemically induced photo-degradation, Adachi et al. and Kumar et al. revealed physically induced photo-degradation of the devices which occur due to carrier accumulation, resulting in severe degradation in solar cell performance (Adachi et al., 2009; Kumar et al., 2010). Their studies established this fact that amount of accumulated charge carriers and degree of degradation of an OSC are closely related to each other.

Mechanical degradation is less studied mode of degradation as compared to other extrinsic and intrinsic degradation modes. However, it is essential to address for the *R2R* manufacturing and the operational stability of OSCs, in particular for the portable and outdoor applications (Savagatrup et al., 2015). The flexible modules of OSCs often go through the substantial bending, shearing and deformation, and therefore, require resistance to these mechanically induced degradations. Mechanically induced degradations (stress) could affect polymer-fullerene layer, the interfacial layers, electrodes and the interfaces (Cheng & Zhan, 2016). Moreover, in case of their

installation and exposure to the real world atmospheric conditions, the devices could face severe mechanical degradation including delamination, cracking, scratches, punctures and bending etc. (Bruner et al., 2014). The punctures and edge delamination facilitate the water and oxygen ingress which eventually cause further delamination of the modules (Krebs et al., 2014). Consequently, as discussed earlier, the penetration of oxygen and water equally affect all the layers and their interfaces.

As long as the photoactive layer concerned, Awartani et al. in their recent work highlighted two critical mechanical parameters of BHJ photoactive layer namely stiffness and ductility that are correlated to the device performance (Awartani et al., 2013). Adequate knowledge of these factors is essential to provide insight into the performance, stability, and underlying degradation phenomena that could occur during the material's service life (Chung et al., 2011). Their study concluded that the P3HT:PCBM based blend increased the elastic modulus and lowered the crack onset strain. Bruner et al. recently reported their findings on molecular intercalation and cohesion of BHJ OSCs (Bruner et al., 2013). Their findings suggest that polymer-fullerene BHJ layer is cohesively weak resulting in thermomechanical failure within the BHJ layer and is influenced by the formation of a bimolecular crystal phase within the BHJ layer.

Dupont et al. discussed the importance of inter-layer adhesion in *R2R* processed OSCs (Dupont et al., 2012). Their work suggests that poor adhesion between adjacent layers may results in in loss of device performance due to delamination driven by the thermo-mechanical stresses in the device. In particular, their study revealed that interface of BHJ layer with the PEDOT:PSS was found to be the weakest. In summary, all the aforementioned degradation factors comprise an intriguing aspect of

interdisciplinary research which requires a team of experts in organic chemistry, device physics, polymer science, interfacial engineering and microstructural determination.

2.4.3 Strategies to Improve Device Stability

It is vital that for the successful performance of an OSC, the device must be extrinsically and intrinsically stable. The OSC modules must resist to mechanical, oxidative, irradiation, thermal and photo-chemical instabilities. The electrode, the interfacial layers and most importantly the photoactive layer and their interfaces should not be susceptible to degradation factors. Several strategies have been adopted to address the stability concerns associated with the operational lifetime of an OSC. This section briefly describes a few strategies to improve intrinsic and extrinsic stability of an OSC.

2.4.3.1 Encapsulation

Encapsulation is one of the key measures which are taken to ensure extrinsic stability. Oxygen and water are the known degradation factors; therefore, it is natural to encapsulate the devices in various ways (Jørgensen et al., 2012). In addition, it also prevents the device from mechanical instabilities such as scratches and bending etc. However, the photovoltaic properties of an encapsulated device depend on the encapsulation material and method (Cheng & Zhan, 2016). In general, OSCs are encapsulated with the glass plates; however, it is not compatible with flexible solar cell modules. Therefore, in recent years, organic based encapsulation materials have been employed to protect OSCs (Krebs, 2006; Sapkota et al., 2014; Tanenbaum et al., 2012). Elkington et al. employed a bisphenol A-based epoxy resin to use as an encapsulation material on BHJ OSCs (Elkington et al., 2014) . The encapsulant proved to be a barrier against the degradation in air. Similarly, Peters et al. demonstrated a highly stable PCDTBT:$PC_{71}BM$ based device by using UV curable epoxy glue as top encapsulation

layer (Peters et al., 2011). The device lifetime approached to around 7 years which is one of the longest ever reported life of OSCs. Recently, metal oxides along with MgF_2 in a layered structure (Gomez et al., 2015) and GO (Kim et al., 2014) have been employed to encapsulate the OSCs that lead to the highly stable device exhibiting several hundred hours of operational life. Combination of organic-inorganic materials such as epoxy resin and glass can also be used as an encapsulant (Aluicio et al., 2014; Roesch et al., 2013).

2.4.3.2 Interfacial Engineering to Enhance Performance of OSCs

The basic structure of an OSC comprises of photoactive layer sandwiched between two electrodes. However, it is now considered as essential to insert interfacial layers at the interface of electrodes and photoactive layer, making them integral part of BHJ OSCs. However, most commonly used interfacial materials are susceptible to the degradation and significantly reduce the device performance. Therefore, several alternatives have been explored during the past few years to address stability concern associated with pristine interfacial materials.

Hole transport layer. PEDOT:PSS is the most commonly employed HTL material , but it favors the device degradation due to its acidic and hygroscopic nature. Ultimately, it corrodes the underneath ITO which further diffuse into the photoactive layer. Therefore several alternative materials have been reported to work as HTLs in OSCs. Among them metal oxides based HTL are the most studied alternatives to the acidic PEDOT:PSS (Lattante, 2014; Zhao et al., 2010). Metal oxides such as NiO (Yang et al., 2012), V_2O_5 (Meyer et al., 2011), WO_3 (Tan et al., 2012) and MoO_3 (Chen et al., 2012) have been widely used as HTLs in OSCs (Kim et al., 2015). All these materials can be processed from solution, and thus are compatible with *R2R* production (Girotto et al., 2011; Manders et al., 2013; Zilberberg et al., 2011). Recently, GO has been

employed as a potential HTL material in BHJ OSCs (Cheng et al., 2015; Li et al., 2010). Go is an oxidize state of graphene which possess excellent properties such as high transparency, excellent electrical conductivity and very good mechanical properties to act as an HTL (Gao et al., 2011). Another alternative is to use combination of metal oxide/GO along with PEDOT:PSS to compliment the drawbacks of each of the individual materials (Lee et al., 2016; Rafique et al., 2016).

Electron transport layer. LiF or Ca and ZnO are the most commonly employed ETLs in conventional and inverted geometry BHJ OSCs, respectively. These materials are unstable in ambient atmosphere due their reactivity with oxygen, water (for LiF and Ca), air and light (for ZnO) (Cheng & Zhan, 2016). In addition, vacuum deposition is not compatible with *R2R* manufacturing. In this context, metal oxides such as CrO_x (Wang et al., 2010), Cs_2CO_3 (Li et al., 2006), TiO_2 (Huang et al., 2015) and electron extracting polymers (Nikiforov et al., 2013) have been employed as alternative ETLs. Moreover, ZnO can be modified in a number of ways to overcome the stability issues associated with the single ZnO ETL (Cao et al., 2014). Metal doping of ZnO is commonly used to enhance the electron transport characteristics (Kim, 2014). In addition, several other structures of ZnO such as nanowires, nanorods, nanoflakes and nanowalls are also reported in the literature as ETLs (Mbule et al., 2013). Like HTL, GO can also be used as an ETL material to improve the efficiency and stability of OSCs. D.H. Wang et al. demonstrated PCDTBT:PC_{71}BM BHJ OSCs employing an ETL of stretchable GO by stamping transfer (Wang et al., 2013). The resultant device showed enhanced efficiency and stability as compared to pristine device without any interlayer. Efficacy of GO as an ETL has been reported by several other works (Jayawardena et al., 2013; Kim et al., 2015).

2.4.3.3 Morphology Control in the BHJ Photoactive Layer

Photoactive layer comprises of BHJ of polymer-fullerene is the most important component of an OSC. Although, BHJ OSCs are showing promising results in terms of efficiency and stability, however, the morphology of each donor-acceptor material differs significantly, particularly, in terms of domain size and degree of interpenetration between domains (Zheng, et al., 2015). Due to shorter diffusion length of excitons the active layer must comprises of interpenetrating network morphology consisting of optimized domain size of both donor and acceptor constituents to facilitate the migration of excitons to the donor- acceptor interface and their splitting into the free charge carriers so that the charge carriers can be extracted. Ideally, the domain size of donor-acceptor fragments must be in the range of 10-20 nm (Yu et al., 1995).

Inclusion of third component in addition to donor-acceptor fragments is a popular approach to enhance the device performance (Ameri et al., 2013; An et al., 2016; Lu et al., 2015). A third component could be a cross-linker to enhance the thermal stability (Derue et al., 2014; He et al., 2013), modified fullerene derivatives acting as cross linker to thermally stabilize the device (Chen et al., 2015; Cheng et al., 2011), inclusion of compatibilizers to enhance the thermal and mechanical stabilities (Chen et al., 2014; Sivula et al., 2006) and employing insulator polymer as a third agent to simultaneously increase thermal and mechanical stabilities (Ferenczi et al., 2011). In addition to improve the thermal and mechanical stability, inclusion of third agent can also enhance the air and photostability (Jung et al., 2011; Kim et al., 2012). In addition, solvent additives also enhance the device performance. In this context, Peet et al. incorporated a few volume percent of alkanedithiols in the PCPDTBT:PCBM blend which results in an enhanced efficiency from 2.8% to 5.5% through altering the bulk heterojunction morphology (Peet et al., 2007). Moreover, optimization of processing parameters of the photoactive blend such as preparation of solution, formation of thin

film, and post treatment such as thermal annealing can enhance the stability of an OSC (Cheng & Zhan, 2016; Dittmer et al., 2000).

2.4.3.4 Use of Inverted Geometry and Alternative Electrode to Enhance Stability

The normal architecture BHJ OSC generally comprises of a low *WF* Al electrode which is sensitive to oxygen and moisture. As a result it reacts with atmospheric oxygen and water and they further diffuse into the whole device though the top cathode. In order to overcome this issue, inverted geometry has been developed in which position of cathode and anode is interchanged. The inverted device showed much better air stability as compared to the normal architecture OSCs while the efficiencies are still comparable with that of normal architecture (Dey et al., 2011; Lan et al., 2014; Lee et al., 2015; Nam et al., 2015; Şahin et al., 2005).

As discussed earlier, Al is susceptible to oxygen and water, therefore, silver has been widely used as an alternative anode material. As a noble metal, silver is more stable than Al upon exposure to ambient atmosphere (Tavakkoli et al., 2011). Recently, H.R. Yeom et al. employed silver and gold top electrode in PTB7:$PC_{71}BM$ based inverted OSCs and the resultant devices exhibited high stability and photovoltaic performance (Yeom et al., 2015). Sio et al. in their recent work employed MoO_3/Ag anode in P3HT:PCBM based inverted device that led to enhanced stability (Sio et al., 2012).

In order to achieve high stability and efficiency in BHJ OSCs, an in depth knowledge of degradation mechanism in OSCs is essential. Moreover, aforementioned strategies must be adopted in order to mitigate the degradation factors and ensure the higher operational stability of the solar cells.

2.5 Conclusions

OSCs employing BHJ structure have attracted extensive attractions in recent years. Tremendous research is focused to increase the device performance in terms of efficiency, stability and production cost. Under optimized conditions device efficiency of above 10% and several thousand hours of life time has already been reported. In this review chapter, fundamental aspects of BHJ OSCs ranging from design properties to device physics, performance characteristics, stability/degradation mechanisms and strategies to improve device performance, have been discussed.

The improvement in the device performance can be attributed to the development of new organic semiconductor materials specifically synthesized to use in OSCs. Moreover, it is also attributed to the development of optimized device physics framework that enables the rational approach to the design of OSC structure including photoactive and transport layers, electrodes, interfaces and choice of suitable material for every layer and interface. The multistep process from light absorption to the charge extraction has been understood largely, and factors affecting this whole process are briefly discussed. Further, the origin of performance characteristics of a BHJ OSC such as V_{oc}, J_{sc}, *FF* and *EQE* etc. has been highlighted.

The intrinsic and extrinsic degradation effects that arise either from material's properties such as migration of constituent materials at interfaces of OSCs or extrinsic factors such as molecular oxygen and water ingress, heat, light irradiation and mechanical stress have been summarized. Most of the factors are thermodynamic, oxidative, photochemical, morphological and mechanical modes of degradation. Furthermore, this review chapter highlights the strategies to improve the device performance in terms of improving the stability while mitigating the device degradation factors.

CHAPTER 3: LAYER BY LAYER CHARACTERISATION OF DEGRADATION PROCESS IN PCDTBT:$PC_{71}BM$ BASED NORMAL ARCHITECTURE POLYMER SOLAR CELLS[2]

3.1 Overview

This work demonstrates the stability and degradation of OSCs based on PCDTBT:$PC_{71}BM$ photoactive blend layers as a function of ageing time in air. Analysis of the stability and degradation process for the OSCs was conducted under ambient air by using current-voltage (*I-V*) measurements and x-ray photoelectron spectroscopy (XPS). The interface between photoactive layer and HTL (PEDOT:PSS) was also investigated. Device stability was investigated by calculating decay in PCE as a function of ageing time in the air. The PCE of devices decrease from 5.17 to 3.61% in one week of fabrication, which is attributed to indium and oxygen migration into the PEDOT:PSS and PCDTBT:$PC_{71}BM$ layer. Further, after aging for 1000 h, XPS spectra confirm the significant diffusion of oxygen into the HTL and photoactive layer which increased from 3.0 and 23.3 % to 20.4 and 35.7 % in photoactive layer and HTL, respectively. Similarly, the indium content reached to 17.9 % on PEDOT:PSS surface and 0.4 % on PCDTBT:$PC_{71}BM$ surface in 1000 h. Core-level spectra of active layer indicate the oxidation of carbon atoms in the fullerene cage, oxidation of nitrogen present in the polymer matrix and formation of In_2O_3 due to indium diffusion. A steady fall in the optical absorption of the active layer during ageing in ambient air has been observed and it reduced to 76.5% of initial value in 1000 h. On the basis of these

[2] **The work presented in Chapter 3 has been published in Elsevier: "Organic Electronics (Rank: Q1, Impact Factor: 3.47)" as**

Rafique et al. (2017). Layer by layer characterization of the degradation process in PCDTBT:$PC_{71}BM$ based normal architecture polymer solar cells. *Organic Electronics, 40*, 65-74.

experimental results, key parameters that account for the degradation process and stability of OSCs in order to improve the device performance are discussed.

3.2 Introduction

Solar energy harvesting has become one of the major areas of research for the current and upcoming technologies. In this context, polymer-based OSCs have drawn special interest due to their tunable properties, low manufacturing cost, roll to roll production compatibility, solution processed and light weight (Chen et al., 2013; Sun et al., 2010; Synooka et al., 2014). To date, the progress in the OSCs development has been intensified and power PCEs of more than 10% have been successfully demonstrated (Li et al., 2012; Trost et al., 2015). In order to bring the OSCs into the market with full success, along with the high efficiencies and low manufacturing cost, longer devices lifetime is much needed (Ecker et al., 2011).

Basically, the polymer solar cells employ BHJ of blended donor and acceptor components as a photoactive layer which is sandwiched between two electrodes. In order to enhance the functionality of these devices often interfacial layers namely HTL and ETL are introduced at the interface between the photoactive layer and electrodes (Duan et al.,2013; Po et al., 2011). However, a short lifetime of the OSCs is observed to be one of the stability constraints since there is always a presence of degradation process throughout the device. The unique degradation mechanisms affecting the photoactive layer, interfacial layers and the electrodes is rather a complex phenomenon and are not yet fully understood. These multilayers and interfaces of metal/organic, organic/organic materials significantly influence the overall performance (Bao et al., 2014). Recent reports on the lifetime stability of OSCs highlighted two major problems regarding the device stability. Firstly, the extrinsic stability which requires proper encapsulation of devices to prevent the environmentally induced degradation mainly

caused by oxygen and moisture present in the air (Ecker et al., 2011; Udum et al., 2014). Secondly, the intrinsic stability which is related to the materials and interfaces present in the OSCs (Jørgensen et al., 2008; Zeng et al., 2015). Device instability comprises a range of complex phenomenon simultaneously in play of which presumably not all have been identified. Some of them are interrelated and occur at the same time such as diffusion of oxygen from atmosphere, and migration of indium into the HTL and active layer due to ITO corrosion caused by acidic nature of PEDOT:PSS (Jørgensen et al., 2012). All these factors prove to be a bottleneck in device performance and hence, better understanding of these constraints is needed.

A variety of different techniques and approaches have been employed in recent years to investigate the degradation mechanisms leading to device failure (Katz et al., 2006; Reese et al., 2010; Schafferhans et al., 2010; Seemann et al., 2009). Analytical techniques such as time of flight - secondary ion mass spectroscopy (TOF-SIMS) and XPS have been employed by many groups to study the degradation effects, in particular, the chemical changes in OSCs with time (Kettle et al., 2015). However, TOF-SIMS is only semi-quantitative in certain situations, so XPS being a quantitative characterization technique, is expected to give better overview of compositional changes caused by device degradation (Norrman et al., 2010). Hintz et al. by the XPS analysis of exposed poly (3-hexylthiophene) (P3HT) active layer to oxygen, showed that both photo-oxidized and physisorbed oxygen is present, which are one of the root causes of degradation (Hintz et al., 2010). Norrman et al. studied the degradation in P3HT:$PC_{61}BM$ photoactive layer due to water and oxygen, and showed by the XPS analysis that the chemical changes taking place at the interface of active layer and HTL are the major cause of instability (Norrman et al., 2010). Similarly, Seo et al. deduced by XPS the partial oxidation of P3HT and configuration of sulfoxide (R-SO-R) on the sulphur atom of thiophene ring after longer degradation hours (Seo et al., 2014).

However, most of works have focused on P3HT degradation studies but it lacks the broad absorption profile necessary to cover large proportion of solar spectrum (Peet et al., 2007), therefore new materials such as PCPDTBT and PCDTBT etc. have been studied (Kettle et al., 2015; Wang et al., 2012). Several groups recently confirmed the high efficiency and photo-current generation in PCDTBT based solar cells because of its faster charge carrier generation capability and different recombination dynamics as compared to P3HT (Banerji et al., 2010; Etzold et al., 2011; Wang et al., 2012).

In this work, the stability and degradation effects related to oxygen and indium diffusion in the PCDTBT:$PC_{71}BM$ based BHJ OSCs with PEDOT:PSS HTL by using photovoltaic characterizations and XPS, respectively, were investigated. Fabrication was carried out by easy, solution processed spin coating technique and devices were aged in ambient atmosphere for degradation analysis. Chemical, optical, compositional and morphological properties were characterized and their effects on the photovoltaic performance as well as long-term stability were studied. Based on the experiments, key physical parameters that account for the OSC degradation process such as indium and oxygen diffusion which consequently result in rapid device failure can be identified. Hence, this study leads to better understanding of degradation processes which occur in BHJ OSCs during their fabrication and ageing phase.

3.3 Materials and Methods

3.3.1 Materials

PEDOT:PSS solution (PH1000) has been purchased from H.C. Starck and used as received. Both PCDTBT and $PC_{71}BM$ were purchased from Lumtec, Taiwan. ITO-coated pre-patterned glass substrates with a sheet resistance of 15 Ω per square were purchased from Ossila, UK. All other necessary chemicals such as HPLC chloroform etc. were purchased commercially and used as received without further purification.

3.3.2 Device Fabrication

The reported OSCs were fabricated on 1.5 × 2.0 cm pre-patterned ITO coated glass substrates, with six active pixels on each substrate and an active area of 30 × 1.5 mm (4.5 mm^2) for every pixel. The impurities were removed from ITO substrates through sequential cleaning. Substrates were first cleaned with soap, ultrasonication in acetone, isopropanol, and deionized water for 15 min each, and subsequently dried under a nitrogen stream. Thereafter, PCDTBT:$PC_{71}BM$ photoactive blend was first dissolved in chloroform at the concentration of 10mg/ml for each and then mixed at a volumetric ratio of 1:4 by vigorous stirring overnight. Next, PEDOT:PSS aqueous solution was filtered using 0.45 µm PTFE filter (Whatman, Germany) and spun coated onto the substrates at 4000 rpm for 60 s and annealed at 120°C for 30 minutes in air to obtain HTL with desired thickness of 40 nm. Thereafter, PCDTBT:$PC_{71}BM$ blend solution was filtered using 0.25 µm PTFE filter (Whatman, Germany) and spun coated on top of the HTL at 2000 rpm in a glove box for 20 s to obtain ~70nm active layer. Al cathodes with 100 nm thickness were thermally evaporated onto the photoactive layer through shadow masks under vacuum (10^{-6} Torr). Finally, the OSCs were encapsulated with a glass of exactly same dimensions as an active area for characterization in the air with a UV-curable epoxy. In order to study the ageing in the air, the HTL and photoactive layers were replicated on ITO coated glass substrates using spin coating with the same fabrication procedure.

3.3.3 Microscopic and Spectroscopic Analysis

Morphological characterizations were carried out by atomic force microscopy (AFM) model SPM PROBE VT AFM XA 50/500 Omicron, Germany, and field emission scanning electron microscopy (FESEM), JEOL JSM-7600F, Japan. XPS data were analyzed to quantify the migration of degradation elements into the HTL and photoactive layer as a function of ageing in the air by using PHI 5000 Versa Probe

Scanning ESCA Microprobe (PHI 5000 Versa Probe II, USA), equipped with monochromatic Al-Kα (hν = 1486.6 eV) X-ray source. The XPS curve fittings for core level spectra were drawn using Multipack software (VERSION 9, ULVAC-PHI, Inc. Japan) which allows the deconvolution of each spectrum into the individual fitting of mixed Gaussian-Lorentzian components. The optical absorption spectra of the samples were recorded by Perkin Elmer Lambda 750 UV/Vis/NIR spectrophotometer, USA over the range of 300-800 nm.

3.3.4 Device Parameters

The current-voltage (I–V) characteristics of the OSCs were measured using Keithley 236 Source Measure Unit (SMU) at room temperature. Solar cell performance was tested by using an air mass 1.5 Global (AM 1.5 G) solar simulator with an irradiation intensity of 100 mW/cm^2 illuminated from the ITO side. The light intensity calibration was performed with a Newport power meter 1918-R with calibrated Si-detector 818-UV.

3.4 Results

This work is mainly focused on the device operational stability and degradation factors which cause the instability in the device performance. Current density- voltage (*I-V*) characteristics of the devices were measured under illumination and in dark, and data were collected over a period of seven days to record the decrease in the PCEs as a function of exposure time to ambient air. Further, to understand the degradation process via chemical changes in the OSCs and the role that ambient atmosphere and indium diffusion played in the degradation process, XPS survey and core-level spectra for freshly prepared samples and after 1000 h of ageing in ambient air have been obtained. In addition, the fall in optical properties of the PCDTBT:$PC_{71}BM$ layer due to ageing in ambient air have also been studied. Moreover, the change in the morphology of the Al

electrode after exposing to the ambient air for 1000 h has been characterized. The schematic representation of the current work is shown in Figure 3.1.

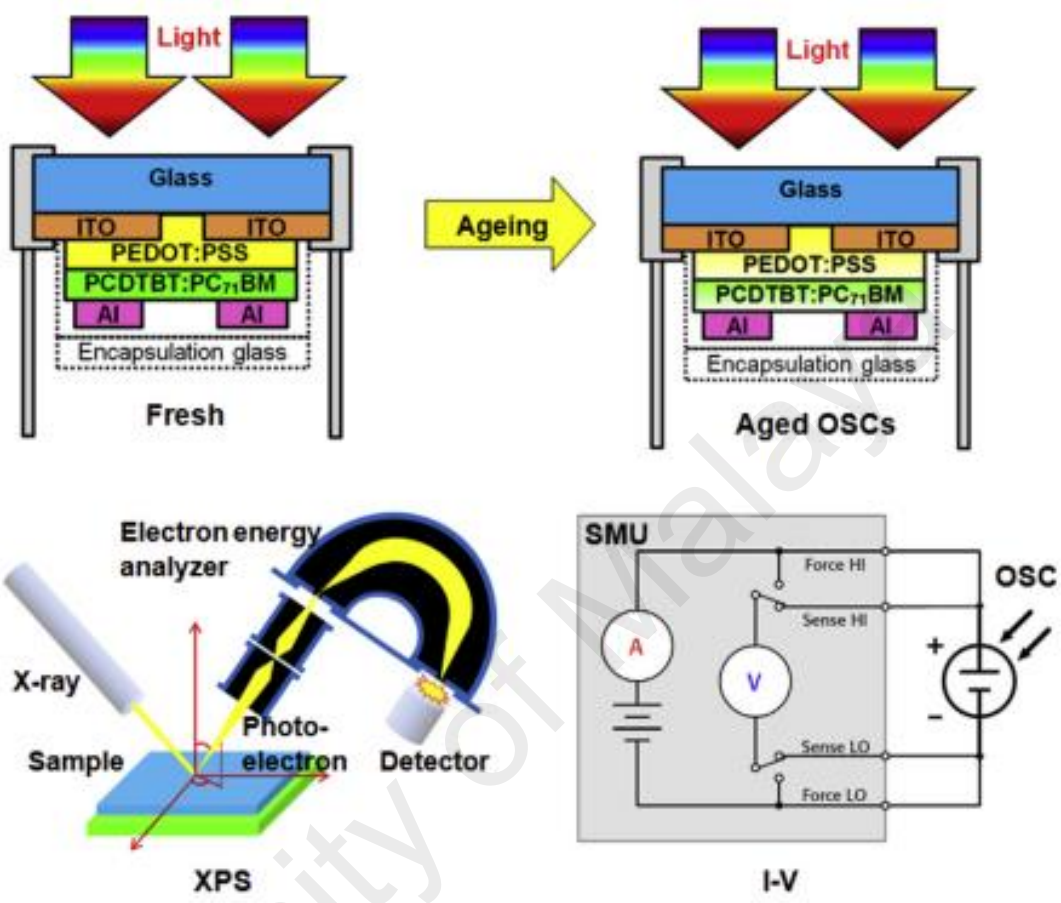

Figure 3.1: Schematic showing the OSCs characterized by XPS and *I-V* measurement in fresh and aged conditions.

3.4.1 Photovoltaic Characterizations

The OSCs lifetime stability was investigated by calculating the decay in PCE as a function of ageing time in air (Kim et al., 2014). I-V characteristics were measured under standard conditions of an encapsulated device over the period of one week. The *I-V* characteristics of the solar cells at 100 mW/cm^2 are shown in Figure 3.2 (a, b) and Table 3.1.

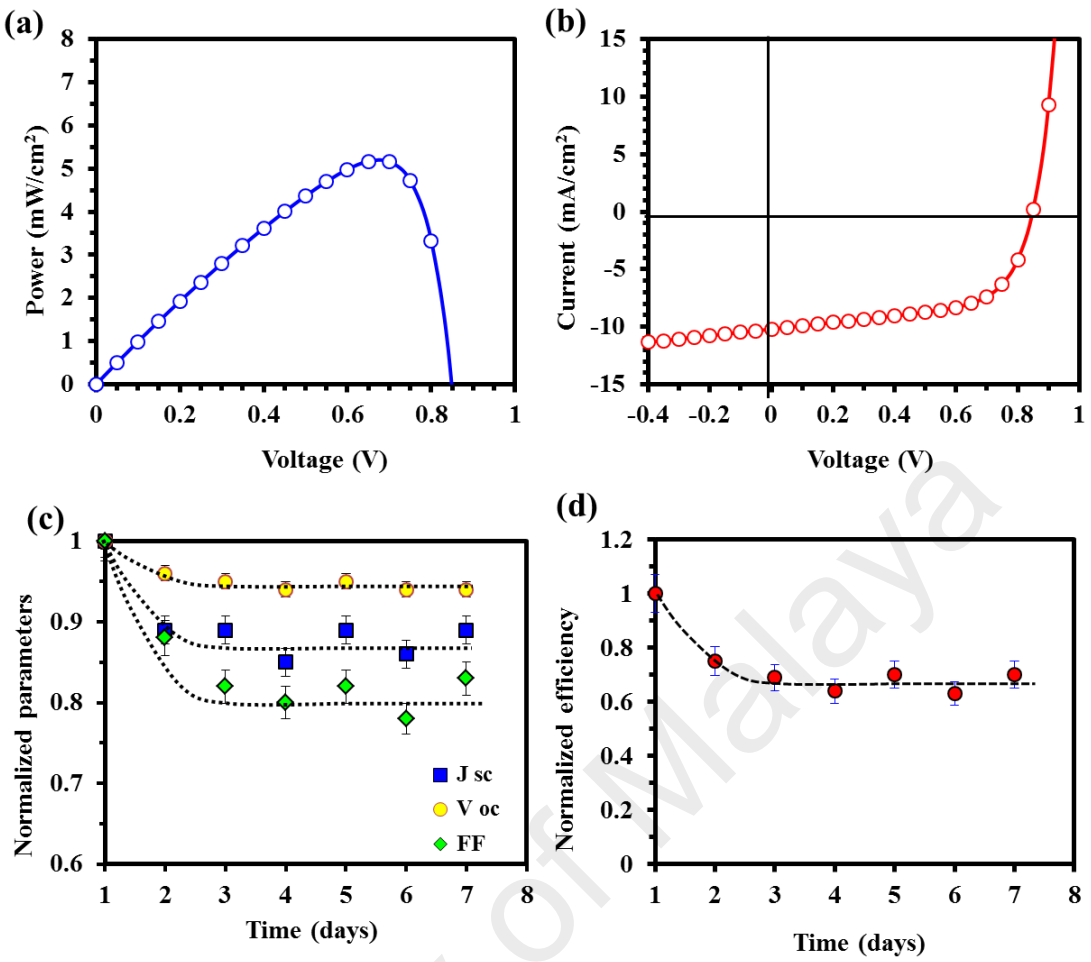

Figure 3.2: The curves show (a) output power (*P*) vs. voltage (*V*), (b) *I V* characteristic for fresh device, the variation in (c) J_{sc}, V_{oc}, *FF* and (d) *PCE* (%) normalized to their initial values for seven days.

From the comparison between the initial and final measurements, it can be observed that a considerable decrease in the solar cell performance occurred due to ageing in air. The cells initially demonstrated a reasonable PCE of 5.17% with a (*Voc)* of 0.84 V, (J_{sc}) of 10.2 mA/cm^{-2} and (*FF)* of 60.3%. The PCE reduced to 3.61% with *Voc* as 0.79 V, *Jsc* as 9.2 mA/cm^{-2} and *FF* as 49.8% over a period of one week. All the photovoltaic parameters for an entire week are presented in the Table 3.1. From the normalised parameters presented in Figure 3.2(c, d), the PCE of the solar cells rapidly reduced initially to 70% of its initial value within first three days of ageing. The devices observed to be relatively stable during the remaining period of time. There were no

significant decay recorded in (V_{oc}) values while (J_{sc}) and *(FF*) reduced to about 87% and 80% of their initial values respectively.

Table 3.1: Photovoltaic performance parameters for the solar cell devices calculated prior to the device degradation tests and subsequent 7 days. Devices were measured by global (AM 1.5 G) solar simulator.

Ageing time (Days)	***Jsc (mA/cm^{-2})***	***Voc (V)***	***FF (%)***	***PCE (%)***
1	10.2	0.84	60.3	5.16
2	9.08	0.81	52.8	3.87
3	9.07	0.80	49.2	3.56
4	8.67	0.79	48.0	3.30
5	9.07	0.79	49.2	3.61
6	8.77	0.79	46.8	3.26
7	9.08	0.79	49.8	3.61

For an OSC device, the degradation phenomenon rely on both bulk and interface phenomena, and involves degradation of the interfaces, degradation of active layer, interfacial layers and electrode degradation, morphological, optical and macroscopic changes such as formation of particles, bubbles, diffusion of water from atmosphere, corrosion and diffusion of ITO, delamination and initiation of cracks and voids etc. (Norrman et al., 2010). All these factors make this process a complex set of phenomena and it is thus a challenging job to identify some or all of them. It becomes even more difficult to quantify each of these degradation factors to what extent each of them contributes in the overall deterioration of the OSCs. In this work, a more detailed understanding of these degradation factors which cause the instability in the device photovoltaic performance have been sought and investigated every layer of the normal architecture cell structure. Although, the device stability data for up to 7 days (140

hours) of fabrication has been presented in Figure 3.2 and Table 3.1, the degradation study was prolonged to 1000 hours in order to develop a deeper understanding of degradation factors affecting the device performance at every layer level.

3.4.2 XPS Analysis of HTL and Photoactive Layer with Aging

To explore the effect of ambient atmosphere exposure on the chemical changes in PCDTBT:$PC_{71}BM$ active layer and PEDOT:PSS HTL, XPS measurements on PCDTBT:$PC_{71}BM$ and PEDOT:PSS thin films are carried out. Figure 3.3 shows the representative survey spectra for both layers ranging from 0 to 800 eV. Data were recorded before and after ageing of samples.

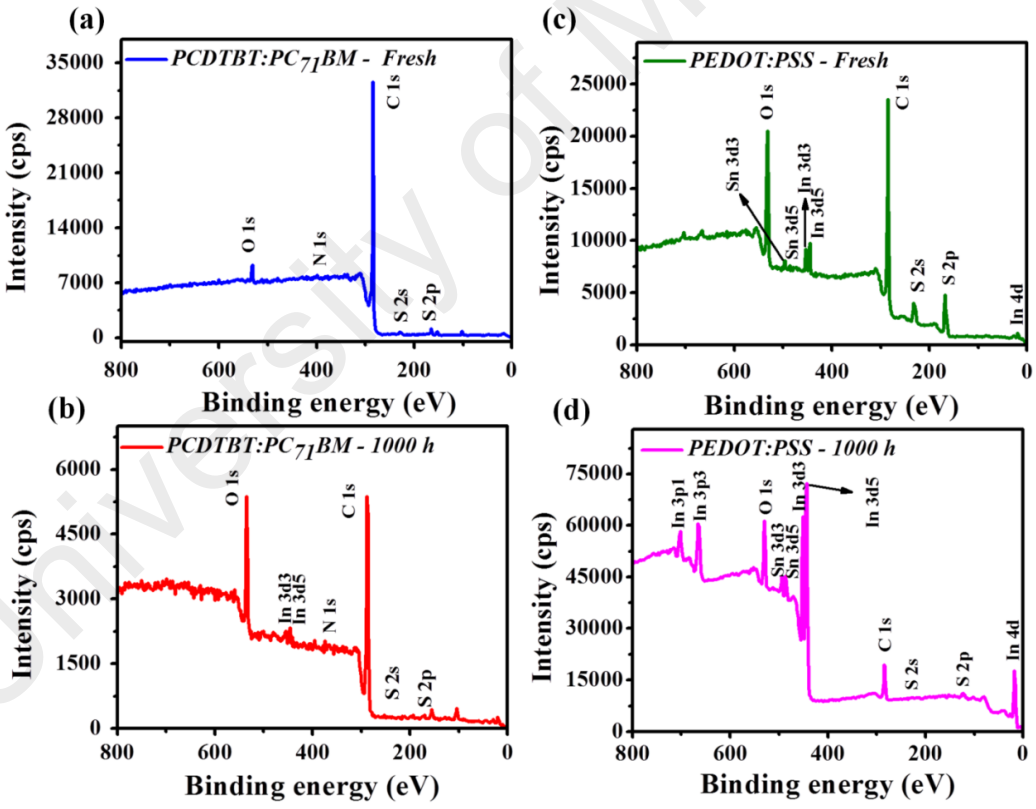

Figure 3.3: Survey spectra for (a, b) PCDTBT:$PC_{71}BM$ and (c, d) PEDOT:PSS films recorded for fresh sample and after 1000 h of aging in ambient atmosphere.

3.4.2.1 Change in Elemental Concentration of HTL with Ageing

Figure 3.4(a) shows the elemental concentration of PEDOT:PSS films for freshly prepared, 250 and 1000 h ageing, whereas the data are obtained for Figure 3.4 from XPS survey spectra of PEDOT:PSS presented in the Figure 3.3. Around 1.1% concentration of indium in freshly prepared PEDOT:PSS films was detected, whereas, the tin concentration was almost negligible (<0.1%) until 250 h of ageing. Indium and tin concentration reached to 17.9 and 2.1 % in 1000 h of ageing, respectively. There was no significant increase recorded in oxygen content in first 250 h which on further ageing of the device for 1000 h in air reached from 23.3 (freshly prepared) to 35.7 %. Sulphur content was also reduced from 7.2% in the fresh sample to 0.7% in 1000 h aged sample. Like oxygen, there was no significant change detected in sulphur content in first 250 h. According to Kettle et, al. in their study on chemical changes of active layer, substantial decrease in the sulphur concentration between 250 and 1000 h is equated with an increase in oxygen content in the similar time span (Kettle et al., 2015). Relatively stable concentration of oxygen in first 250 h is attributed to the fact that PEDOT:PSS initially have the tendency to both gain and loose oxygen; and initially, until 250 h , oxygen loss offsets the oxygen gain and later oxygen gain observed to be the dominant process (Norrman et al., 2010).

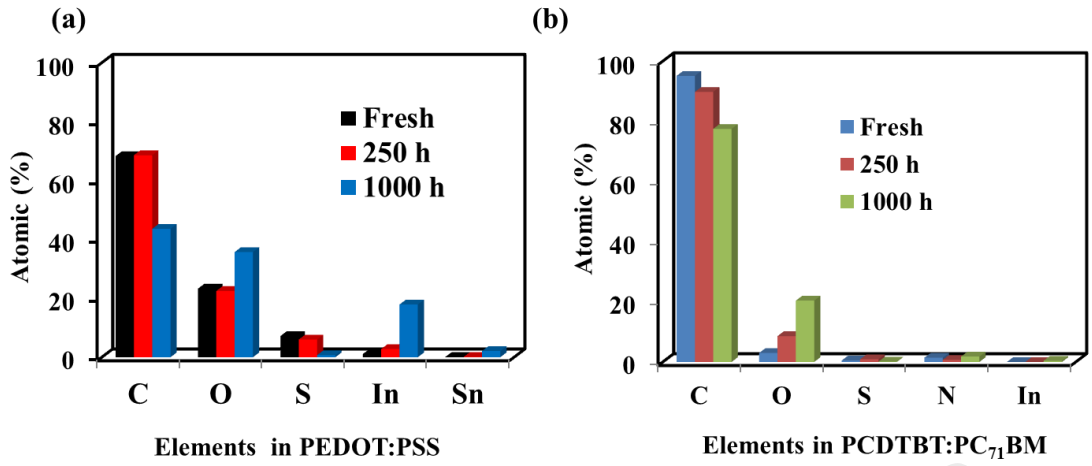

Figure 3.4: Data acquired from XPS survey spectra of (a) PEDOT:PSS and (b) PCDTBT:$PC_{71}BM$ films, presented in Figure 3.3 as a function of ageing time, with a graph showing atomic concentration (%) of each element in PEDOT:PSS and PCDTBT:$PC_{71}BM$ layer.

3.4.2.2 Change in Elemental Concentration of Photoactive Layer with Ageing

PCDTBT:$PC_{71}BM$ samples were replicated as described and characterised by XPS to analyze the relative changes in the surface composition which occurred during ageing in ambient atmosphere for 1000 h. Figure 3.4(b) show the relative atomic concentration (%) for each element of PCDTBT:$PC_{71}BM$ films at 0, 250 and 1000 h. Representative survey spectra for freshly prepared and 1000 h aged samples is shown in Figure 3.3(a and b). It is clear that oxygen content has remarkably increased from 3% in the fresh sample to 20.4 % in 1000 h sample. Contrary to PEDOT:PSS films where no significant increase recorded in oxygen content during initial 250 h, in PCDTBT:$PC_{71}BM$ active layer, there was a steady increase in the oxygen content throughout the ageing period. Moreover, the carbon content was reduced from 95.1 to 77.5% after ageing. Sulphur reduced to negligible level (<0.1%) after ageing while nitrogen concentration remained almost stable with relatively higher concentration (2.2%) at 100 h of ageing. Initially, no traces of indium at the surface of photoactive layer until 250 h were found, later; it reached to 0.4 % in 1000 h. However, it should be

noticed that XPS with the probe depth of 5 to 10 nm does not represent the bulk properties and represents only the surface composition. Therefore, it might be possible that indium had already diffused from ITO surface into the PEDOT:PSS and further into the photoactive layer but reached to the surface after 1000 h.

3.4.2.3 PCDTBT:$PC_{71}BM$ Chemical Changes

To ascertain the chemical changes occurred in the PCDTBT:$PC_{71}BM$ films due to oxygen and indium diffusion, high resolution spectra for each element were recorded. XPS C 1s and O 1s core-level spectra of PCDTBT:$PC_{71}BM$ films show new features and broadening of both spectra after ageing as shown in Figure 3.5. The peaks in the C 1s spectra after ageing show an insignificant shift towards higher binding energies. In C 1s spectra for fresh and aged samples the components at 284.47 and 284.57 eV respectively, are ascribed to C-C bond and the peak shape represents typical of partially-ordered graphite-like materials (Kettle et al., 2015) (Ganguly et al., 2011; Mattevi et al., 2009). The high energy values at 286.76 and 286.84 eV of fresh and aged samples respectively, best match with the carbon singly or doubly bonded to oxygen *i.e.* O-C=O or C-O-C bond (epoxide group) (Bhushan, 2012; Daems et al., 2014; Kumar, et al., 2013). Whereas, the peak present in the fresh sample at 289.49 eV is corresponding to COO- bond (carboxyl groups) as shown in Figure 3.5(a) (Jeong et al., 2008; Mattevi et al., 2009). The intensity of the peaks had significantly reduced after ageing as shown in the C 1s spectra in Figure 3.5(b) which is also evident in the survey spectra and indicates the reduction in carbon content in the polymer matrix. The peak broadening in the aged spectra indicates the significant increase of oxygenated carbon present in the polymer, suggesting that C-O and C=O oxidation of the carbon atoms in the fullerene might occur which cannot be distinguished due to the broadening of peaks (Kettle et al., 2015). These oxidized species might cause severe degradation issues and OSCs performance could significantly decrease.

The deconvulated O 1s spectra before and after ageing are shown in Figure 3.5. The components at 531.37 and 531.96 eV of the fresh and aged sample ascribe to oxygen atoms bonded with carbon atoms in functions such as ketone (C-O-C) and carboxylic acid (COOH and/or -OC-O-CO) (Yusoff et al., 2014). The peak at 533.30 eV in the fresh sample is attributed to the C-O bond which implies that oxygen atoms are directly bonded to carbon atoms in the polymer backbone (Mittal, 2004; Rosenthal et al., 2010; Schweiger et al., 2015), in sound agreement with the literature values (Kettle et al., 2015). Generally, the O species having binding energies between 531-533 eV are likely attributed to C-O or C=O species (Guo et al., 2013). In the aged sample, the peak at 533.30 eV disappeared and a new peak at 529 eV emerged which corresponds to C=O bond (Sabu et al.,2012).

The N 1s spectra for fresh and aged sample in Figure 3.5 showed a sharp and defined peak at ~ 402 eV which correspond to N-O formation (Kettle et al., 2015). This indicates the oxidation of nitrogen present in the polymer matrix. Another shoulder peak at 402.31eV in fresh sample may also correspond to N-O surface species or an N atom bonded to another N atom (Fuge et al., 2003; Miller et al., 2002). A new peak emerged at 398.29 eV after ageing of sample is attributed to C-N or C=N bond (Dementjev et al., 2000; Guo et al., 2013). The shakeup structures in both fresh and aged samples are emerging at 404.51 and 405.31eV respectively and correspond to some form of oxidized nitrogen species (Fechler et al., 2013; Feng, 2015; Gao, 2015; Radovic, 2004).

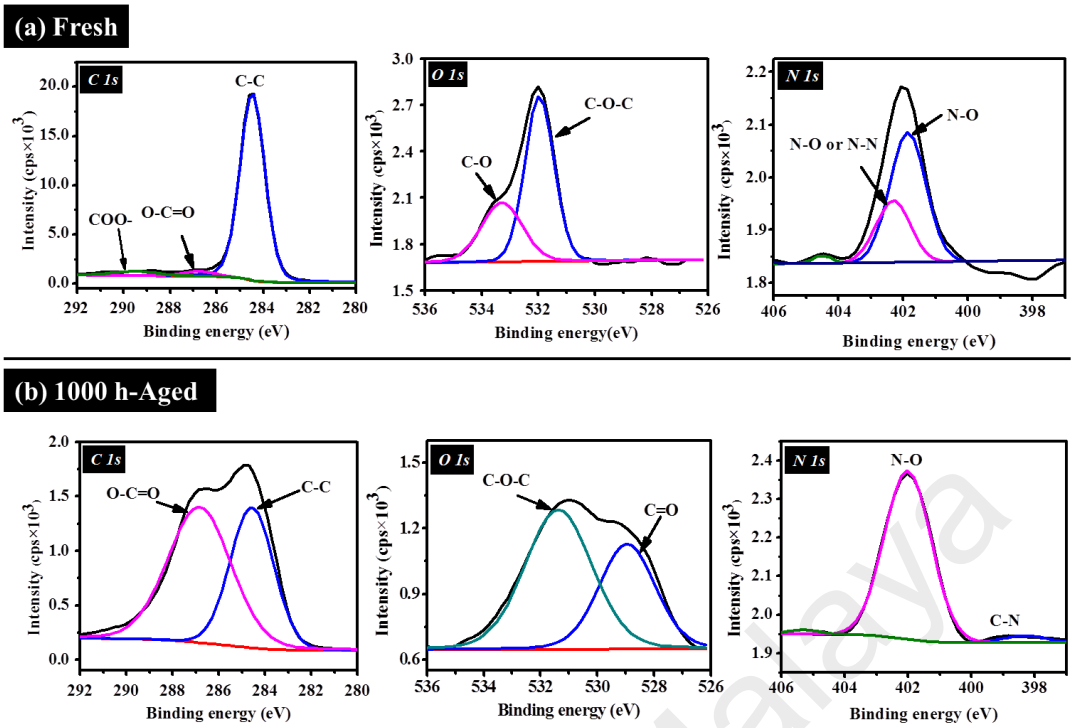

Figure 3.5: High resolution XPS C 1s, O 1s and N 1s spectra of PCDTBT:$PC_{71}BM$ films for (a) as prepared and after (b) 1000 h of ageing.

Due to the negligible level of sulphur content (< 0.1%) in the aged sample, the curve fitting for sulphur is not shown in Figure 3.6. The S content was observed from S 2p peaks in the fresh sample and it shows two 2p doublets. The peak at 163.65 eV corresponds to carbon bonded sulphur (Kettle et al., 2015), is most likely due to presence of little amount of sulphur in the sample due its existence in the PCDTBT polymer (Yusoff et al., 2014). Moreover, contributions from aromatic carbon-sulphur motifs of the PCDTBT molecule structure in the form of C=S bond or thiophenic sulphur species is found at 165.02 eV (Fechler et al., 2013). Figure 3.6(b) shows the core level spectra for indium present in photoactive blend after 1000 h of ageing. Since no indium content was found in the freshly prepared sample, therefore, the core-level spectra for the fresh sample is not included here. The In 3d spectra have two components, the main In $3d_{5/2}$ peak has been found at 444.92 eV and attributed to the characteristic lines of In_2O_3 (Shao et al., 2016; Sharma et al., 2011). A second and

relatively smaller peak was found at 452.63eV which is In $3d_{3/2}$ component of the In 3d spectrum (Kim et al., 2014; Shao et al., 2016).

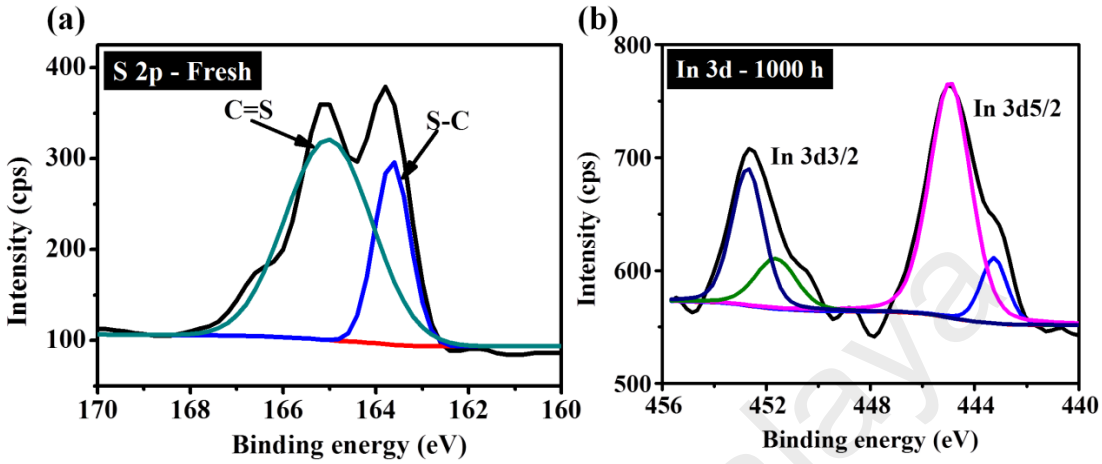

Figure 3.6: High resolution XPS spectra for (a) S 2p fresh and (b) In 3d 1000 h aged sample.

3.4.3 Decay in the Absorption of Photoactive Layer with Ageing

Since the absorption is an important parameter that deals with the overall performance of the photovoltaic devices, it is, therefore, worthy to investigate it in detail. PCDTBT:$PC_{71}BM$ blend degradation was monitored by measuring the evolution of absorption versus exposure time in ambient air as shown in Figure 3.7. As discussed by Tournebize et al. in their study on the photostability of active layer polymer, it is essential to focus on the initial stages of degradation, which have a key impact on the device performance (Tournebize et al., 2015), because initially, a few percent fall in optical absorption of the polymer may lead to a drastic change in the device performance (Tromholt et al., 2012). The normalized decay of absorption for the samples measured at 0, 25, 50, 100 and 1000 h of preparation show a linear decrease in the optical absorption of the polymer. During initial 100 h the absorption fell down to 92.02 % of initial value which continued to decrease until it reached to 76.56 % in 1000

h. The peaks at 377 and 479 nm exhibit slightly more pronounced decrease in the absorption (undesired) of the aged samples which is indicative of the atmospheric induced degradation of the polymer due its exposure to air (Endale et al., 2014).

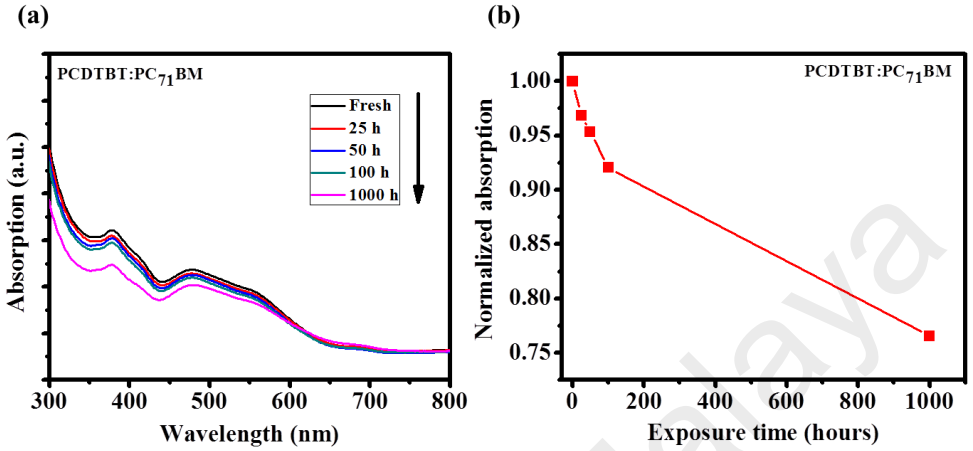

Figure 3.7: (a) Evolution of the PCDTBT:$PC_{71}BM$ absorption (300-800 nm) versus exposure time to ambient air (Fresh - 1000 h), (b) Decay of the normalized PCDTBT:$PC_{71}BM$ absorption upon exposure in ambient atmosphere.

3.4.4 Morphological Analysis of Photo-active Layer

It is evident from the photovoltaic results that a sharp decrease in the device performance occurred within the first 72 h of device ageing, in this context; apart from other factors the morphology of the photo-active blend layer has a crucial influence on the device performance. Thus, AFM and SEM analysis of PCDTBT:$PC_{71}BM$ photo-active layer were performed for freshly prepared and 72 h aged samples. AFM images in Figure 3.8 show the evolution of surface morphology with aging, both freshly prepared (Figure 3.8b) and 72 h (Figure 3.8d) aged samples revealed quite smooth surface with almost similar morphological features, however, the root mean square roughness (RMS) value, in an area of 1 µm × 1 µm, for the aged films (1.86 nm) is much greater than that of freshly prepared (1.07 nm) sample. The SEM images also present a flat sheet of polymer with morphology features very similar to that observed

in AFM images. Some impurities or probably some clusters of the organic material were found on the surface (i.e. encircled in the Figure 3.8c) of 72 h aged sample which likely occurred due to aggregation of organic constituents of photo-active layer with the ageing, in good agreement with previously reported data (Seck et al., 2015).

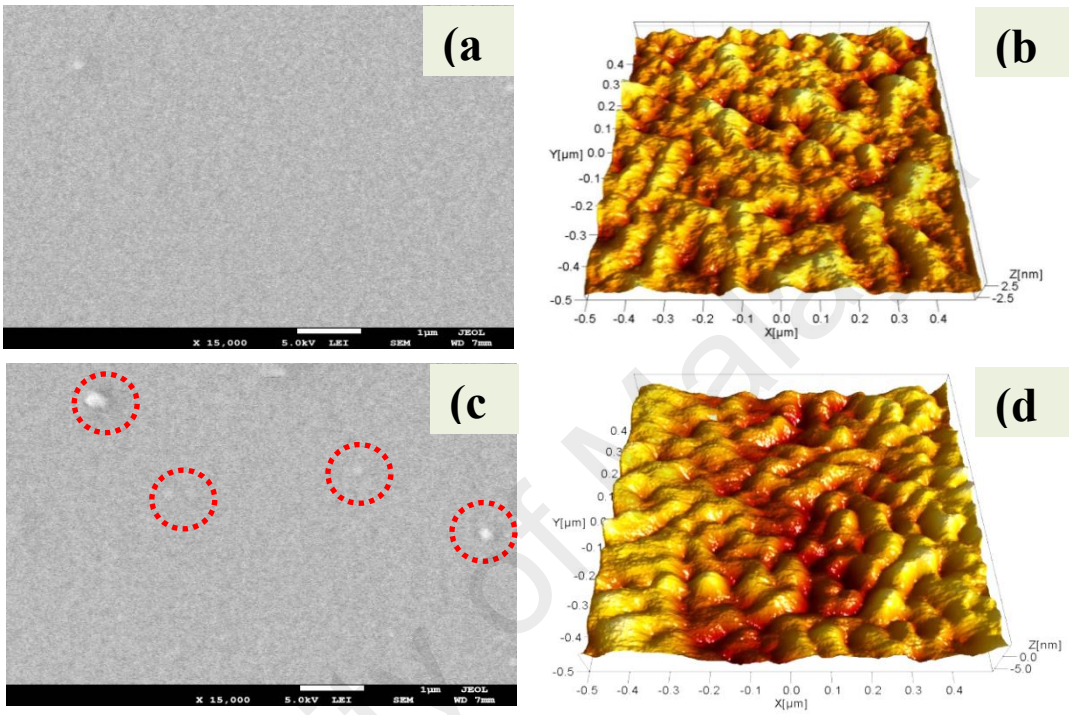

Figure 3.8: SEM and AFM images of PCDTBT:$PC_{71}BM$ films (a, b) Fresh and (c, d) after 72 h of ageing at ambient atmospheric conditions.

3.4.5 SEM Analysis of Aluminium Electrode Degradation

Effect of Al cathode exposure to the high humidity air has also been characterized. The devices were exposed to ambient air in order to observe the possible damage due to water ingress. SEM results exhibit severe damage of Al electrodes caused by moisture and oxygen. SEM images of the freshly deposited Al electrode in Figure 3.9 (a, b) exhibit a void-free surface without much height deviation. Moreover, SEM images in both fresh and aged sample show grain surface texture consisting of small Al grains. Although the grains are densely packed, however, no definite order

among them is visible, in good agreement with previously reported results (Kaune et al., 2011). Whereas, in the aged samples (Figure 3.9 (c, d)) micron sized voids and bubble-like protrusions appeared which are similar to the previously reported ageing effects (Glen et al., 2015).

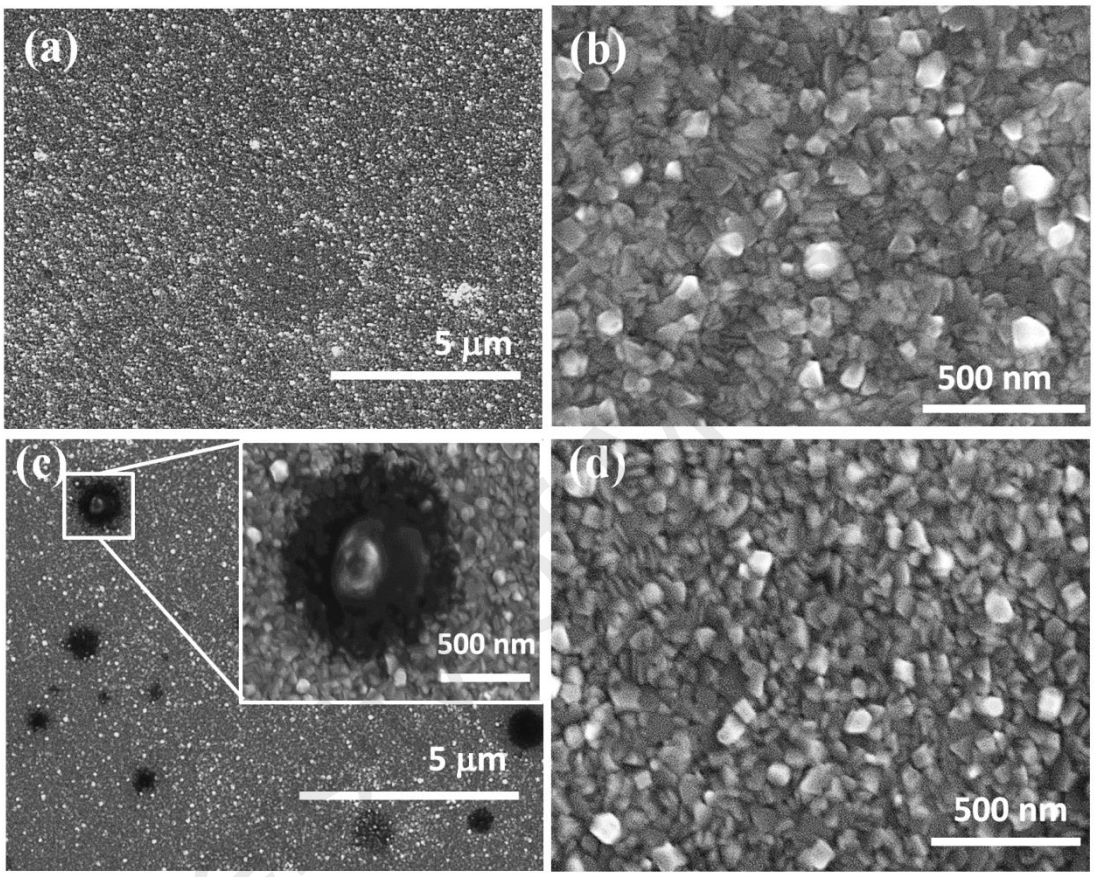

Figure 3.9: FESEM images of Al electrodes for (a, b) as deposited samples and (c, d) after exposing to the ambient atmosphere for 1000 h.

3.5 Discussion

From the XPS and photovoltaic results, it is believed that the OSCs in ambient air exhibit significant instability due to indium and oxygen diffusion into the HTL as well as the photoactive layer. The devices and films were tested under prolonged exposure to ambient air. It is evident from the photovoltaic results that the device initially showed rapid decay in efficiency, however, relatively stable performance of the

device after 72 h and until 1000 h is attributed to the proper encapsulation of the devices which overcomes the device degradation and limits the hazardous effect of ambient air on the device performance but it is expected to die within very short time of fabrication in case of an un-encapsulated device (Stratakis et al., 2014). The sharp decay in the device photovoltaic performance within 24 hours is mainly attributed to the instability of the interface between ITO and PEDOT:PSS. Initially the degradation is predominately due to indium diffusion which immediately started after spin coating of PEDOT:PSS HTL and 1.1% concentration of indium on the surface of freshly prepared PEDOT:PSS films has been detected. PEDOT:PSS etches indium out of ITO which leads to the incorporation of indium in the photoactive layer. The diffusion of indium into the active layer could result in quenching of excitons and accelerates the charge recombination rate due to its ability to act as the charge trapping center (Chen et al., 2013; Warren et al., 1992). This would result in the decay of J_{sc} and *FF* of the device and, therefore, decrease the lifetime stability of the device. Moreover, as the time passes, the efficiencies keep on deteriorating, where after just three days of fabrication the PCE of the device plunges to around 70 % from its initial efficiency, shown in Figure 3.2(d). The decay in the efficiency is mainly attributed to the significant (about 20%) decrease in the *FF* and around 10% decrease in the J_{sc}, however, the V_{oc} of the OSCs remained almost stable with only 5% reduction in its initial value as shown in Figure 3.2(c). In addition, formation of In_2O_3 and presence of oxygenated species caused by oxygen diffusion have been observed to restrict the overall device performance. Interestingly, during the XPS analysis of exposed films of HTL, it was observed that initially the dominating degradation factor is the diffusion of indium which started immediately after the spin coating of PEDOT:PSS HTL. Chang & Chen in their recent investigation on the PEDOT:PSS and ITO interaction, showed that dissolution of indium in PEDOT:PSS aqueous solution also decrease the work function

(Chang & Chen, 2007). This would lead a device to degradation even after encapsulation, predominately in the *FF* and J_{sc} as observed in our work. In case of longer hours of exposure to air, oxygen is also in play along with indium diffusion into the HTL which would also accelerate the indium diffusion (Kawano et al., 2006).

Contrary to HTL, degradation process in PCDTBT:$PC_{71}BM$ photoactive layer was predominately due to oxygen diffusion (Figure 3. 4) which continuously increased in 1000 h. Oxygen can be absorbed from the atmosphere into the active layer through the Al electrodes. Al easily gets oxidize which cause voids and pinholes in case of longer exposure to moisture. These voids facilitate the diffusion of moisture into the underneath layers (Kawano et al., 2006; Seeland et al., 2011) , and this whole oxidation process consequently increases the series resistance (R_s). In addition, areas which are affected by these voids due to deterioration of Al are unlikely to have any contribution towards a working device. Since the photo-active layer and Al electrode will lose contacts in the region under voids, therefore, any free charge carriers generated in this region will be likely to recombine rather than being extracted by the electrode. Hence, Al-active layer interface will act as a charge blocking layer and grow as a function of exposure time to air. This phenomenon significantly accounts in total efficiency loss with time (Glen et al., 2015).

Although, there was no significant change recorded in the morphology of fresh and 72 h aged samples except for the increase in the surface roughness, however, it is vital to record the initial changes in the morphology of the blend film due to ageing because a small deterioration of the morphology could have a drastic effect on the device performance (Tournebize et al., 2015; Tromholt et al., 2012). However, in this work, it is believed that root cause of device degradation is the diffusion of indium into the photoactive layer and the increase in the surface roughness is likely to add in the

overall device degradation as smooth and homogeneous surface is highly desired for an optimum device performance.

The decay in the optical properties of the active layer blend is likely ascribed to deterioration of polymer morphology due to its reaction with ambient atmosphere or even with PEDOT:PSS (Tournebize et al., 2015). Our results match well with observed decay in device photovoltaic stability (Figure 3.2); in addition, XPS survey spectra also confirm the oxygen/moisture ingress into the polymer blend and later on indium diffusion from ITO surface to the photo active layer which could likely hinder its absorption.

The study presented here demonstrate that ageing in ambient air leads to an overall performance loss of PCDTBT:$PC_{71}BM$ based OSCs. Basically, all the characterizations techniques revealed decay in the morphological, compositional and electrical parameters of an OSC with time. Finally, it is vital to note that the presented fabrication procedure is a facile route to ensure a low cost device, since it can be processed on light-weight and flexible substrates, and therefore compatible with large scale roll to roll production. The device performance can be improved by ensuring extrinsic and intrinsic stability with proper encapsulation and finding the alternative of PEDOT:PSS which should not corrode the ITO surface.

3.6 Conclusions

In summary, the degradation process mainly based on chemical and optical changes related to materials and interfaces in BHJ OSCs, has been studied. The XPS data show chemical changes that occur in PCDTBT:$PC_{71}BM$ photoactive layer under ambient atmosphere. The photoactive blend appears as an oxygen containing polymer with oxidation of carbon and nitrogen atoms. XPS survey spectra confirm the penetration of indium and tin into the PEDOT:PSS HTL and further into the photoactive

layer. Substantial increase in indium content at HTL surface in initial 250 h of ageing shows that degradation in HTL initially was predominantly due to indium diffusion which upon ageing for 1000 h also affected by remarkable increase in oxygen content. Whereas, a steady increase in oxygen content at the surface of photoactive layer, has been observed. It was concluded that photoactive material and its interface with HTL and cathode is strongly affected by moisture diffusion along with the diffusion of indium from ITO surface. Optical properties of the device were also affected in ambient atmosphere and the low absorption after degradation was observed. The power conversion efficiency was reduced due to decrease in J_{sc} and *FF*. Overall, this study show the degradation effects related to oxygen and indium diffusion in the photoactive layer and its interface with PEDOT:PSS and Al cathode. It is suggested that higher performance of the device could be achieved by adopting intrinsic and extrinsic stability measures.

CHAPTER 4: STABILITY ENHANCMENT IN ORGANIC SOLAR CELLS BY INCORPORATING V_2O_5 NANOPARTICLES IN THE HOLE TRANSPORT LAYER[3]

4.1 Overview

Synthesis The synthesis of V_2O_5 nanoparticles by a hydrothermal method and their utilization in a PEDOT:PSS buffer layer in a PCDTBT:$PC_{71}BM$ device structure is demonstrated. V_2O_5 nanoparticles were dispersed in the PEDOT:PSS HTL in normal architecture BHJ solar cells. The device performance for both pure PEDOT:PSS and hybrid HTLs were studied and demonstrated to effectively work in BHJ OSCs. From the stability test initially for one week and subsequently for another three weeks, it was confirmed that the OSC device with the incorporation of V_2O_5 nanoparticles in the standard HTL leads to a decrease in device degradation and significantly improves the lifetime as compared to the standard HTL based device. Moreover, the hybrid HTL exhibits better optical properties and a relatively stable band gap as compared to its pristine PEDOT:PSS counterpart. The results indicate that V_2O_5 could be a simple addition into the PEDOT:PSS layer to overcome its stability and degradation issues leading to an effective HTL in BHJ OSCs.

4.2 Introduction

OSCs have gained considerable attraction due to their friendliness to the environment, cheaper generation cost, compatibility with green energy systems and large scale roll to roll production (Huang et al., 2012; Sun et al., 2010). BHJ-OSCs are

[3] **The work presented in Chapter 4 has been published in RSC: "RSC Advances (Rank: Q1, Impact Factor: 3.29)" as**

Rafique et al. (2016). Stability enhancement in organic solar cells by incorporating V_2O_5 nanoparticles in the hole transport layer. *RSC Advances, 6*(55), 50043-50052.

based on an intimate blend of a donor and an acceptor material within the active layer matrix which is then phase separated while coating to create a donor acceptor interface (Irwin et al., 2011; Kettle et al., 2012; Li et al., 2010). Photons are absorbed by these materials to generate excitons which diffuse to the donor–acceptor interface and dissociate into the charge carriers. These charge carriers are then extracted by the respective electrodes (Scharber & Sariciftci, 2013; Wright & Uddin, 2012). These solar cells have layered geometric structure and optimization of each layer is essential to achieve overall performance of the device. It is very important in BHJ OSCs to achieve good ohmic contacts and charge transportation between the electrodes and the active layer. This is limited by the deep energy levels of the donor polymers which create a barrier at the interface between the active layer and either of the electrodes (Griffin, 2014). In order to overcome these issues, HTL and ETL are introduced at the interface between active layer and the electrodes (Duan et al., 2013; Irwin et al., 2011; Jørgensen et al., 2012).

PEDOT:PSS is considered as one of the most widely used HTL materials for the efficient charge transportation. However, there are several stability issues associated with this material due to its shallower energy levels and acidic nature which turns the device to degrade rapidly (Hancox et al., 2012; Schulz et al., 2014; Steirer et al., 2010). In recent years, a lot of research has been carried out to overcome the shortcomings of PEDOT:PSS. Metal oxides have been proved to be a good alternative to it (Lattante, 2014). These metal oxides serve many functions in an OSC such as their use as an active material, transparent electrodes, charge blocking and extraction layers, optical spacers and at the same time they are helpful in enhancing the stability and efficiency (Gershon, 2011). There are several transition metal oxides such as V_2O_5, NiO, Cs_2CO_3, WO_3 and MoO_3 which are being used in the BHJ solar cells and exhibit a wide range of energy levels. Many of them are proved to be more stable than PEDOT:PSS due to their

intrinsic optical, structural and electrical properties (Irani et al., 2013; Julien et al., 2012; Mane et al., 2015; Meyer et al., 2011; Ryu & Jang, 2011; Shrotriya et al., 2006; Zilberberg et al., 2011). In general, metal-oxide charge extraction layers demonstrated to be a good addition in OSCs with overall improvement in efficiency and stability (Ryu & Jang, 2011; Shrotriya et al., 2006).

V_2O_5 is one of the most widely explored materials as an n-type semiconductor due to its very good transparency, wide optical ban dap, and good stability (Irani et al., 2013; Mane et al., 2015). In addition, this metal oxide also provide good interfacial adhesion and enhances the device stability significantly when exposed to ambient environment which are limiting factors in case of PEDOT:PSS HTL (Meyer et al., 2011; Zilberberg et al., 2011). There are several methods which have been employed in the past to deposit this material as an HTL in BHJ OSCs both in normal as well as in inverted structures. Vacuum deposited processes had been widely used to deposit V_2O_5 in the past but these processes are not compatible with the large scale production on account of their high manufacturing costs which lead to a substantial addition in the overall fabrication cost of the device (Julien et al., 2012; Liu et al., 2014). In recent years, efforts have been made to solution deposit the V_2O_5 by using different techniques such as brush painting (Cho et al., 2015), solution processed spin coating (Hancox et al., 2012), sol–gel derived vanadium oxide (Kololuoma et al., 2015; Zilberberg et al., 2011), and several other methods (Irani et al., 2013; Julien et al., 2012; Mane et al., 2015; Meyer et al., 2011; Ryu & Jang, 2011; Shrotriya et al., 2006; Zilberberg et al., 2011). However, still a lot of work is needed to be done to find the best and cheaper ways to deposit these oxides, for optimizing the material properties to get the highly efficient devices compatible with PEDOT:PSS and exhibiting high stability.

One of the main constraints in OSC performance is its stability. OSCs are very sensitive towards various environmentally induced degradations such as decay in chemical, physical, mechanical, structural and optical performance. Consequently the life time of these devices is very short which put limitations for their commercial use. The goal to establish an easy solution processable fabrication procedure to develop a highly stable device by overcoming the reliability issues associated with PEDOT:PSS layer stimulates me to investigate the effect of incorporating the V_2O_5 nanoparticles in PEDOT:PSS layer. Investigations show that HTL with the dispersion of V_2O_5 nanoparticles exhibit much stable device as compared to its pristine counterpart.

4.3 Materials and Methods

4.3.1 Active Materials and the Synthesis of V_2O_5 Nanoparticles

Both PCDTBT and $PC_{71}BM$ were purchased from Lumtec. While PEDOT:PSS solution (PH1000) has been purchased from H.C. Starck and used as received. Figure 4.1 shows the molecular structure of PCDTBT, $PC_{71}BM$ and PEDOT:PSS.

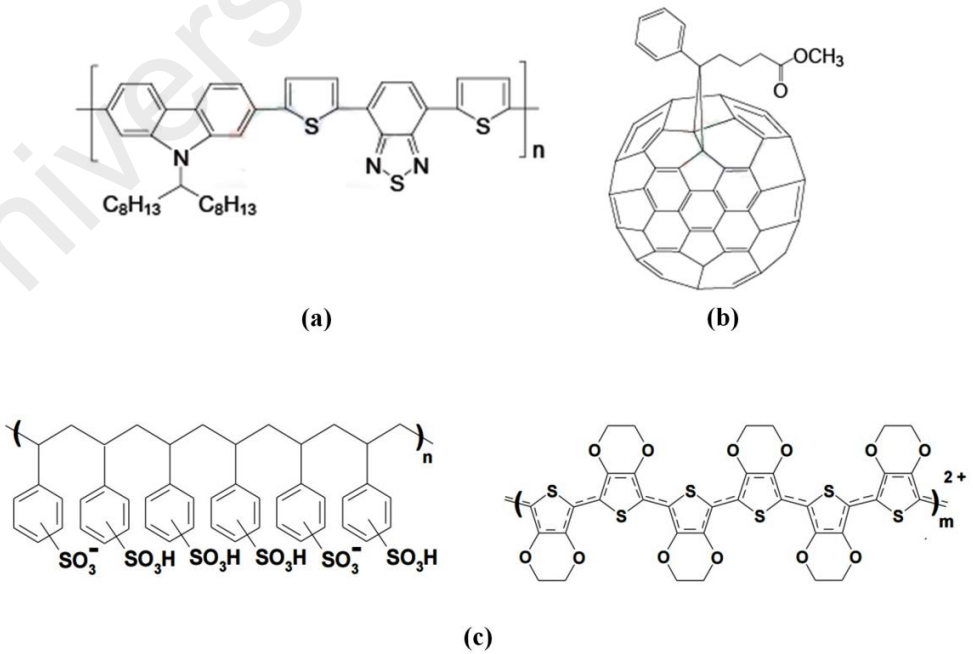

Figure 4.1: Molecular structures of (a) PCDTBT, (b) $PC_{71}BM$, and (c) PEDOT:PSS.

V_2O_5 nanoparticles were synthesis by hydrothermal method. 1 mM of vanadium acetylacetonate was dissolved into 40 mL of deionized water. 10 mg of Hexa-decyl-trimethyl ammonium bromide (CTAB) and 5 mg of trimethylamine N-oxide were dissolved into 20 mL of deionized water. This solution was added drop by drop into the vanadium solution under stirring at 80 °C and left at this temperature for 30 minutes. Whole mixture was transferred to Teflon-lined stainless steel autoclave with capacity of 80 mL and put into an electric oven at 150 °C for 2 hours. The product was collected by centrifuge at 5000 rpm for 1 min, then washed several times with deionized water and left to dry at 50 °C in the oven under vacuum overnight. The powder was followed by calcinations at 450 °C for 2 hours to finally obtain yellowish-brown V_2O_5 nanoparticles. The flow chart for the synthesis procedure has been presented in Figure 4.2.

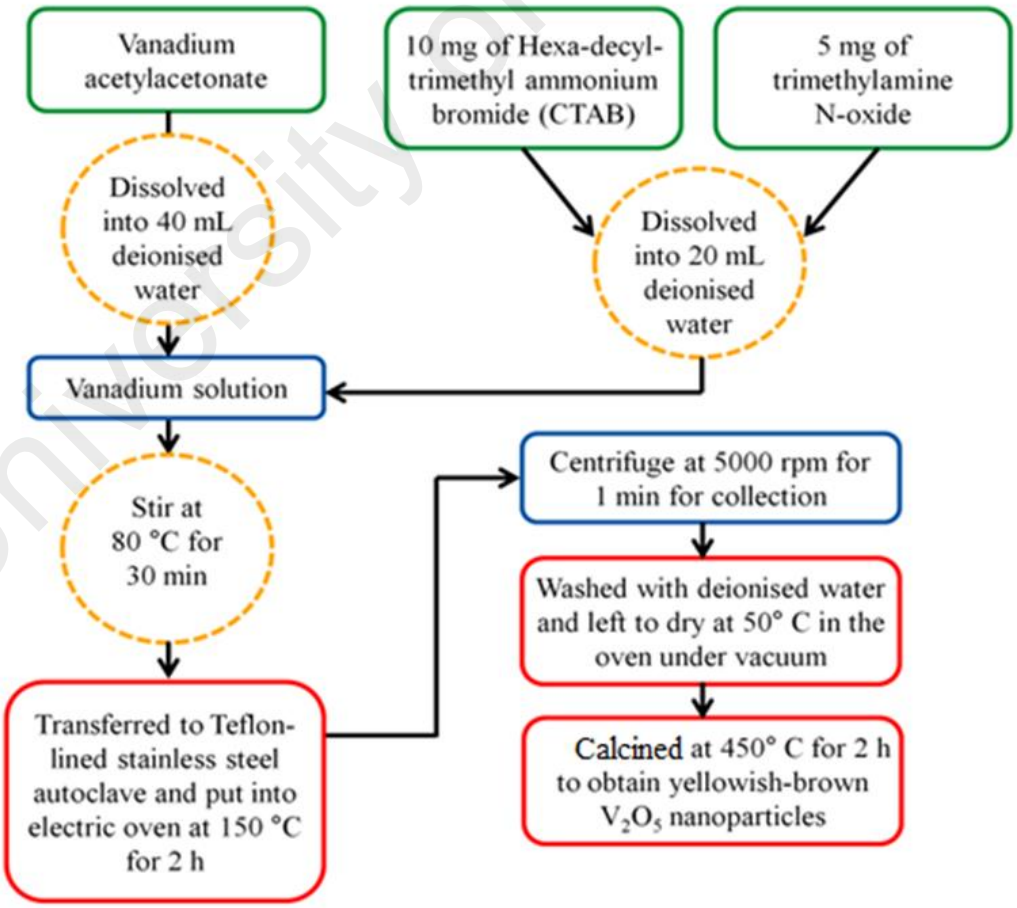

Figure 4.2: Flow chart of V_2O_5 nanoparticles synthesis via hydrothermal method.

4.3.2 Solar Cell Fabrication Procedure

Pre-patterned ITO coated glass substrates, for device fabrication, were provided by Ossila Ltd. UK. The dimensions of the rectangular substrates were 1.5×2.0 cm, with six active pixels on each substrate and an active area of 3×1.5 mm (4.5 mm^2) for every pixel. Those were cleaned first by using normal soap and then sequential ultrasonication in deionized water, acetone and isopropanol for 15 min each. At the end, substrates were dried by (Nitrogen) N_2 stream and treated by O_2 plasma for 5 minutes. PEDOT:PSS was spun coated at 4000 rpm for 1 min and then dried at 120 °C for 30 minutes to achieve the final layer thickness of around 40 nm. The active layer is consisting of PCDTBT as donor material and $PC_{71}BM$ as an acceptor material. The active layer ingredients were dissolved in chloroform with a concentration of 10 mg mL^{-1} and then mixed with the volume ratio of 1: 4 (PCDTBT:$PC_{71}BM$). Mixing was performed by stirring them for 24 hours. After transferring samples into nitrogen-filled glove-box, the final blended active layer was spun coated at 2000 rpm for 20 seconds. Al electrode with thickness of 100 nm was deposited on top of the active layer in vacuum (<10^{-6} torr) by means of thermal evaporation. Finally, all the OSCs devices were encapsulated by sticking a thin glass slide to cover active area of the device using a drop of epoxy glue. In the second set of experiments, PEDOT:PSS was mixed with the V_2O_5 nanoparticles at the concentration of 1 mg mL^{-1} and coating parameters were optimized for the desired thickness of 40 nm. Same fabrication procedure was adopted which is described previously. Figure 4.3 shows two types of fabricated OSCs varied by their HTLs including the energy band diagram for both of them.

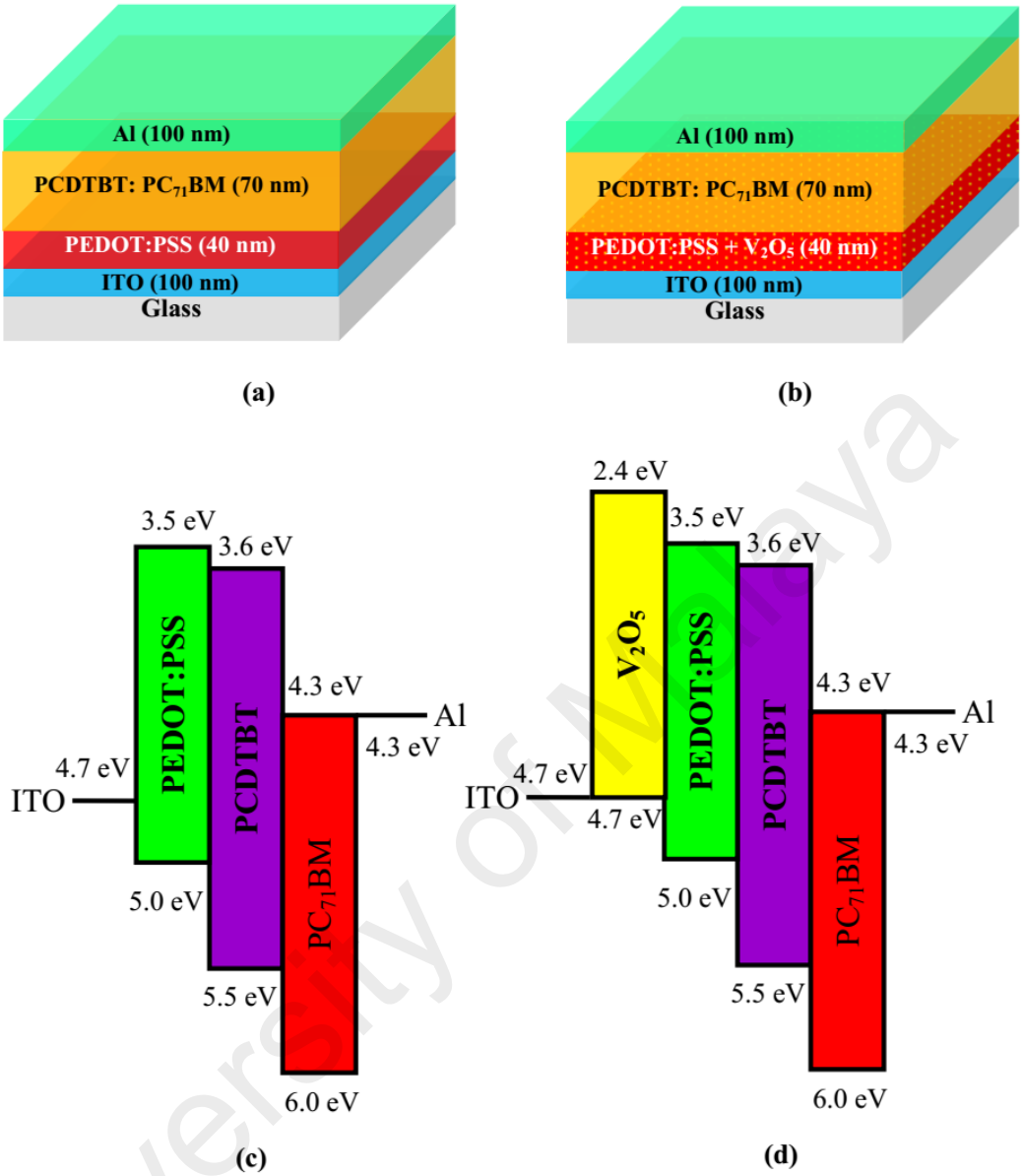

Figure 4.3: Device structure of PCDTBT:$PC_{71}BM$ solar cells with (a) PEDOT:PSS, (b) PEDOT:PSS + V_2O_5 as HTL, and the energy diagram for solar cells with (c)PEDOT:PSS, and (d) PEDOT:PSS + V_2O_5 as HTL.

4.3.3 Characterization

4.3.3.1 Characterization of V_2O_5 Nanoparticles

V_2O_5 nanoparticles were first characterized for their compositional and structural properties. XRD was performed in 2θ scanning range of 10 to 60° by using Ultima-IV (Rigaku, Japan) multipurpose X-ray diffraction system. Powder diffractometer, equipped with Cu K-a source (λ=0.154060 nm) was used to obtain the X-ray diffraction

pattern. Energy dispersive X-ray analysis along with FESEM was performed to obtain the elemental composition by using EDS OXFORD INCA ENERGY 250 (Oxford Instruments, UK) attachment. Raman spectroscopy was performed to measure Raman shifts by a DXR Raman Microscope (Thermo Scientific, USA), equipped with green light excitation (532 nm) laser source at 6 mW power.

4.3.3.2 Characterization of OSC Devices

Thickness of the HTL consisting of a mix blend of PEDOT:PSS and V_2O_5 was measured by surface Profiler (DEKTAK 150 Veeco, UK). Morphological characterizations were carried out by FESEM model JEOL JSM-7600F, Japan and AFM model SPM PROBE VT AFM XA 50/500 Omicron, Germany. Optical measurements of the samples were carried out with the UV-vis spectrophotometer (Perkin Elmer Lambda 750, USA). I-V characteristics of the solar cells were measured by Keithley 236 Source Measure Unit. Solar cell performance was tested by using an air mass 1.5 Global (AM 1.5 G) solar simulator with an irradiation intensity of 100 mW cm^{-2}. The light intensity calibration was performed with a Newport power meter 1918-R with calibrated Si-detector 818-UV.

4.4 Results and Discussion

4.4.1 Structural and Morphological Analysis

XRD pattern of the prepared V_2O_5 nanoparticles is presented in Figure 4.4(a). All the peaks are well indexed to the ICDD PDF-2 (Release 2011) DB card number 01-077-2418 and represent the intense reflections at 15.4126, 20.3651, 21.7817, 26.1387,v31.0528, 32.4078, 33.3502, 34.3418, and 41.3024° . 2θ diffracted peaks show sharp and noise free spectra which confirm the high Crystallinity and well-arranged orthorhombic symmetry of V_2O_5 crystal structure (space group: Pmmn (59)) with cell

dimensions as a = 11.5120, b = 3.5640, c = 4.3680. Both XRD and EDS (Figure 4c) results confirm the high purity of the prepared material.

Phase purity of the synthesized V_2O_5 nanoparticles was confirmed by the Raman spectroscopy due to its high sensitivity towards crystalline V_2O_5 nanoparticles (Wachs & Routray, 2012). Determined spectrum matched well with the reported spectra (Aslam et al., 2015; Lee et al., 2003) and shown in the inset of Figure 4.4(b). The peak at 995cm^{-1} is assigned to the terminal oxygen (V-O) stretching mode occurring due to unshared oxygen. Bands at 696cm^{-1} and 526 cm^{-1} are attributed to V-O-V stretching modes. Peaks at 406cm^{-1} and 283cm^{-1} are exhibiting the bending vibrations of V = O bonds whereas peaks at 487cm^{-1} and 303 cm^{-1} also represent the bending vibrations of different oxygen bonds. Raman peaks at 194cm^{-1} and 142cm^{-1} represent the lattice vibrations (Aslam et al., 2015; Lee et al., 2003).

Two variants of HTL were also characterized for Raman shifts since it is a powerful tool to study the conducting polymers. Resulting spectra for both HTLs are represented in the Figure 4.4(b). Attributions of peak positions are consistent with several reported results (Chang et al., 2014; Teng et al., 2013), showing dominantly the characteristics for PEDOT in either case and contribution of PSS is almost negligible in both cases. Peaks observed at 1563 cm^{-1}, 1500cm^{-1}, 1440cm^{-1}, 1360cm^{-1}, 1252cm^{-1} and 986cm^{-1} are assigned to PEDOT. Moreover, the most obvious difference brought by the addition of V_2O_5 nanoparticles was observed between 1252cm^{-1} and 1563 cm^{-1}. These nanoparticles reduced the intensity of the Raman fingerprints for the peaks attributed to 1252cm^{-1}, 1360cm^{-1}, 1440cm^{-1}, 1500cm^{-1} and 1563 cm^{-1}, furthermore they exhibited narrower band as compared to pristine HTL (Chou et al., 2015; Sakamoto et al., 2005).

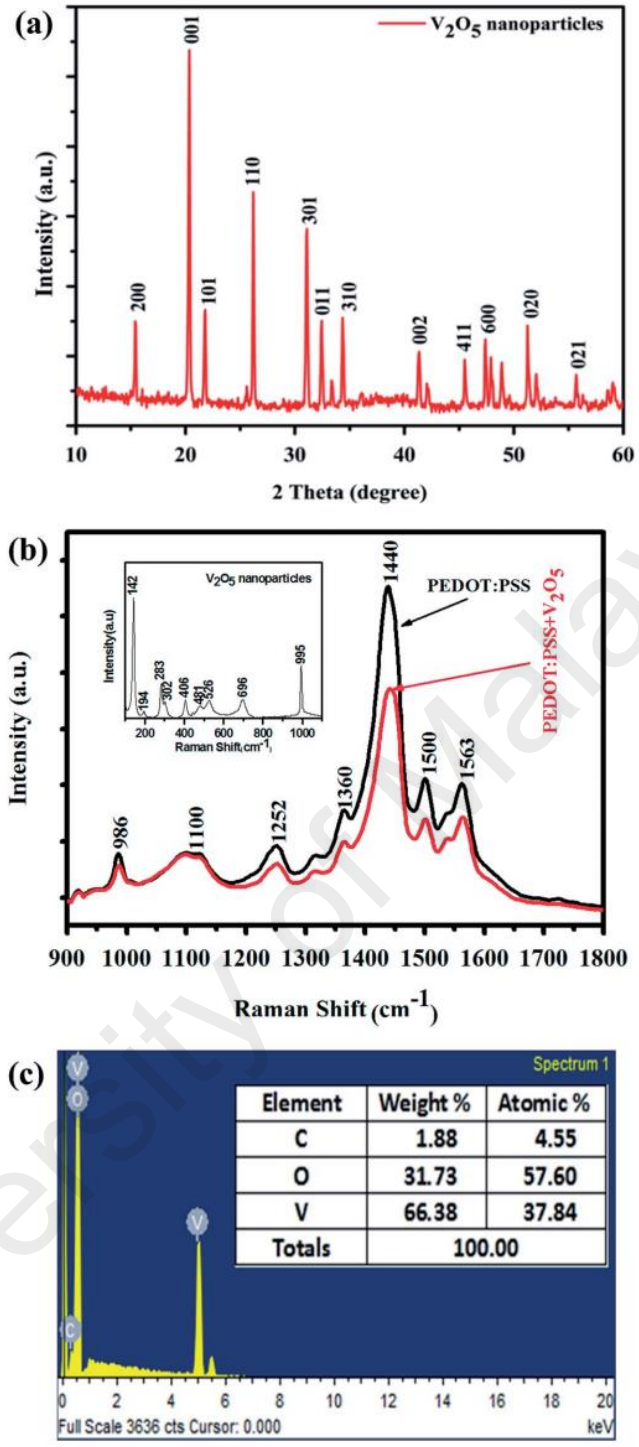

Figure 4.4: (a) XRD pattern of the V_2O_5 nanoparticles synthesis by hydrothermal method, (b) Raman spectra of pristine PEDOT:PSS HTL and its hybrid variant. Inset shows Raman fingerprints for V_2O_5 nanoparticles and (c) EDS spectra of synthesized V_2O_5 nanoparticles.

It is crucial to study surface morphology to ensure the device performance by improving different surface parameters. To compare the two HTL morphologies,

FESEM and AFM characterizations were used. High resolution FESEM images and AFM morphology of both HTLs are presented in Figure 4.5.

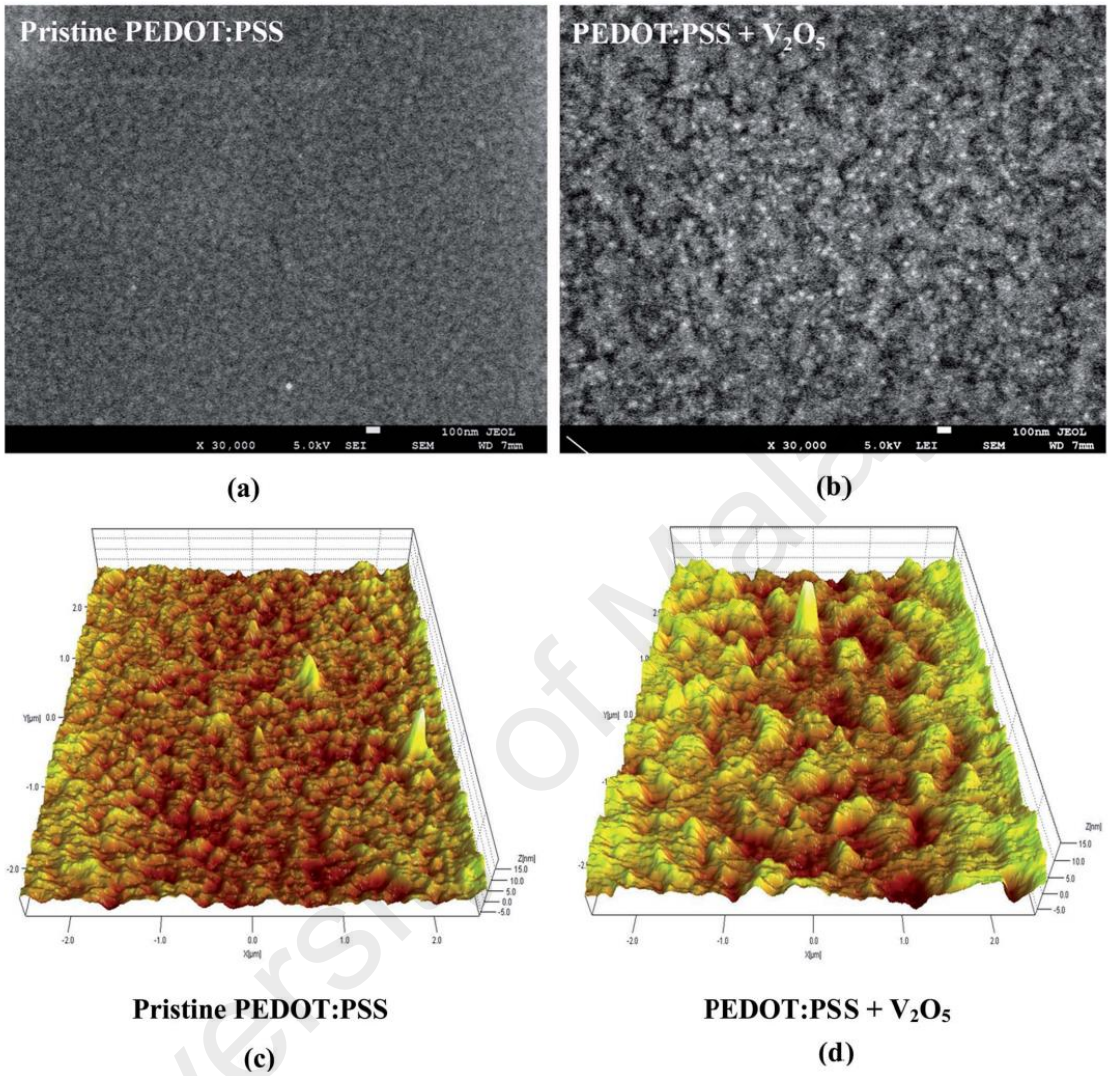

Figure 4.5: FESEM and AFM images for (a, c) pristine PEDOT:PSS HTL and (b, d) Hybrid HTL.

SEM image of the pristine PEDOT:PSS (Figure 4.5(a)) layer shows the smooth and featureless surface morphology as compared to hybrid HTL. Whereas, the hybrid HTL exhibits a loosely packed surface morphology (Figure 4.5(b)); the globules aggregation of discrete nanoparticles on the entire surface are likely to be V_2O_5 particles uniformly distributed within the polymer matrix which confirms the method efficacy of the solution processed fabrication technique that was used to prepare HTLs. Hybrid

HTL shows formation of channels like morphology likely caused by nucleation effect of V_2O_5 particles. Figure 4.5(c) and (d) shows the non-contact tapping mode AFM images of pristine and hybrid HTLs deposited on ITO coated glass substrates. The morphology of the PEDOT:PSS HTL is much smoother than hybrid HTL and surface roughness increased to double due to addition of V_2O_5 nanoparticles. The increase in the roughness was expected and agrees with the reported results in (Huang et al., 2009). Although the roughness of the HTL had increased with the addition of V_2O_5 nanoparticles but it is believed that the particles dispersed on the surface of the HTL can effectively extract the charged carrier due to their high conductivity and at the same time they assist in reducing the leakage current by blocking the negative charge carriers which in turns guarantees a better and stable device. It is reported that the RMS roughness of modified HTL increases slightly with the increase of V_2O_5 concentration in PEDOT:PSS except for high ratio of doping concentration (1:1) (Kim et al., 2015). In this work, it is observed that the addition of V_2O_5 in small amount (1 mg) into PEDOT:PSS has also altered the roughness of modified HTL as shown in Figure 4.5(d). However, the change in device performance is believed to be due to the change in electronic and optical properties of the HTL compared to the morphological change such as the roughness (Kim et al., 2015). Further details are presented in Section 4.4.2.

4.4.2 Optical Transmittance and Band-gap Calculations

In Figure 4.6(a), the transmittance spectra of pristine (PEDOT:PSS) HTL and hybrid HTL (PEDOT:PSS + V_2O_5) to distinguish the ageing effect on the optical properties of the both variants have been reported. Data are shown for the freshly prepared and one month aged samples. The transmittance curves for hybrid HTL show high transmittance of more than 94% in the visible region and did not show any significant reduction in transmittance over one month ageing period. Whereas, the transparency of the pristine PEDOT:PSS of freshly prepared sample is exhibiting

around 89 % transmittance which diminished to 84 % after one month of preparation. It is notable that transmittance of the pristine PEDOT:PSS thin film reduced with time which is undesirable (Sarker et al., 2015). Relatively higher degree of transparency in the hybrid HTL ensures more light absorption by the active layer and therefore an increase in the photo-generation of charges (Ecker et al., 2011).

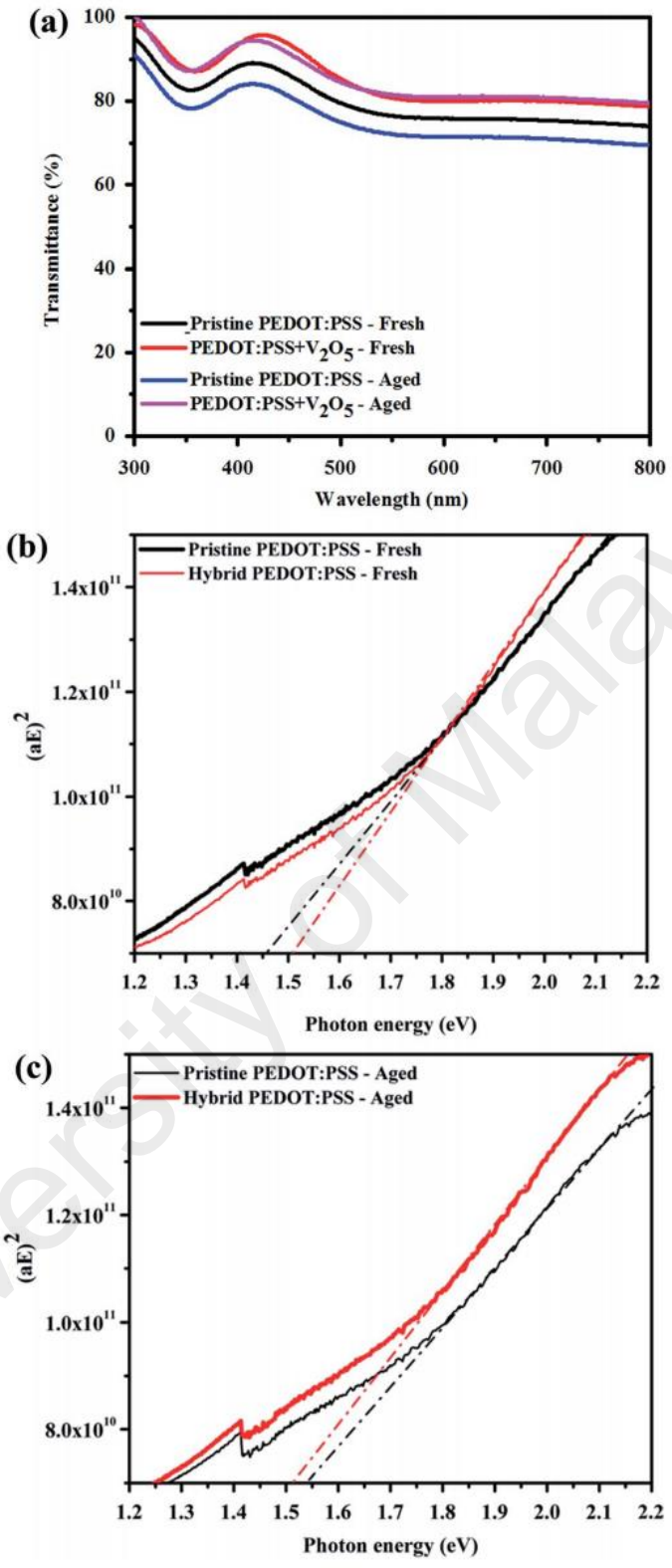

Figure 4.6: The transmittance spectra, for (a) pristine PEDOT:PSS and PEDOT:PSS enhanced with V_2O_5 nanoparticles, the Tauc plot of $(aE)^2$ against the photon energy (E) for (b) freshly prepared HTL variants and (c) aged HTL variants.

In Figure 4.3(c) and (d), the energy band diagram has been presented based on their known energy levels which consist of LUMO and HOMO values. It can be seen that the presence of V_2O_5 has further facilitated the extraction of holes from the active component (PCDTBT) to PEDOT:PSS layer and then to the ITO via V_2O_5. In principle, a significant difference of V_2O_5 LUMO level as compared to LUMO levels of both PEDOT:PSS and the active component (PCDTBT) has potentially created a restriction for electrons flow to the ITO and consequently made V_2O_5 as good electron blocking component between the ITO/active layer interfaces. In this section, the optical energy gaps for the freshly prepared and aged samples of pristine and hybrid PEDOT:PSS HTLs have been determined via the optical absorption spectroscopy. The square of absorption coefficient and photons energy $(\alpha E)^2$ is related to the band gap (E_g) and calculated by the following expression (Mane et al., 2015; Reddy et al., 2013).

$$\alpha h\nu = \alpha_O\left(h\nu - E_g\right)^n \quad \ldots\ldots\ldots\ldots \textit{(4.1)}$$

Where E_g is the band gap corresponding to a particular transition occurring in the samples, ν is the transition frequency, *h is* Planck's constant, *n* is the exponent which can be taken as 1/2, 3/2, 2 and 3 depending on the band transition classifications. Whereas, $\alpha = 2.303\ A/t$, *A* and *t* are absorption and thickness of the films respectively (Muhammad & Sulaiman, 2011). Extrapolated values from the straight line to the abscissa determine the optical band-gap. Figure 4.6(b) and (c) show the Tauc plot, i.e. $(aE)^2$ versus photon energy of pristine and hybrid HTLs. For the direct allowed transition, the optical band gap transition energy for pristine PEDOT:PSS varied from 1.46 to 1.55 eV when the data were collected after one month. Whereas, the optical energy gap for hybrid HTL was found to be around 1.51 eV slightly higher than the energy gap of fresh pristine PEDOT:PSS HTL which is believed to be due to the presence of V_2O_5 nanoparticles, a well-known high work function metal oxide.

However, it remained unchanged during this period of time exhibiting high degree of stability in the transition energy which consequently helps in improving the device performance especially in cell stability. Thus, the improvement in the device performance is also attributed to the optical properties of V_2O_5 (Lee et al., 2014). The variation in transmittance and band gap energy of the both variants of HTL are summarized in Table 4.1.

Table 4.1: The variations in transmittance and band gap energy of pristine and hybrid HTLs due to ageing for one month.

Sample	***Transmittance (%)***		***Band gap energy (eV)***	
	Fresh	Aged	Fresh	Aged
Pristine PEDOT:PSS	89	84	1.46	1.55
PEDOT:PSS+ V_2O_5	94	94	1.51	1.51

4.4.3 Organic Solar Cell Device Characteristics

Photovoltaic properties of the OSCs based on PCDTBT:$PC_{71}BM$ active layer with pristine HTL, PEDOT:PSS, and its modified variant with the incorporation of V_2O_5 nanoparticles were investigated. The efficiency and life time stability of both types of devices were investigated by performing I–V measurements and reduction in the PCEs was recorded over a period of 4 weeks. The solar simulations were performed at the light intensity of 100 mW cm^{-2}. Figure 4.7 shows the I–V characteristics for both OSCs. The two variants of OSCs showed a decline in both (J_{sc}) and (V_{oc}) as shown in Figure 4.7(a) and (b). However, OSC devices with pristine PEDOT:PSS HTL exhibited more decay in both parameters than that of with hybrid HTL. After the first week, the pristine device demonstrated a minor degradation, mainly the decrease of the device (V_{oc}) from 0.8 to 0.75 V. After four weeks the device continued to degrade and (V_{oc}) value reduced to 0.70 V. While, in the hybrid device the (V_{oc}) for freshly prepared

device is about 0.85 V which showed minor degradation in first week with (V_{oc}) of 0.80 V. After four weeks the hybrid device showed no further reduction in the (V_{oc}).

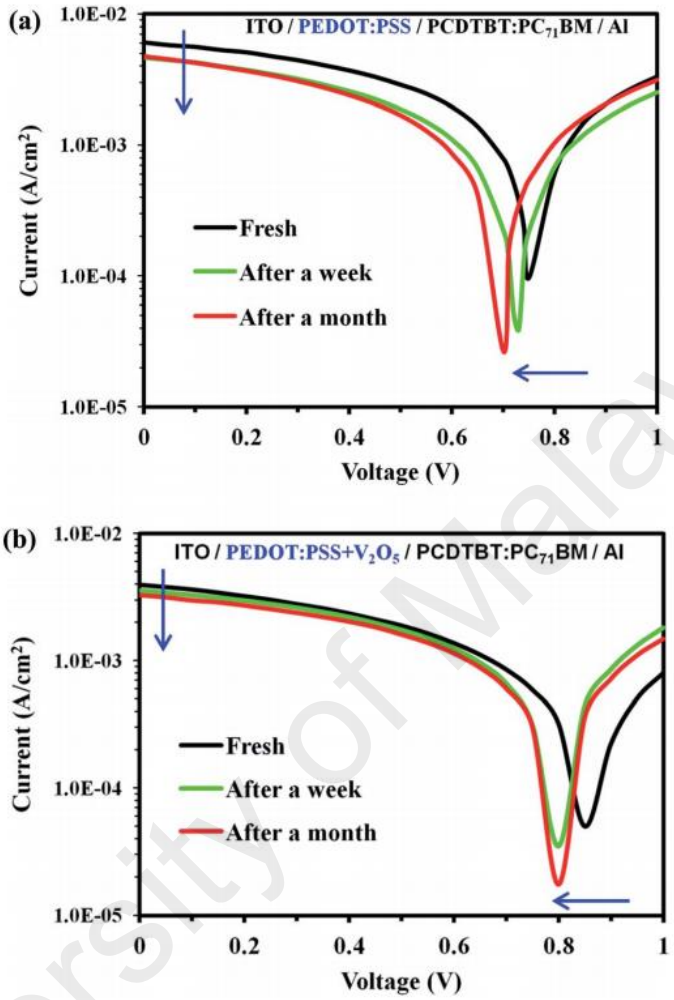

Figure 4.7: The current-voltage (*I-V*) characteristic in fresh condition, after one week, and after 4 weeks for OSCs with (a) PEDOT:PSS, and (b) PEDOT:PSS+V_2O_5 HTL layer.

From the normalized efficiency calculated over the period of four weeks as shown in Figure 4.8, it is evident that that device with the hybrid HTL was consistently much stable as compared to the device with pristine PEDOT:PSS layer. It retained about 90 % of its efficiency, whereas the standard device reduced to around 65 % of its initial efficiency over this entire period of time.

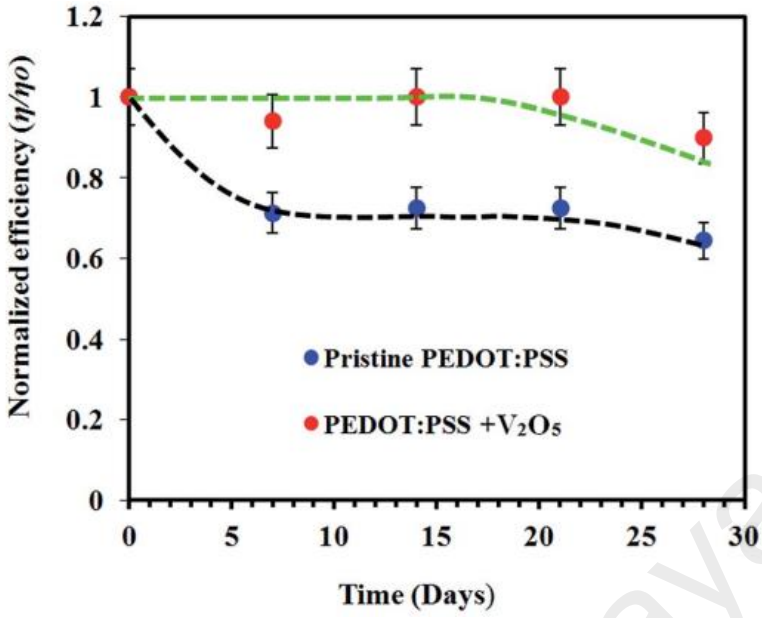

Figure 4.8: Normalized efficiency (η/η_o) of both OSCs with pristine PEDOT:PSS layer and PEDOT:PSS + V_2O_5 nanoparticles layer measured for 28 days (four weeks).

The improvement in the device stability and overall performance was due to the intrinsic features of the metal oxide nanoparticles which were incorporated in the HTL. Our results were also consistent with the previous studies showing that V_2O_5 effectively prevent the leakage current in both normal as well as inverted geometries. It proved to be more stable as compared to conventional PEDOT:PSS layer (Kösemen et al., 2014; Shrotriya et al., 2006; Escobar et al., 2013; Wang et al., 2012). The addition of these nanoparticles forms an organic–inorganic hybrid buffer layer which protects the active layer and at the same time maintains the device performance (Chen et al., 2011). Moreover, in recent years, it is studied that conventional PEDOT:PSS layer does not provide good adhesion at the interfaces (Dupont et al., 2012). Whereas, V_2O_5 proved to be better in adhesion (Escobar et al., 2013) at the interface between active layer and HTL and at the same time it also helps in transport of charged carriers to the electrode. Relatively better performance of the hybrid device is also attributed to the better transmittance and stable band gap of the hybrid HTL as compared to its pristine

counterpart. Furthermore, it mitigated the adverse effects of PEDOT:PSS acidic nature on ITO over the time due to its favorable optical, structural and electrical properties which in turns had given us a more stable device as compared to the standard cell.

4.5 Conclusions

This work has successfully demonstrated the fabrication of air stable PCDTBT:$PC_{71}BM$ based polymer solar cells with V_2O_5 modified HTL to address the reliability issues associated with conventional PEDOT:PSS layer. The results show that the mixing of V_2O_5 + PEDOT:PSS has a major impact on the device life time stability. Based on this study, results were evident that V_2O_5 based HTL could significantly reduce the degradation in OSCs device performance than pristine PEDOT:PSS HTL. The device with hybrid HTL retained 90 % of its PCE even after four weeks of ageing compared to the pure PEDOT:PSS HTL where overall efficiency reduced to around 65 % of its initial value. In addition to remarkably better stability, both HTLs and active layers were fabricated by the simple and solution processed method, which greatly simplifies the fabrication process and reduced the overall cost. This study thus showed the importance of buffered layers in OSCs with an emphasis on improving the HTL if long operational devices are to be achieved. A further in depth study of metal oxide based HTLs and their interfaces with the BHJ and ITO electrodes are needed to be investigated in future.

CHAPTER 5: BULK HETEROJUNCTION ORGANIC SOLAR CELLS WITH GRAPHENE OXIDE HOLE TRANSPORT LAYER: EFFECT OF VARIED CONCENTRATION ON PHOTOVOLTAIC PERFORMANCE[4]

5.1 Overview

This chapter reports the solution processable hole transport layer (HTL) for bulk heterojunction organic solar cells (BHJ OSCs) based on varied concentration of graphene oxide (GO) in aqueous suspension. The effects of varied concentration of GO at 1, 2 and 4 mg/ml on the morphological, optical, electrical and photovoltaic properties of the OSCs have been studied. Device with the lowest concentration and least thickness of GO showed most optimized performance with a power conversation efficiency (PCE) of 2.73 % as compared to the higher concentration where the PCE reduced to 0.67 and 0.22 % for the devices with HTL of 2 and 4 mg/ml, respectively. The remarkable reduction in the device performance at higher concentration is mainly attributed to a drastic decrease in the short circuit current that reduced from 8.14mA/cm^2 to 2.90 and 1.10 mA/cm^{2}at 2 and 4 mg/ml, respectively. Similarly, the increased series resistance (R_s) from 6.89 Ω/cm^{2}to 9.54 and 11.51Ω/cm^2 has also reduced the device performance. Optical transmittance has been decreased from more than 85% to less than 80% in the overall wavelength region at higher concentrations. Both the insulating properties of GO at higher thickness of HTL due to high

[4] **The work presented in Chapter 5 has been published in ACS: "Journal of Physical Chemistry C (Rank: Q1, Impact Factor: 4.50)" as**

Rafique et al. (2016). Polymer bulk heterojunction organic solar cells with graphene oxide hole transport layer: Effect of varied concentration on photovoltaic performance. *The Journal of Physical Chemistry C*, *121*(1), 140-146.

concentration and inhomogeneous surface characteristics lead to a decrease in the device performance.

5.2 Introduction

The potential of a facile, low cost, solution processable, role to role manufacturing process has made BHJ OSCs very promising candidate to address growing concerns related to the implementation of green energy harvesting (Jagadamma et al., 2014; Li et al., 2015; Rafique et al., 2016). In OSCs, photovoltaic parameters such as open circuit voltage (V_{oc}), short circuit current (J_{sc}) and fill factor (FF) are greatly relied on the interfacial characteristics between the photoactive layer and the electrodes as well as the bulk properties of the materials (Yun et al., 2011). Due to these reasons, the interfacial layers namely HTL and ETL are essential for improving the efficiency and stability of OSCs (Yang et al., 2012). Several key factors such as high transmittance, optimum morphology, high conductivity, stability and efficiency have been considered for the use of these promising interfacial layers (Cao et al., 2016b; Lian et al., 2014).

Poly (3, 4-ethylenedioxythiophene)-poly (styrenesulfonate) PEDOT:PSS is the current state of the art standard interfacial layer on the transparent ITO anode to facilitate the extraction of holes, blocking of electrons and improve the surface morphology at the interface (Crispin et al., 2006; Espinosa et al., 2011; Wakizaka et al., 2004). It possesses several advantages including its excellent transparency in the visible region, high electrical conductivity, easy solution processing in aqueous dispersion and its high work function (Nardes et al., 2008; Po et al., 2011; Zhao et al., 2015). However, PEDOT:PSS as an HTL also favors device degradation due to its hygroscopic and acidic nature, resulting in severe device instability (Jagadamma et al., 2014; Varnamkhasti et al., 2012). To address these issues, inorganic metal oxides such as NiO

(Park et al., 2010; Yang et al., 2012), V_2O_5 (Meyer et al., 2011) and MoO_3 (Chen et al., 2012) have been investigated among others to replace PEDOT:PSS. However, deposition of these materials normally involves costly vacuum techniques that are incompatible with the large scale role to role production (Yun et al., 2011). Therefore, development of a facile, solution processable and cost effective method is in high demands. In this context, solution processable GO has been recently reported by several groups to serve as an HTL in OSCs (Liu et al., 2012; Smith et al., 2014). GO is the one atomic layer thick graphene sheet functionalized with oxygen groups (hydroxyl (OH) and epoxy group) on its basal plane and various other types at the edges (Ding et al., 2015). It possesses excellent electrical, optical and thermal properties, a large surface area and a high young's modulus, which makes it suitable for a variety of applications including OSCs, fuel cells, light emitting diodes (LEDs), sensors and field effect transistors etc. (Yu et al., 2011; Yu et al., 2010). Stratakis et al. demonstrated the use of GO as an HTL in BHJ OSCs that outperformed the device with pristine PEDOT:PSS HTL on merits of their stability and efficiency (Stratakis et al., 2014). Similarly, Zhou et al. and Smith et al. also reported the BHJ OSCs fabricated with GO HTL and exhibiting high efficiency and stability (Smith et al., 2014; Zhou et al., 2015). Efficacy of GO as an HTL in BHJ OSCs, for both normal and inverted architectures, has been confirmed by many other reported works (Yusoff et al., 2014; Cheng et al.; He et al., 2014). Thus, GO has the substantial potential to serve as an HTL in OSCs with superior performance and device life time as compared to the conventional PEDOT:PSS HTL. However, device performance with GO HTL is extremely sensitive to its thickness due to insulating characteristics of GO. In addition, the thickness of the GO films is also highly dependent on the GO concentration in any solvent, in particular, the aqueous suspension. To date, there has been no report published with optimized experimental conditions with regard to concentration and consequently thickness of GO as an HTL.

Several groups reported the efficacy of GO as an HTL and each of them reported the results with different concentration and experimental conditions for the fabrication of GO HTL in BHJ OSCs. For example, Li et al. reported GO for the very first time as an HTL in P3HT based BHJ OSCs and used an optimized concentration of 8 mg/ml in aqueous dispersion (Li et al., 2010). However, the thickness was optimized to be ~ 2 nm for a PCE of 3.5%. In another study, Yang et al. utilized GO aqueous dispersion at 2 mg/ml concentration to deposit GO HTL in a BHJ OSC (Yang et al., 2012). Similarly, Cheng et al. also reported BHJ OSC with UV treated GO HTL at the concentration of 1.25 mg/ml (Cheng et al., 2015). Therefore, optimization of GO concentration and corresponding thickness are much needed to move towards the standardized conditions for deposition of GO as an HTL.

In this study, the solution processed GO HTLs in the PCDTBT:$PC_{71}BM$ photoactive blend based BHJ OSCs have been investigated. GO in aqueous suspension was prepared at varied concentration and deposited at fixed spinning speed. The changes in surface properties due to different concentrations and an overall effect on the thickness were investigated. Surface morphology, optical and electrical properties, and photovoltaic performance were evaluated to correlate the performance of OSCs with varied concentration of GO as HTLs.

5.3 Materials and Methods

5.3.1 Preparation of GO HTLs

The GO solution was prepared by following simplified hummer method reported elsewhere Ming (Ming, 2010). Three different concentrations were considered for GO HTL aqueous dispersion: 1, 2 and 4 mg/ ml. The freshly prepared GO aqueous solution of varied concentration was spun coated on cleaned, pre-patterned ITO substrates (15

Ω/ sq.) at spin rate of 6000 rpm for 40 s. After the spin coating the films were annealed at 150 °C for 5 min in air and allowed to cool down at room temperature.

5.3.2 Characterization of GO HTLs

Surface morphology of the GO films was characterized using tapping mode of atomic force microscopy (AFM, Agilent Technologies 5500 Scanning Probe Microscope) and field emission scanning electron microscope (FESEM) model JEOL JSM-7600F, Japan. Structural analysis of the samples was performed by DXR Raman Microscope (Thermo Scientific, USA) with 532 nm laser irradiation source of 6 mW power. The optical transmittance spectra of spun coated GO layers were measured using Perkin Elmer UV-visible diffuse reflectance spectrophotometer (Lambda 650) over the wavelength range of 200 to 800 nm. The thickness of the GO films was estimated using surface profiler (DEKTAK 150 Veeco, UK).

5.3.3 Fabrication of PCDTBT:$PC_{71}BM$ Based Solar Cells

Normal architecture BHJ OSCs were fabricated on pre-patterned ITO coated glass substrates. The substrates were cleaned with detergent, ultrasonicated in deionized (DI) water, acetone, isopropyl alcohol and rinse with DI water. The cleaned substrates were blown with dry nitrogen stream and further treated with oxygen plasma for 5 min to obtain a hydrophilic surface state for GO HTL. The PCDTBT:$PC_{71}BM$ photoactive blend solution was prepared by dissolving 10 mg of PCDTBT and $PC_{71}BM$ in 1 mL of chloroform, separately. The constituents of photoactive layer were kept on stirring at room temperature for ~ 24 h and further mixed by vigorous stirring overnight at the ratio of 1:4 for the PCDTBT and $PC_{71}BM$, respectively. The prepared solution was filtered with 0.25 µm PTFE filters (Whatman, Germany) prior to spin casting at an optimized speed of 2000 rpm for 60 s, resulting in a thickness of ~ 70 nm.

5.3.4 Characterization of Solar Cells

Measurement of the photovoltaic performance was carried out using a Keithley 236 (Keithley Co.) source measurement unit. Air Mass 1.5 Global (AM 1.5 G) solar simulator with an irradiation intensity of 100mW/cm^2 was used to measure the solar cell performance. The light intensity calibration was carried out using a Newport power meter 1918-R with calibrated Si-detector 818-UV.

5.4 Results and Discussion

Figure 5.1(a) and 5.1(b) describe the device structure of OSCs using the GO HTLs and corresponding energy level diagram. The devices were fabricated with varied concentration (1, 2 and 4 mg/mL) of GO in aqueous suspension and consequently the varied thickness using fixed spin coating conditions. The OSCs were fabricated by the consecutive spin coating of GO HTLs (2-10 nm as shown in Figure 5.2(a), PCDTBT:$PC_{71}BM$ as an active layer (70 nm) and thermally evaporated aluminium (100 nm) as a cathode on ITO anode. The fabrication of OSCs is described in the experimental section. GO nanosheets were synthesized by the chemical exfoliation of graphite powder using simplified Hummers method, further, GO aqueous suspension was prepared in DI water at the concentration of 1, 2 and 4 mg/mL. GO exhibits several unique properties including its tunable energy levels, easy functionalization, facile and low cost synthesis process, and its two dimensional structure. In order to fabricate a high performance OSC device with GO as an HTL, a highly uniform, ultra-thin and smooth surface with full coverage of ITO is recommended. However, it is difficult to deposit a homogeneous HTL of GO in the range of 1-3 nm with uniform full coverage of ITO anode. Therefore, the device performance is significantly affected due to direct contact of ITO and photo-active layer at the non-covered regions. In addition, at higher concentration, aggregation of GO flakes is observed which gives rise to high root mean

square (RMS) roughness values; consequently, the non-uniform and overlapping GO flakes are likely to suppress the transportation of holes.

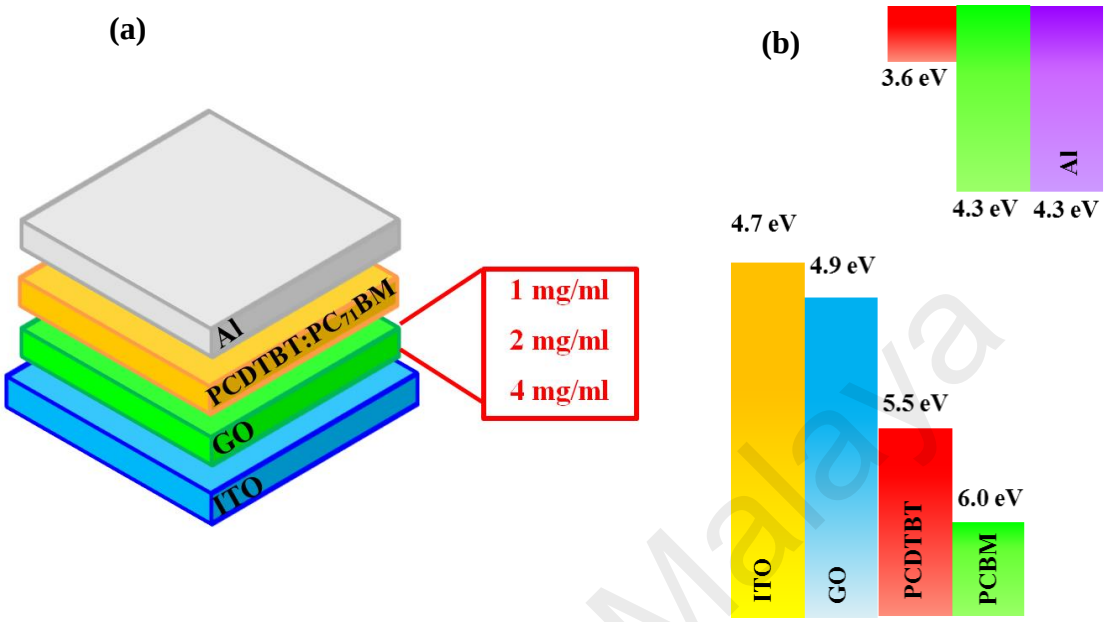

Figure 5.1: (a) Schematic device structure and (b) energy level diagram of the PCDTBT:$PC_{71}BM$ based devices with GO HTLs of varied concentration.

Raman spectroscopy has been extensively used to characterize the graphene based materials. The Raman spectra presented in Figure 5.2(b) for all three HTL concentration variants showed two well-known bands i.e. the D band and G band. The peaks at ~1347 cm^{-1} are ascribed to the D-band, which represents the structural disorder defects and partially disordered structured of the sp^2 domain (Bajpai et al.,2012; Fu et al., 2013), while the peaks at ~1598 cm^{-1} correspond to the G-band, which shows the planer configuration of sp^2 bonded carbon corresponding to GO (Hafiz et al., 2014). The existence of G band of GO at a higher region indicates the extensive oxidation of graphite which lead to the distortion of its planar structure (Dehsari et al., 2014). At the higher frequency end of the spectra, three peaks at ~2710, 2940 and 3190 cm^{-1} are observed. A relatively strong and pronounced peak at 2940 cm^{-1} is the combination of D and G band and denoted as D+G band which is ascribed to the disorder induced

combination mode (Delgado et al., 2008). The peaks at 2710 and 3190 cm^{-1} correspond to an overtone of D band and often referred as 2D band (Bajpai et al., 2012; Wang et al., 2013). There is a significant increase in the intensity of the D and G bands at 2 and 4 mg/ml which likely occur due to increase in the concentration and consequently the increased Raman scattering.

Since the transmittance is one of the important parameters which govern the overall performance of the solar cell devices, therefore, Figure 5.2(c) reports the optical transmittance of GO films in order to distinguish effects arising from varied concentration of GO aqueous suspension. The films at 1 and 2 mg/ml do not significantly alter the transparency of ITO and show high transmittance values of more than 85% in the overall wavelength range. However, in the case of higher concentration (4 mg/ml), it yielded a more pronounced reduction in the transmittance of the film. It can be observed that the transmittance of the GO-4mg/ml film is almost 15% lower compared with the transmittance of pristine ITO and ITO/GO (1 and 2 mg/ml) samples in the region of ~ 400-800 nm. The observed decay of transmittance in the ~ 400-800 nm region could potentially bring a substantial effect on the photo-generated current (J_{sc}) of the device. Thus the device efficiency could be significantly reduced due to low transmittance as well as other factors such as high surface roughness and increased R_s values etc. (Yusoff et al., 2014; Jeon et al., 2014). These results are in good agreement with the current photovoltaic studies of the corresponding devices. Relatively low transmittance is ascribed to the increased concentration which consequently increases the thickness as well as the surface roughness of the film, as a result diminishes the transmittance.

R_s, is another important parameter to determine the overall device performance; generally, low R_s values are desirable. For the device with GO HTL of 1 mg/ml

concentration, R_s is estimated to be 6.89 Ω/cm^2. At high concentrations, a linear increase in the R_s values has been observed and it increased to almost double of the lowest concentration (11.51 Ω/cm^2) at 4 mg/ml. Comparatively low R_s values suggest the better charge transportation ability and a homogeneous morphology, as compared to the devices fabricated at high concentration. The R_s values as a function of varied concentration of GO has been presented in Figure 5.2(d) and Table 5.1.

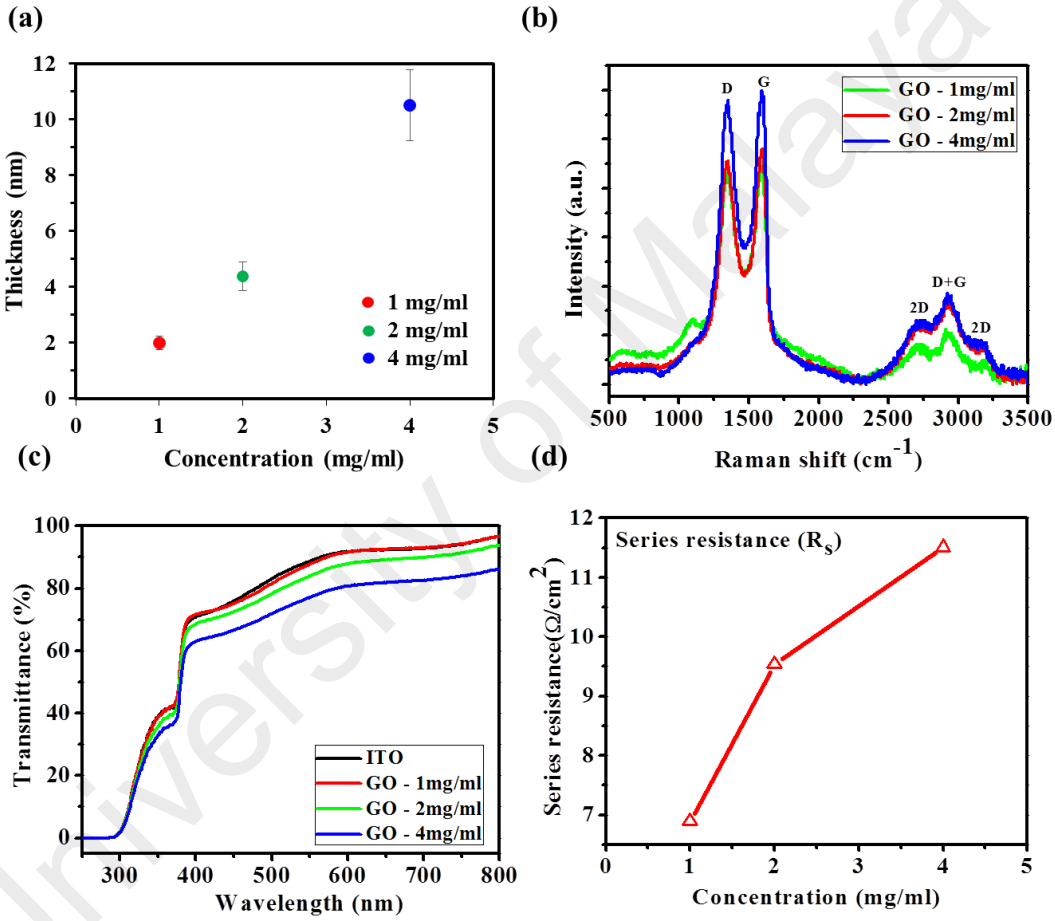

Figure 5.2: (a) Thickness vs concentration plot (b) Raman spectra of GO films, (c) optical transmittance and (d) series resistance (R_s), at 1, 2 and 4mg/ml concentration.

5.4.1 SEM and AFM Morphology of GO on ITO

The influence of the different concentration of GO in aqueous suspension on the surface morphology of spin coated GO films was analyzed based on AFM topographical images and FESEM surface scans, as shown in Figure 5.3. The RMS roughness values for the films at 1, 2 and 4 mg/ml are calculated to be 2.88, 2.53 and 5.16 nm respectively. RMS value slightly reduced in case of 2 mg/ml as compared to 1 mg/ml because this concentration likely results in planarization of the surface. Moreover, RMS surface roughness has significantly increased at 4 mg/ml which caused a substantial decrease in the device performance. The surface texture for all three concentration variants can also be seen in SEM images where it is clearly visible that at 4 mg/ml, GO has aggregated and it is exhibiting stem like structures on entire surface due to aggregation of these flakes. The SEM results matched well with the AFM morphology analysis. Comparatively uniform surface texture is observed for the HTL deposited with concentration of 1 and 2 mg/ml as shown in Figure 5.3(a) and 5.3(b). HTL morphology significantly influences the R_s values and generally, a homogeneous and full-covered HTL morphology yield low R_s which is highly desired. However, in this study, GO at 1mg/ml exhibited a reasonably uniform surface and an ultrathin layer (Figure 5.3(a)) but it lacks in full ITO coverage of ITO surface. Therefore, uncovered regions may cause a direct contact of photo-active layer with ITO which could lead to a significant decrease in device performance. At higher concentrations, although the HTL is providing full coverage of ITO but increase in roughness and thickness lead to a radical decrease in device performance. As discussed above, GO exhibits its full functionality if it is in the form of an ultrathin layered structure. Stacking of many atomic layers in case of thicker HTLs may diminishes the favorable properties of GO and predominately exhibits the insulating properties. Hence, the device performance is observed to be drastically decreased.

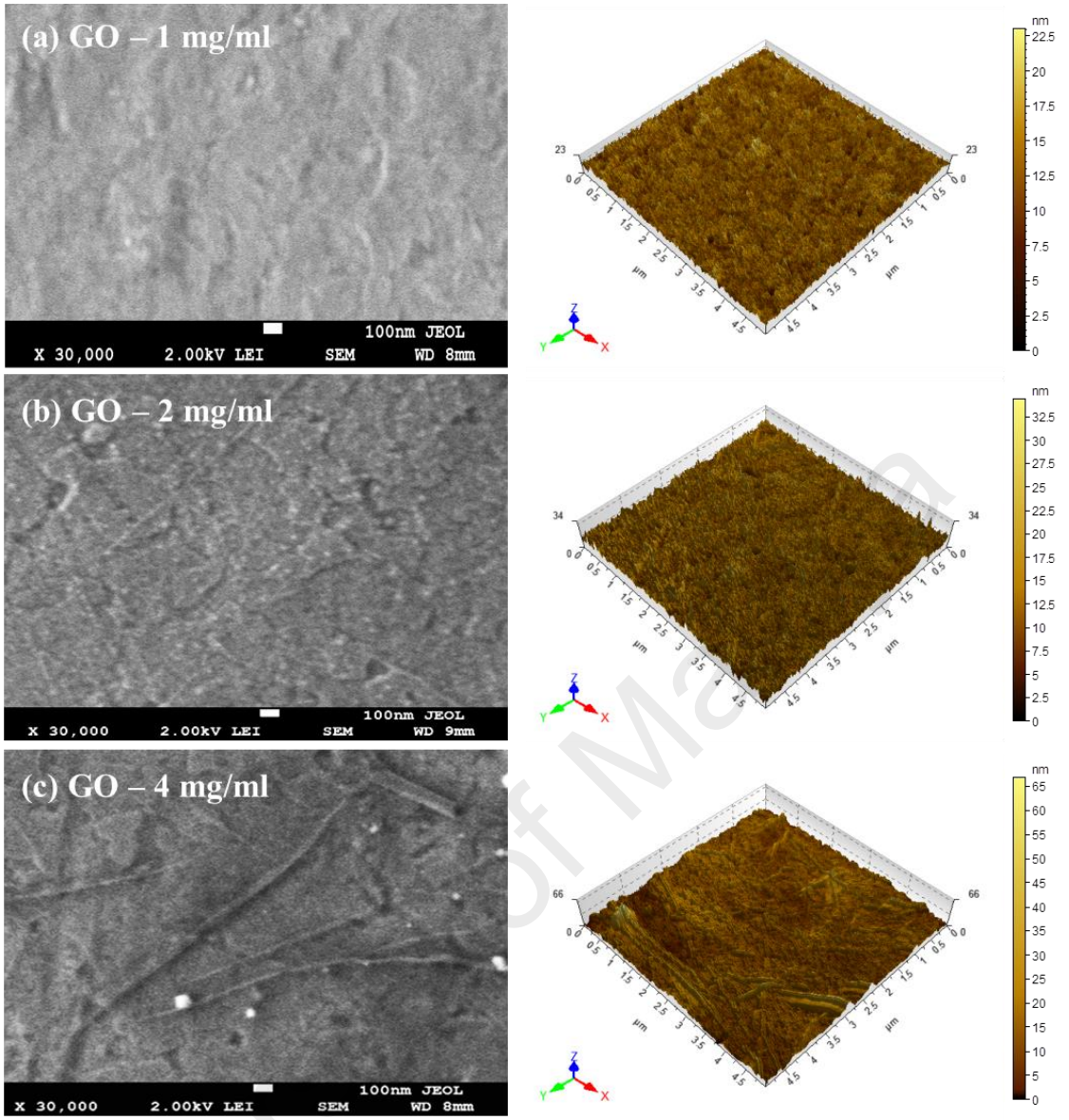

Figure 5.3: AFM topography image and SEM surface scan of GO films at the concentration of (a) 1 mg/ml (b) 2 mg/ml and (c) 4 mg/ml.

5.4.2 Photovoltaic Performance

The OSCs devices have been characterized in dark conditions by Keithley source measure unit at low voltage range from -1 to 1 V in order to calculate the rectification ratio (*RR*) of each device. *RR* values were calculated by obtaining the ratio of the forward current to the reverse current at a certain applied voltage, i.e. I_F/I_R. Figure 5.4a shows rectification behavior of each device and it is observed that the OSCs with the thinnest GO layer produced by 1 mg/ml GO solution exhibited the highest RR;

while the OSC with thickest GO HTL formed from 4 mg/ml GO solution showed lowest RR than the others. This indicates that an asymmetry current density – voltage (*J-V*) characteristic is increased with the decreasing GO concentration as well as the thickness as HTL in OSCs.

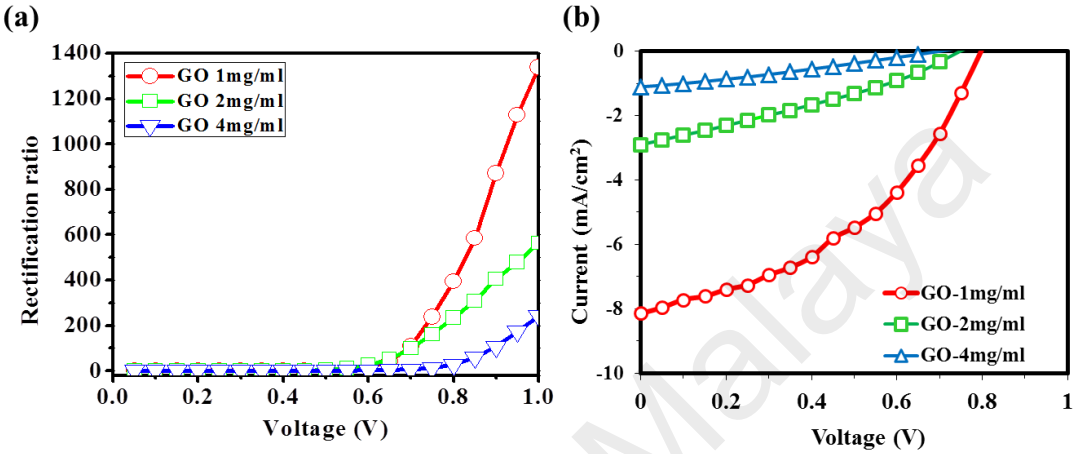

Figure 5.4: (a) Rectification ratio of the OSCs with GO HTL variant and (b) *J-V* characteristics of the devices fabricated with GO based HTLs of varied concentration at 1, 2 and 4 mg/ml.

Figure 5.4(b) represents the *J-V* characteristics under illumination of the OSCs fabricated with GO HTLs of varied concentration, consequently the varied thickness also, and performance characteristics of the devices are summarized in Table 5.1. A clear trend of decreasing in PCE with increasing GO concentration and film thickness can be observed. The lowest concentration (1 mg/ml) and thinnest HTL yielded the best results and all solar cells parameters were improved as compared to its high concentration and thicker HTL variants. The improved PCE is mainly attributed to the substantially increased short circuit current (J_{sc}), and comparatively improved open circuit voltage (V_{oc}) as well as fill factor (*FF*). In addition, the enhanced performance is also attributed to smooth surface morphology and decreased R_s as compared to the HTL of higher concentration. The performance of high concentration HTLs is substantially

decreased, most likely due to the significant increase in R_s resulting in substantially lower J_{sc} and slightly lower transmittance of the film with thickness of ~10 nm, moreover, V_{oc} and *FF* also comparatively decreased.

Table 5.1: OSCs photovoltaic performance parameters for GO HTL variants of 1, 2 and 4 mg/ml concentration calculated under illumination and their series resistance(R_s).

GO HTL Concentration	**J_{sc} (mA/cm^2)**	**V_{oc} (V)**	**FF**	**η (%)**	**R_s(Ω/cm^2)**
1 mg/ml	8.14	0.80	0.42	2.73	6.89
2 mg/ml	2.90	0.74	0.31	0.67	9.54
4 mg/ml	1.10	0.65	0.31	0.22	11.51

Experimental results show that device fabricated with GO HTL at concentration of 1mg/ml demonstrated best performance. The optimized thickness of GO HTL is about 1-3 nm in this work. However, it still lacks the full coverage of ITO and excessive voids and openings will weaken the charge extraction ability of HTL due to direct contact of ITO with that of photo-active layer. When high concentration and consequently thicker HTL is used, the R_s value is observed to increase significantly and reduce the device performance greatly. Performance of the OSCs fabricated with GO HTL could be enhanced by optimizing the concentration as well as the surface morphology and thickness of HTL. In general, an ultrathin GO HTL with full coverage of ITO surface would yield a high performance. Moreover, we can reduce the band-gap between GO and photoactive layer by introducing conventional PEDOT:PSS interfacial layer between GO and PCDTBT:$PC_{71}BM$ photo-active layer to form a bi-layer HTL structure that would facilitate the transportation of charges towards the ITO. PEDOT:PSS with the band-gap of 5.1 eV will provide a very good ascending step for the holes to hop.

5.5 Conclusions

In summary, it is demonstrated that the ultrathin GO films (thickness = 1-3 nm) processed from aqueous dispersion at concentration of 1 mg/ml are a promising candidate for HTLs in OSCs as compared to their high concentration variant HTLs. However, HTL concentration and thickness are two critical parameters which are needed to be optimized for enhanced performance. The decay in device performance is observed to be mainly driven through a substantial decrease in J_{sc} and a significant increase in the R_s values at higher concentrations. Moreover, the V_{oc}, FF and PCE also reduced as a function of increasing concentration. The efficiency values obtained in our results are slightly lower than the previously reported data, however, owing to the advantage of solution processability, nonacidic nature (contrary to PEDOT:PSS), suitable electrical and optical properties of GO thin films as an HTL indicate its promising future. For the further optimization of OSCs, development of a novel composite of GO with that of PEDOT:PSS and metal oxide is currently underway.

CHAPTER 6: SIGNIFICANTLY IMPROVED PHOTOVOLTAIC PERFORMANCE IN POLYMER BULK HETEROJUNCTION SOLAR CELLS WITH GRAPHENE OXIDE /PEDOT:PSS DOUBLE DECKED HOLE TRANSPORT LAYER[5]

6.1 Overview

This work demonstrates the high performance graphene oxide (GO) / PEDOT:PSS doubled decked hole transport layer (HTL) in the PCDTBT:$PC_{71}BM$ based bulk heterojunction organic photovoltaic device. The devices were tested on merits of their power conversion efficiency (PCE), reproducibility, stability and further compared with the devices with individual GO or PEDOT:PSS HTLs. Solar cells employing GO/PEDOT:PSS HTL yielded a PCE of 4.28% as compared to either of individual GO or PEDOT:PSS HTLs where they demonstrated PCEs of 2.77 and 3.57%, respectively. In case of single GO HTL, an inhomogeneous coating of ITO caused the poor performance whereas PEDOT:PSS is known to be hygroscopic and acidic which upon direct contact with ITO reduced the device performance. The improvement in the photovoltaic performance is mainly ascribed to the increased charge carriers mobility, short circuit current, open circuit voltage, fill factor, and decreased series resistance. The well matched work function of GO and PEDOT:PSS is likely to facilitate the charge transportation and an overall reduction in the series resistance. Moreover, GO could effectively block the electrons due to its large band-gap of ~ 3.6 eV, leading to an increased shunt resistance. In addition, the improvement in the reproducibility and stability has also been observed.

---

[5] **The work presented in Chapter 6 has been published in Nature: "Scientific Reports (Rank: Q1, Impact Factor: 5.23)" as**

Rafique et al. (2017). Significantly improved photovoltaic performance in polymer bulk heterojunction solar cells with graphene oxide/PEDOT:PSS double decked hole transport layer. *Scientific Reports, 7*(39555), 1-10.

6.2 Introduction

Organic photovoltaic devices (OPVs) employing donor-acceptor BHJ structure are considered promising next generation solar cells due to their advantages over traditional counterparts, including lower costs, increased flexibility, lighter weight plus solution processed R2R production compatibility (Kanwat & Jang, 2014; Pan et al., 2016; Rafique et al., 2016). Although this class of solar cells has seen significant progress, further development in both efficiency as well as stability are still needed for their widespread commercial applications (Savagatrup et al., 2015). During recent years, considerable research has been focused on interfacial engineering of OPVs, in particular, on the introduction of an interfacial layer between ITO anode and a photo-active layer that could facilitate the transport of holes, blocking of electrons and reduce the charge recombination and leakage (Duan et al., 2013; Lattante, 2014). This layer is often termed as HTL.

PEDOT:PSS is regarded as state of the art HTL which is being used as a standard material for BHJ OPVs because of its high work function, easy solution process-ability, high conductivity and high optical transmittance (Lee et al., 2014; Vitoratos et al., 2009). However, owing to the highly acidic and hygroscopic nature of PEDOT:PSS, it favors the device degradation in number of ways (Jagadamma et al., 2014; Norrman et al., 2010). The chemical interaction between PEDOT:PSS and ITO causes the corrosion of ITO which gives rise to severe instability in device performance (Ecker et al., 2011). In addition, it absorbs the oxygen and water from the air which further penetrate to subsequent layers to eventually reduce the device performance (Kanwat & Jang, 2014). Therefore, research has been focused to either replace or improve PEDOT:PSS by introducing inorganic semiconductors such as V_2O_5 (Chen et al., 2011; Zilberberg et al., 2011), NiO (Wang et al., 2014), WO_3 (Chen et al., 2012) or MoO_3, (Xie et al., 2013) among others, to address the reliability issues related to

PEDOT:PSS. However, deposition of these oxide materials normally involves intensive costs related to high vacuum techniques which are incompatible with the large scale roll to roll OSCs production.

In this context, solution processed aqueous dispersion of GO has been recently used by several groups as an HTL material for ITO anode (Jeon et al., 2014; Liu et al., 2012; Stratakis et al., 2014). GO is the derivative of one atom thick graphene comprises of hydroxyl (OH) and epoxy group on its basal plane and carboxyl groups (COOH) at the edge (Ding et al., 2015). GO, in aqueous dispersion, exhibits a unique heterogeneous electronic structure due to the presence of mixed sp^2 and sp^3 hybridizations (Loh et al., 2010). However, it lacks good Ohmic contact due to its insulating properties (Yu et al., 2014). Moreover, it is difficult to obtain the full coverage coating of GO at a time. Therefore, recently combination of GO and PEDOT:PSS have been reported to effectively work as an HTL in OSCs. It is reported that use of a thin layer of GO underneath PEDOT:PSS can effectively prevent corrosion of ITO and its further diffusion into the photoactive layer (Dehsari et al., 2014). Lee et al. in their recent work on planar heterojunction perovskite solar cells, used GO/PEDOT:PSS HTL structure to obtain a stable device with power conversion efficiency (PCE) of 9.74 % (Lee et al., 2016). Similarly, Yu et al. demonstrated highly efficient polymer light emitting diodes (PLEDs) and OSCs with GO and PEDOT:PSS composite layer as an HTL (Yu et al., 2014). Park et al. used GO/PEDOT:PSS bi-layer HTL in P3HT:PCBM based BHJ OSCs and demonstrated a PCE of 3.53% (Park et al., 2012). In this context, PCDTBT: $PC_{71}BM$ photoactive blend layer in BHJ OSCs has been used during this study. PCDTBT, as donor polymer, is expected to yield high efficiency and photo-current generation due to its faster charge carrier generation capability and different recombination dynamics as compared to P3HT (Banerji et al.,

2010; Etzold et al., 2011; Wang et al., 2012). In addition, PCDTBT WF matches well with that of GO and PEDOT:PSS as compared to P3HT.

In the present study, findings suggest the enhanced efficiency of PCDTBT:$PC_{71}BM$ based OPVs, using a solution processed GO/PEDOT:PSS double decked layer as an HTL. It is suggested that combination of GO/PEDOT:PSS as an HTL may complement the shortcomings of either of individual materials. GO in combination with PEDOT:PSS as an HTL exhibited a high efficiency and stability as compared to either of single PEDOT:PSS or GO HTLs. This study investigated the electrical, optical, chemical and morphological properties and their effects on the performance of the OPVs.

6.3 Materials and Methods

6.3.1 Materials

PEDOT:PSS aqueous suspension (PH1000) was purchased from H.C. Starck and used as received. Both PCDTBT and $PC_{71}BM$ have been purchased from Lumtec, Taiwan. Pre-patterned ITO-coated glass substrates with a sheet resistance of 15 Ω per square were purchased from Ossila, UK. Graphite flakes has been purchased from Asbury Inc. (USA). Potassium permanganate ($KMnO_4$, >99%), sulphuric acid (H_2SO_4, 98%), phosphoric acid (H_3PO_4, 98%), and hydrochloric acid (HCl, 35%) for GO synthesis, were obtained from R & M Chemicals. All other necessary chemicals such as chloroform etc. were purchased commercially and used as received without further purification.

6.3.2 Synthesis of GO

In the present study, GO was synthesized following a simplified hummers method (Ming, 2010). Namely, graphite flakes, H_3PO_4, H_2SO_4, and $KMnO_4$ were mixed in an appropriate amount at room temperature by using a magnetic stirrer. The mixture

was kept on stirring for about 72 h so that complete oxidation of the graphite could be achieved. After oxidation of graphite, H_2O_2 solution along with ice was used to stop the oxidation. The synthesized GO was subjected to washing for three times with 1 M of HCl aqueous suspension and several times with DI water to achieve a neutral pH. During washing process with DI water, the exfoliation of GO was experienced, which resulted in formation of thick brown GO solution and finally followed by the emergence of the GO gel. The concentration of obtained GO gel was determined for further studies.

6.3.3 Device Fabrication Procedure

Pre-patterned ITO coated glass substrates were cleaned with consecutive ultrasonic agitation in acetone, isopropyl alcohol (IPA) and DI water for 20 minutes each. The substrates after drying with nitrogen stream were subjected to oxygen plasma treatment to form a hydrophilic surface state. The GO aqueous solution was prepared at the concentration of 1 mg/ml in DI water, while, PEDOT:PSS solution was filtered by using 0.45 µm PTFE filters (Whatman, Germany). The doubled decked (GO/PEDOT:PSS) HTLs were deposited by sequential spin coating of GO and PEDOT:PSS at 6000rpm for 60 seconds onto the ITO coated substrates and post-annealed at 150 °C for 5 min in ambient room conditions. For the performance comparison, individual GO and PEDOT:PSS HTLs were also deposited and annealed at the same conditions. To perform further fabrication steps, all the materials and substrates were transferred to nitrogen (N_2) filled glove box. To fabricate the photo-active layer, both PCDTBT (donor) and $PC_{71}BM$ (acceptor) were dissolved in chloroform at the concentration of 10mg/ml by vigorous stirring overnight and further mixed at the ratio of 1: 4, respectively. The prepared blend was first filtered by 0.25 µm PTFE filters and then spun coated at an optimized speed of 2000 rpm for 60 s onto PEDOT:PSS, GO and GO/PEDOT:PSS HTLs. Next, Al electrodes were thermally evaporated onto the active layer through shadow masks under vacuum with the pressure

of 10^{-6} Torr. Thereafter, the fabricated devices were encapsulated with glass covering the active area by using UV-curable epoxy for the characterizations in the air.

6.3.4 Instrumentations

The surface morphologies of the all three types of HTLs were analyzed by atomic force microscopy (AFM) using tapping mode of Agilent Technologies 5500 Scanning Probe Microscope. Cross-section images were taken by field emission scanning electrons microscopy (Hitachi, SU8220 Scanning Electron Microscope). Raman spectra of all types of HTLs were measured by a DXR Raman Microscope (Thermo Scientific, USA), by using green light excitation (532 nm) laser source with 6 mW power. Optical properties were measured by a Perkin Elmer UV-visible diffuse reflectance spectrophotometer (Lambda 650) in the range of 250–800 nm. XPS analysis of prepared GO was carried out by PHI 5000 Versa Probe Scanning ESCA Microprobe (PHI 5000 Versa Probe II, USA), equipped with monochromatic Al-Kα ($h\nu$ = 1486.6 eV) X-ray source. The curve fittings for core level spectrum was performed by using Multipack software (VERSION 9, ULVAC-PHI, Inc. Japan) which allows the deconvolution of each spectrum into the individual fitting of mixed Gaussian-Lorentzian components.

Current density-voltage (*J-V*) characteristics of OPVs were measured using a Keithley 236 (Keithley Co.) source measurement unit. Photovoltaic performance was measured by using an Air Mass 1.5 Global (AM 1.5 G) solar simulator with an irradiation intensity of 100 mW/cm^2. The light intensity was calibrated using a Newport power meter 1918-R with calibrated Si-detector 818-UV.

6.4 Results and Discussion

In the present study, the BHJ OPVs were fabricated with single GO, PEDOT:PSS and double decked GO/PEDOT:PSS as HTLs. GO possesses several

unique advantages, including its tunable energy levels, facile solution processed, low cost synthesis, its two-dimensional structure and easy functionalization(Liu et al., 2014). However, it is essential to fully cover the ITO surface with a uniform and very thin layer to achieve an optimum performance with a GO HTL. Moreover, post deposition annealing is also recommended to remove the oxygen function groups and consequently the electrical properties of GO could be improved (Jeon et al., 2014). It is difficult to deposit highly uniform thin layer of GO with full coverage of ITO surface. As a result, poor holes extraction to ITO anode can be expected because of the direct contact of BHJ photo-active layer with the ITO at the uncovered regions. In addition, non-uniform surface coverage by GO may also lead to inhomogeneous electrical properties yielding a poor reliability of the device performance (Lee et al., 2016). Similarly, standard PEDOT:PSS HTL also exhibits severe stability issues. To address these point, low temperature (150 °C) solution processed approach to fabricate BHJ OPVs with sequential spin coating of GO and PEDOT:PSS was used and compared with that of individual GO or PEDOT:PSS HTLs on merit of their efficiency, reproducibility and stability. The schematic of the current work is presented in Figure 6.1.

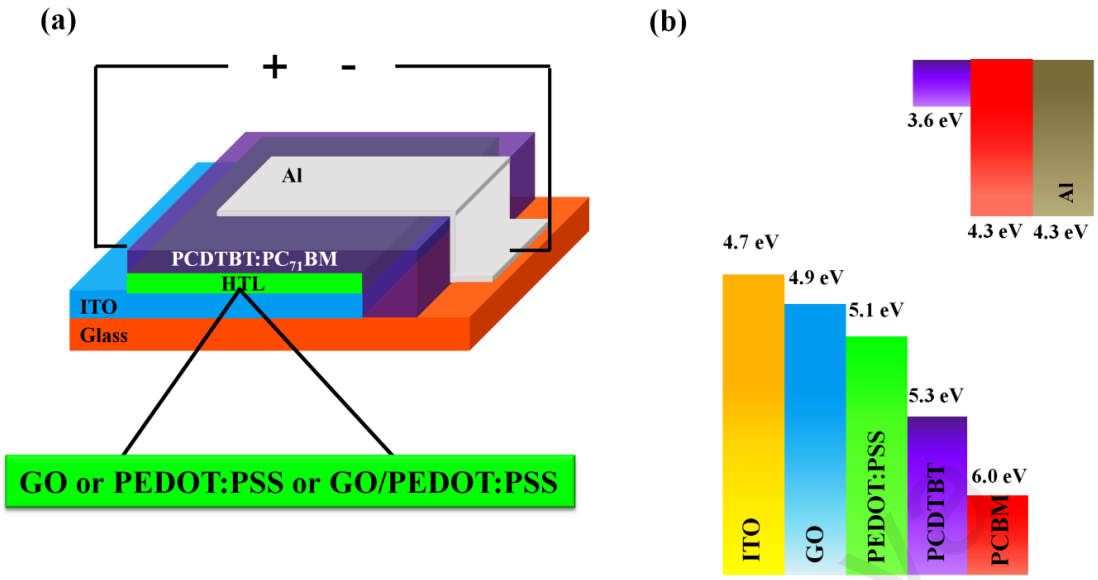

Figure 6.1: (a) Schematic illustration of the BHJ OPVs with GO, PEDOT:PSS and GO/PEDOT:PSS HTLs and (b) The energy band diagram showing the energy levels of all the materials used in OPVs of current study.

6.4.1 Spectroscopic Characterizations

The optical and structural properties of each HTL deposited on ITO coated glass substrates have been investigated prior to device fabrication. Transmittance spectra of all three types of HTLs along with bare ITO are shown in Figure 6.2(a). These layers show high transmittance in the overall wavelength range of more than 87%. The optical transparency of HTLs is very important in order to absorb maximum light by photo-active layer. It can be observed that the transmittance spectra of the ITO/PEDOT:PSS and ITO/GO/PEDOT:PSS is almost 15% higher compared with the transmittance of pristine ITO and ITO/GO in the region of ~ 400-500 nm. However, no pronounced change in transmittance spectra for any of the HTLs is observed in the overall wavelength region except the aforementioned wavelength range. The observed difference of transmittance in the ~ 400-500 nm region could potentially bring a significant effect on the photo-generated current (J_{sc}) of the device and hence the better

efficiency is expected in case of ITO/PEDOT:PSS and ITO/GO/PEDOT:PSS, in good agreement with the photovoltaic studies of the corresponding devices.

Raman spectroscopy is the most commonly used non-destructive technique to analyze the quality and structure of the carbon based materials, in particular, it is being used to investigate the defects and ordered and disordered structures of graphene (Some et al., 2013). Raman spectrum was collected for GO/PEDOT:PSS double decked structure as shown in Figure 6.2(b). For comparison, the spectra of single GO and PEDOT:PSS HTLs were also collected. Raman spectrum for single GO HTL shows both D and G bands appearing at 1350 and 1600 $cm^{-1,}$ respectively. It is well known that D band appearing in the range of 1200 to 1500 cm^{-1} corresponds to structural defects and partially disordered structures of the sp^2 domains, whereas, G band appearing from 1500 to 1600 cm^{-1} is associated with E_{2g} - vibration mode of sp^2 carbon (Some et al., 2013; Zhang et al., 2014). The wide band towards high frequency end of the spectrum features three peaks at around 2720, 2930 and 3190 cm^{-1}. The peak at 2790 cm^{-1} is corresponding to an overtone of D band and attributed as 2D band, whereas, the peak at 2930 cm^{-1} arise from contribution of both D and G bands and often termed as D+G band (Bajpai et al., 2012; Delgado et al., 2008). The shoulder peak at ~ 3190 cm^{-1} also ascribes to an overtone of D band (2D). The Raman spectrum for GO/PEDOT:PSS films also illustrated D and G bands but with significantly decreased intensity of the peaks as shown in Figure 6.2b. In addition, the spectrum is featured with some bands from PEDOT:PSS polymer in low frequency range between 500 to 1100 cm^{-1} which confirms the method efficacy of double decked layer fabrication. The GO/PEDOT:PSS HTL also features the 2D, D+G and 2D bands at 2700, 2930 and 3170 cm^{-1} but with significantly low intensity as compared to pure GO films. The Raman spectrum for PEDOT:PSS HTL shown in Figure 6.2(c) exhibits Raman finger prints for PEDOT and PSS. Most of the peaks are attributed to PEDOT and negligible contribution of PSS is

observed in the spectrum, in good agreement with previously reported data (Rafique et al., 2016; Sakamoto et al., 2005). A strong vibrational band observed at 1440 cm^{-1} is attributed to PEDOT and related to symmetric $C\alpha = C_\beta$ (- O) stretching mode. In addition, the following bands are related to PEDOT vibrational modes such as: 1562 cm^{-1} is ascribed to $C\alpha = C_\beta$ asymmetrical stretching, 1364 cm^{-1} to C_β - C_β stretching deformations and 1255 cm^{-1} to C_α - C_α inter-ring stretching vibrations (Chang et al., 2014; Farah et al., 2012). The peaks at 986 and 573 cm^{-1} correspond to the oxyethylene ring deformation (Teng et al., 2013).

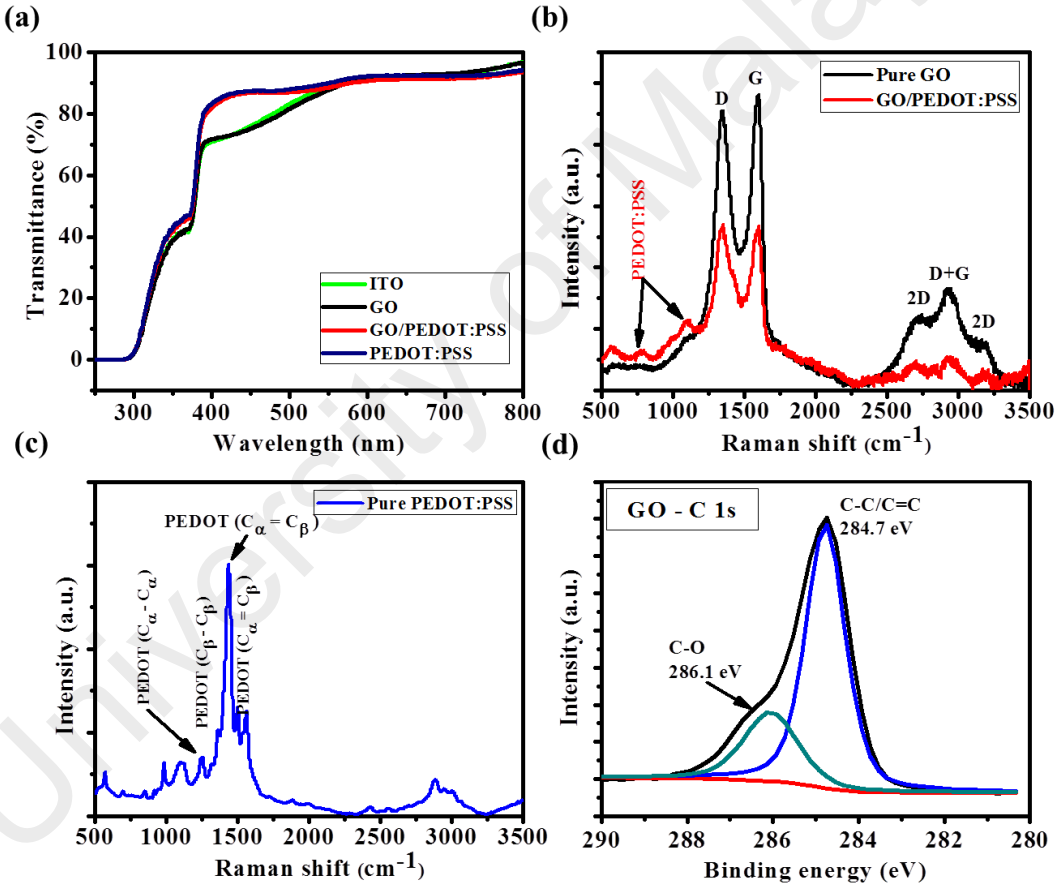

Figure 6.2: (a) Transmittance of GO, PEDOT:PSS and GO/PEDOT:PSS films deposited on ITO coated substrate and that of bare ITO substrate. (b) Raman spectra for GO, GO/PEDOT:PSS and (c) PEDOT:PSS HTLs. (d) Deconvoluted XPS C 1s spectrum of GO.

The core level XPS C 1s spectrum of the GO presented in Figure 6.2(d) is decomposed into two components, the sharp and high intensity peak at 284.7 eV is ascribed to sp^2 carbon aromatic rings (C-C/C=C) and relatively low intensity peak at 286.1 eV corresponds to C-O bond (Some et al., 2013; Wang et al., 2014). These peaks confirm the presence of carbon atoms in different functional groups , i.e. the non-oxygenated rings and oxygen related functional groups (Kim et al., 2015; Some et al., 2012).

6.4.2 Morphological Study of HTLs

Film morphology of an HTL significantly influences the electrical properties of the device, in particular, the R_s and shunt resistance (R_{sh}). In general, a smooth and fully-covered HTL morphology may induce a higher R_{sh} and low R_s which is highly desirable to enhance the performance of OSCs (Jeon et al., 2014). It is therefore vital to control the morphology of the HTLs. In the present study, the AFM topography images of the all three HTLs on ITO were taken as shown in Figure 6.3. RMS roughness values of GO, PEDOT:PSS and GO/PEDOT:PSS films in an area of 5 μm × 5μm were calculated to be 2.88, 1.56 and 1.99 nm, respectively. As compared to the recently reported results (3.2 nm) for spin coated GO films (Lee et al., 2016), the RMS roughness of our samples is comparatively improved but it is still significantly higher than PEDOT:PSS HTL. The single GO HTL is inhomogeneous with overlapping GO flakes across the surface as visible in AFM image (Figure 6.3(a)) and could not cover the ITO surface with high uniformity. Consequently, the non-uniform and overlapping GO flakes could suppress the transportation of holes while the uncovered areas may lead to direct contact of ITO and photo-active layer and hence the performance of OSCs with GO as HTLs could significantly reduce (Ding et al., 2015). By applying PEDOT:PSS on GO (GO/PEDOT:PSS HTL), RMS roughness reduced to 1.99 nm

(Figure 6.3e), comparable with single PEDOT:PSS (Figure 6.3c), which indicate that deposition of PEDOT:PSS on GO results in smoothening of the irregular GO surface.

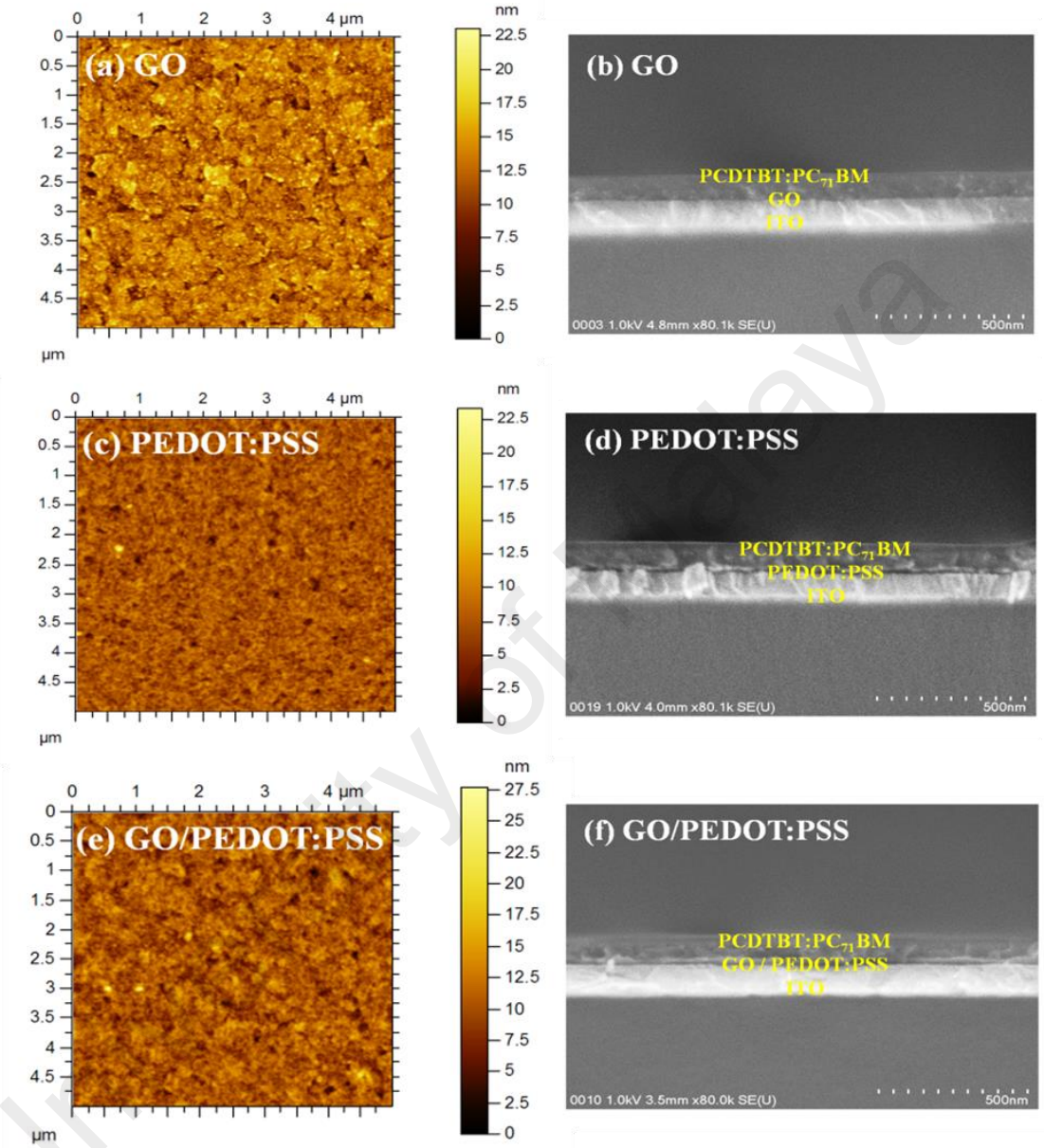

Figure 6.3: The AFM surface topography images and SEM cross-sectional images with complete device, of (a, b) GO (c, d) PEDOT:PSS and (e, f) GO/PEDOT:PSS HTLs.

Figure 6.3 shows cross-sectional SEM images of the solar cells fabricated with each of the GO, PEDOT:PSS (Figure 6.3d) and GO/PEDOT:PSS (Figure 6.3f) HTLs. The thickness of PCDTBT:$PC_{71}BM$ were observed to be uniform (approx. 75 nm) regardless of the HTLs. The single GO film was very thin (around 1-3 nm) to distinguish as shown in Figure 6.3(c). The thickness of both PEDOT:PSS and GO/PEDOT:PSS HTLs was approximately the same and calculated to be around 30 nm.

6.4.3 Photovoltaic Characteristics

In order to analyze the photovoltaic characteristics, it is important to explain the role of HTL during the OPVs operation. In normal architecture BHJ OSCs, the photo-active layer is irradiated with solar light via ITO/HTL bottom electrode side, while the active layer absorbs the solar light (photons) and generates electrons- holes pairs, the so-called excitons. Further, these excitons dissociate into the electrons in the lowest unoccupied molecular orbital (LUMO) and holes in the highest occupied molecular orbital (HOMO), at the donor-acceptor interface. Therefore, the HOMO level of the donor polymer should match well with the work-function of HTL to facilitate the transportation of holes through HTLs to the anode (Stratakis et al., 2014). In this context, PCDTBT with the HOMO of 5.3 eV was utilized along with the GO/PEDOT:PSS HTL. The device with PCDTBT as donor polymer provides better holes extraction since energy levels from PCDTBT/ PEDOT:PSS/ GO/ ITO provide good ascending steps for the holes to hop. The energy level diagram for each element used in this study and the device structure is presented in Figure 6.1. Reference devices with only GO and PEDOT:PSS as an HTL were also fabricated for comparison. In addition, the performance of GO is somehow thickness dependent and one can achieve an optimum performance with the GO layer of 1-3 nm (Li et al., 2010). Therefore, the thickness and concentration of GO were optimized, and with the spinning conditions

described in the experimental section, a layer of approximately 1-3 nm was obtained as shown in Figure 6.4(a).

Figure 6.4(b) shows the typical current density-voltage (*J-V*) characteristics under illumination of the PCDTBT:$PC_{71}BM$ OSC devices with GO, PEDOT:PSS and GO/PEDOT:PSS as the HTLs, and the corresponding extracted device parameters are summarized in Table 6.1. As shown in *J-V* curves, the devices using the GO/PEDOT:PSS double decked HTL showed superior performance as compared to the individual GO or PEDOT:PSS HTLs with a V_{oc} of 0.82 V, a J_{sc} of 10.44 mA/cm^2 , *FF* of 0.50 and a *PCE* (η) of 4.28 %. In comparison, the devices with only PEDOT:PSS as an HTL exhibited a relatively low performance with V_{oc} of 0.80 V, a J_{sc} of 9.49 mA/cm^2, a *FF* of 0.47 and an η of 3.57 %. Whereas, the device with single GO exhibited poor performance with a V_{oc} of 0.80 V, a J_{sc} of 7.90 mA/cm^{2,} a *FF* of 0.44 and a *PCE* of 2.77 %. Relatively poor performance of the devices with individual GO HTL is mainly attributed to inhomogeneous GO layer with high surface roughness that lead to suppression and an inefficient transportation of holes. As a result, the device efficiency is significantly reduced. For the devices based on GO/PEDOT:PSS HTL, the improvement is attributable to high J_{sc}, *FF* and V_{oc} values as compared to either of GO or PEDOT:PSS HTLs. Additionally, the GO/PEDOT:PSS HTL also exhibited reduced R_s than GO or PEDOT:PSS single HTLs, as shown in Figure 6.4(c). Relatively low R_s value in case of GO/PEDOT:PSS HTL suggest the better charge transportation ability of the double decked structure as compared to single GO and PEDOT:PSS based devices. As discussed above and presented in the energy diagram in Figure 6.1, the WF of GO (4.9 eV) matches well with PEDOT:PSS (5.1 eV) which likely results in an efficient charge extraction and transportation to ITO. Moreover, GO could effectively block the electrons owing to its large band-gap of ~ 3.6 eV (Lee et al., 2016).

Table 6.1: Device photovoltaic performance characteristics of PCDTBT:$PC_{71}BM$ OPVs incorporating GO, PEDOT:PSS and GO/PEDOT:PSS as the HTLs.

Anode interlayer	J_{sc} (mA/cm^2)	V_{oc} (V)	*FF*	Mobility, μ (cm^2/Vs)	η (%)
GO	7.90	0.80	0.44	4.04 x 10^{-4}	2.77
PEDOT:PSS	9.49	0.80	0.47	3.78 x 10^{-4}	3.57
GO/PEDOT:PSS	10.44	0.82	0.50	7.47 x 10^{-4}	4.28

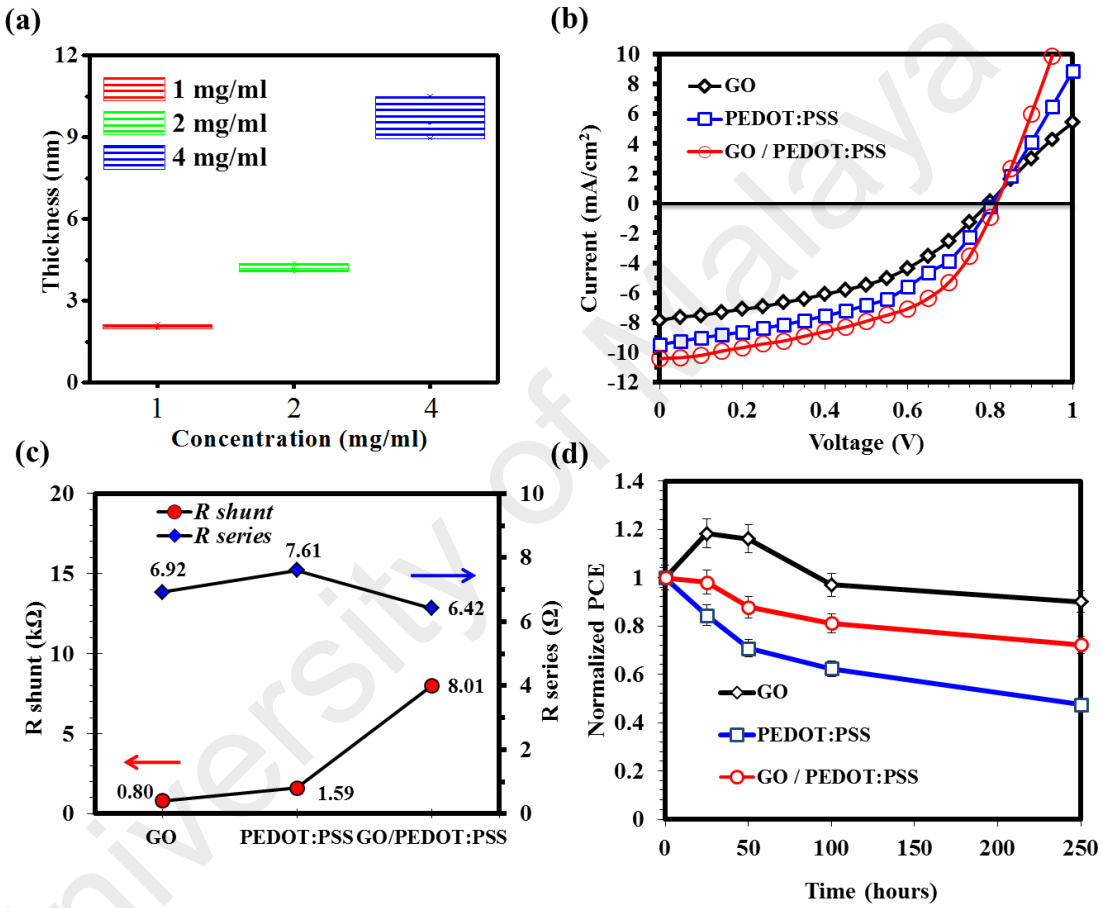

Figure 6.4: (a) Thickness *vs* concentration plots for GO. (b) *J-V* characteristics of OPVs with GO, PEDOT:PSS and GO/PEDOT:PSS as an HTL. (c) R_{sh} and R_s calculated from *J-V* curves under illumination conditions. (d) Stability test of OPVs over 250 h.

Since operational stability of the OPVs is one of the most important factors for their widespread commercialization, therefore, the operational stability of all type of HTLs was explored. Figure 6.4(d) shows the decay in PCE as a function of exposure

time in ambient atmosphere. The devices with single GO HTLs or with GO/PEDOT:PSS HTLs showed better stability as compared to single PEDOT:PSS HTLs in which the efficiency decreased to more than 50% of initial value. The instability in the PEDOT:PSS HTL is attributed to corrosion of indium due to acidic nature of PEDOT:PSS with high pH value (Wong et al., 2002). With the passage of time indium diffuses into the HTL and further to active layer which causes severe damage to the device performance. The improved stability in case of single GO/PEDOT:PSS HTL is expected because a thin layer of GO underneath PEDOT:PSS serves as a barrier against the direct contact of PEDOT:PSS with ITO surface.

The effective carrier mobility or the so-called ambipolar mobility for all three devices was then determined by space-charge-limited-current (SLCL) method under positive voltage up to 10 V in dark. Figure 6.5 shows *log J* vs. *log V*, several conduction regimes have been identified from the plots based on their gradient values, such as: $I \sim V^1$ with slope 1 is an Ohmic regime, $I \sim V^2$ with slope 2 is an SCLC regime, while $I > V^2$ with slope > 2 is a trap regime. The ambipolar mobility has been calculated from the SCLC regime by the following equation:

$$J = \frac{9}{8}\varepsilon\varepsilon_o\mu\ \frac{V^2}{L^3} \quad \text{..... (6.1)}$$

Where J is the current density within the conduction regime, ε is the relative dielectric constant, ε_o is the vacuum permittivity, L is the active layer thickness, V the voltage within the conduction regime and μ represents the mobility (Yang et al., 2012). Figure 6.5 and Table 6.1 show the change of ambipolar mobility for the devices with GO, PEDOT:PSS and GO/PEDOT:PSS HTLs. The ambipolar mobility increased from 3.78 x 10^{-4} cm^2 V^{-1} s^{-1} in case of PEDOT:PSS HTL to 4.04 x 10^{-4} cm^2 V^{-1} s^{-1} for single GO HTL and finally to 7.47 x 10^{-4} cm^2 V^{-1} s^{-1} for the device with GO/PEDOT:PSS

double decked HTL, which is almost double of the either of the individual GO or PEDOT:PSS HTLs, and in good agreement with the PCEs of corresponding devices. A quantitative comparison of ambipolar mobility of the OSCs with GO, PEDOT:PSS and GO/PEDOT:PSS HTLs confirmed that use of GO/PEDOT:PSS layer promoted the charge carriers transportation and extraction, particularly the hole mobility, resulting in optimized photovoltaic performance (Yu et al., 2014). Since the only difference in the device architecture is the utilization of different HTLs therefore the increase in the accumulative charge carrier mobility is predominately due to the increased hole mobility using a GO/PEDOT:PSS double decked layer that can lead to balanced charge carrier transportation with an electron-blocking ability and a reduction of the suppression between the HTL and the active layer (Yu et al., 2014). Thus, OSCs with high PCEs were realized using GO/PEDOT:PSS double decked layer.

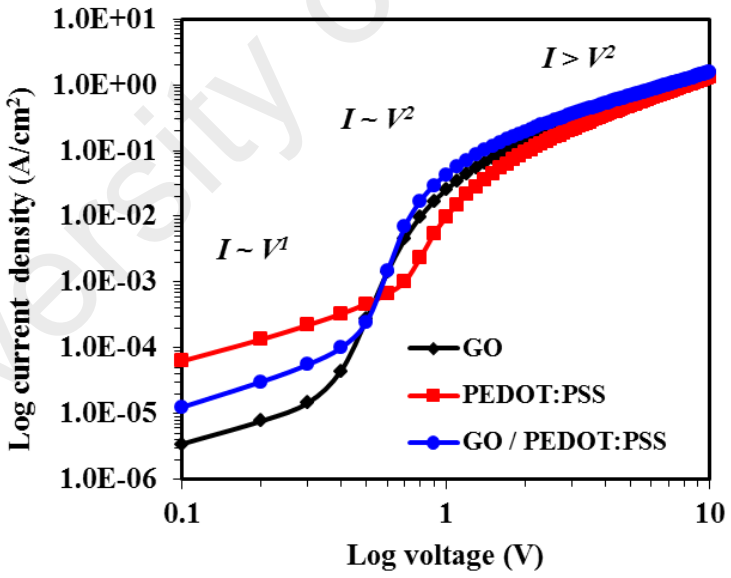

Figure 6.5: Double logarithmic characteristic (*Log V vs. log J*) exhibiting effective charge carrier mobility of PCDTBT:$PC_{71}BM$ based OPVs with GO, PEDOT:PSS and GO/PEDOT:PSS as the HTLs.

In order to confirm the reproducibility and reliability of the GO/ PEDOT:PSS HTLs, the important photovoltaic parameters were recorded and presented in Figure 6.6.

The GO/ PEDOT:PSS HTL exhibited fairly good reproducibility with minor variations in V_{oc}, J_{sc} and PCE. On the contrary, the device with GO HTL showed comparatively wide variations in V_{oc}. However, a relatively wider variation is observed in *FF* of all HTLs which could be attributed to the absence of ETL in our device structure.

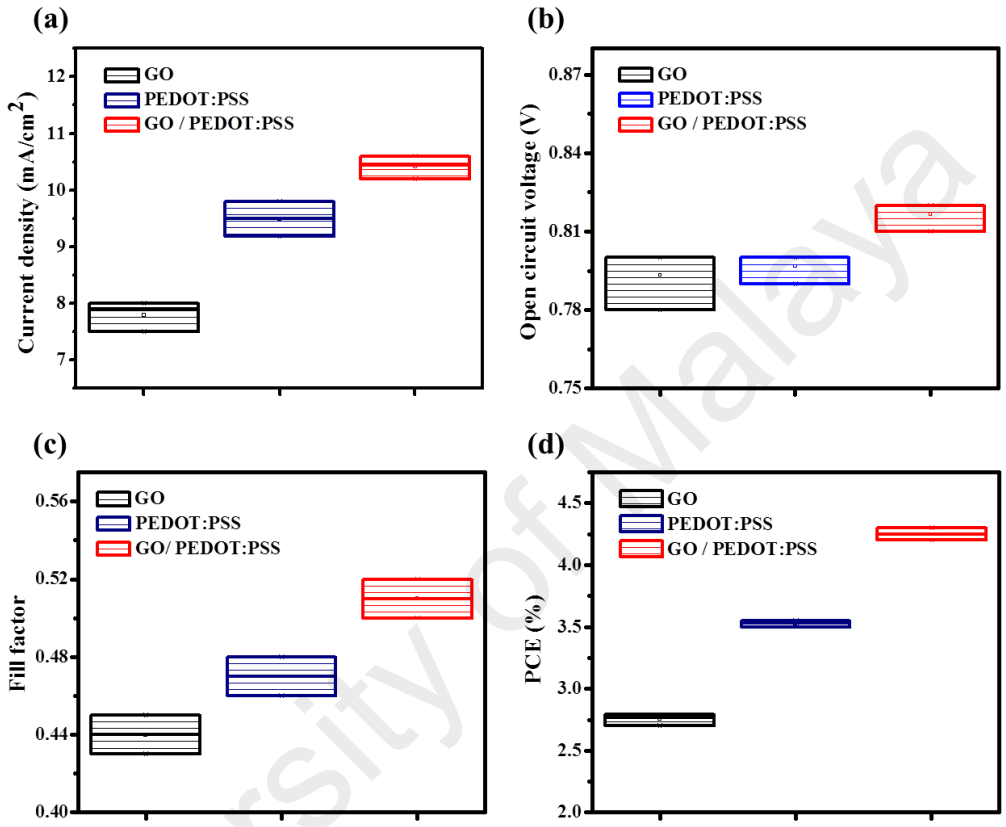

Figure 6.6: Photovoltaic performance parameters including (a) J_{sc} , (b) V_{oc} , (c) *FF* and (d) PCEs (%) of PCDTBT:$PC_{71}BM$ based OPVs with GO, PEDOT:PSS and GO/PEDOT:PSS as the HTLs.

The selection of double decked GO/PEDOT:PSS HTL played a vital role in the improved device efficiency and stability. It has been reported that use of either of individual GO or PEDOT:PSS as HTLs in OPVs may cause severe instability issues at the anode interface (Jørgensen et al., 2012; Lee et al., 2016).The hygroscopic and acidic PEDOT:PSS aqueous suspension could react with both the ITO as well as the photoactive layer. Similarly, single and ultrathin GO layer could cause a non-uniform

coating on ITO which would provide a direct contact of ITO and photoactive layer at the non-covered regions and drastically reduces the device performance. Interestingly, the combination of GO and PEDOT:PSS in a double decked structure is a compatible solution to compliment the drawbacks of both individual materials. To the best of my knowledge, there is no report on photovoltaic performance, reproducibility and stability of PCDTBT:$PC_{71}BM$ based devices with GO/ PEDOT:PSS double decked layer.

6.5 Conclusions

In summary, the performance, reproducibility and stability of GO/PEDOT:PSS double decked hole transport layers in PCDTBT:$PC_{71}BM$ based OPVs are reported. The GO/PEDOT:PSS is a promising candidate to replace conventional PEDOT:PSS or single GO HTLs by complimenting the drawbacks of both individual materials. The GO/PEDOT:PSS HTL retained its efficiency as well as reproducibility yielding a highly stable device. It demonstrated a J_{sc} = 10.44 mA/cm^2, V_{oc} = 0.82 V, FF =0.50, and PCE = 4.28 %. A well matched work function of GO/PEDOT:PSS = 4.9 eV/5.1 eV with that of PCDTBT (5.3 eV) donor material facilitates the hole transportation to ITO. The improved performance is also attributed to decreased R_s which are highly desired for carrier transportation and collection as evident from charge carrier's mobility results. Moreover, the high R_{sh} of GO also helps to suppress carrier recombination. Both parameters were calculated from *J-V* curves. GO is probably inducing effective blocking of electron due to its large band gap of ~ 3.6 eV. In addition to the reasonably improved efficiency, reproducibility and stability, the preparation of HTLs as well as photoactive layer are based on a facile, flexible and R2R compatible solution process, which remarkably simplifies the overall fabrication process and lowers the fabrication cost.

CHAPTER 7: CONCLUSIONS AND FUTURE CHALLANGES.

7.1 Conclusions

Organic photovoltaic materials open up the new pathways to develop solar cells modules based on a facile, solution processable and R2R compatible fabrication techniques. However, like any burgeoning OSC related technology there are several instability issues that need to be addressed to move beyond the laboratory. The biggest obstacles in their widespread commercialization are their low efficiencies and shorter life time as compared to that of already developed technologies. In this context, this PhD thesis successfully describes the degradation factors effecting device stability, and performance achievements of OSCs by overcoming the stability issues associated with the HTL. One crucial step was the identification of the degradation factors pertaining to device instability in ambient air, in particular related to the HTL. Further to address those factors by introducing organic-inorganic hybrid HTLs consisting of conventional PEDOT:PSS material along with V_2O_5 and/or GO. Moreover, a range of characterization techniques were presented, which have been used in the current work. It was shown that many characteristics such as device architecture, material combinations, ITO diffusion, oxygen ingress, concentration ratios and layer thicknesses can significantly affect the device performance. During this work, the overarching theme was to study metal oxides (V_2O_5) and/or GO in HTL of BHJ OSCs with the aim to ensure utilization of a facile, flexible, low cost and R2R compatible solution process, which remarkably simplifies the overall fabrication process. This dissertation can be subdivided into three major sections. A summary of each of the section is presented here followed by a brief outlook of the future challenges and strategies to follow-up the present work.

In the first step, stability and degradation issues pertaining to each layer of the normal architecture BHJ OSCs as a function of exposure time to ambient air were discussed. The BHJ OSCs were fabricated and their photovoltaic performance was evaluated. It was shown, that indium and oxygen diffusion are one of the main causes of device degradation which cause deterioration of chemical, optical, morphological and photovoltaic characteristics of the device. This study was mainly focused on identifying and addressing the stability constraints brought by PEDOT:PSS due to its acidic nature and instability issues due to device exposure in ambient atmosphere.

In the second set of experiments, the stability issues associated with the PEDOT:PSS were addressed, by incorporating V_2O_5 nanoparticles in the PEDOT:PSS HTL to develop an organic-inorganic hybrid HTL. The resultant device has significant improvement in stability while maintaining the efficiencies comparable to that of pristine PEDOT:PSS HTL.

In the third section, GO was utilized as an HTL in the PCDTBT:$PC_{71}BM$ based BHJ OSCs. At first, the GO concentration was optimized for the best photovoltaic performance. Further, the optimized concentration was utilized as an under-layer in GO/ PEDOT:PSS double decked HTL. The resultant devices were tested on the merits of their stability, efficiency and reproducibility and compared with those containing either of GO or PEDOT:PSS HTLs. The device with double decked HTL has successfully overcome the drawbacks of any of the individual GO or PEDOT:PSS HTL.

In conclusion, we optimized the fabrication parameters by adopting a facile and solution processable fabrication process by simply spin coating of HTL as well as photoactive layer. Degradation factors, particularly in context of HTL, were identified and successfully addressed by employing V_2O_5 and GO based HTLs. Moreover, the

operational stability of the OSCs have been remarkably improved by employing hybrid HTLs as compared to pristine PEDOT:PSS HTLs.

7.2 Future Challenges

There are a number of challenges that still need to be addressed to accomplish the current work, which were not possible to do within the frames of this study. In particular:

a) Further studies of metal oxides and/or GO have to be carried out to develop optimized processing conditions of the layers for the manufacturing of efficient OSCs. These optimized fabrication conditions for the metal oxides and/or GO can be implemented to manufacture tandem solar cells.
b) Degradation studies should be extended to develop optimized atmospheric chambers for an in-depth analysis of degradation factors such as humidity, oxygen, and electrode corrosion and diffusion etc.
c) Several important points should be addressed pertaining to device fabrication, stability and degradation study such as, improved buffered layers, proper encapsulation, high efficiency and stability, increased geometrical FF and fabrication of large scale R2R solar cell modules.

REFERENCES

Aluicio-Sarduy, E., Baidak, A., Vougioukalakis, G. C., & Keivanidis, P. E. (2014). Phosphorimetric characterization of solution-processed polymeric oxygen barriers for the encapsulation of organic electronics. *The Journal of Physical Chemistry C, 118*(5), 2361-2369.

Ameen, M. Y., Pradhan, S., Suresh, M. R., & Reddy, V. (2015). MoO_3 anode buffer layer for efficient and stable small molecular organic solar cells. *Optical Materials, 39*, 134-139.

Ameri, T., Dennler, G., Lungenschmied, C., & Brabec, C. J. (2009). Organic tandem solar cells: A review. *Energy & Environmental Science, 2*(4), 347-363.

Ameri, T., Khoram, P., Min, J., & Brabec, C. J. (2013). Organic ternary solar cells: A review. *Advanced Materials, 25*(31), 4245-4266.

An, Q., Zhang, F., Zhang, J., Tang, W., Deng, Z., & Hu, B. (2016). Versatile ternary organic solar cells: A critical review. *Energy & Environmental Science, 9*(2), 281-322.

Anderson, D., Goldemberg, J., & Johansson, T. B. (2004). *World Energy Assessment: Overview: 2004 Update*: United Nations Publications.

Armin, A., Velusamy, M., Wolfer, P., Zhang, Y., Burn, P. L., Meredith, P., & Pivrikas, A. (2014). Quantum efficiency of organic solar cells: Electro-optical cavity considerations. *ACS Photonics, 1*(3), 173-181.

Aslam, M., Ismail, I. M., Salah, N., Chandrasekaran, S., Qamar, M. T., & Hameed, A. (2015). Evaluation of sunlight induced structural changes and their effect on the photocatalytic activity of V_2O_5 for the degradation of phenols. *Journal of Hazardous Materials, 286*, 127-135.

Awartani, O., Lemanski, B. I., Ro, H. W., Richter, L. J., DeLongchamp, D. M., & O'Connor, B. T. (2013). Correlating stiffness, ductility, and morphology of polymer: fullerene films for solar cell applications. *Advanced Energy Materials, 3*(3), 399-406.

Aygül, U., Hintz, H., Egelhaaf, H.-J., Distler, A., Abb, S., Peisert, H., & Chassé, T. (2013). Energy level alignment of a P3HT/fullerene blend during the Initial steps of degradation. *The Journal of Physical Chemistry C, 117*(10), 4992-4998.

Badawy, W. A. (2015). A review on solar cells from Si-single crystals to porous materials and quantum dots. *Journal of Advanced Research, 6*(2), 123-132.

Bagnall, D. M., & Boreland, M. (2008). Photovoltaic technologies. *Energy Policy, 36*(12), 4390-4396.

Bailo, D., Generosi, A., Albertini, V. R., Caminiti, R., De Bettignies, R., & Paci, B. (2012). Time-resolved morphological study of 'PEDOT:PSS'hole transporting layer for polymer solar cells. *Synthetic Metals, 162*(9), 808-812.

Bajpai, R., Roy, S., Rafiee, J., Koratkar, N., & Misra, D. (2012). Graphene supported nickel nanoparticle as a viable replacement for platinum in dye sensitized solar cells. *Nanoscale, 4*(3), 926-930.

Banerji, N., Cowan, S., Leclerc, M., Vauthey, E., & Heeger, A. J. (2010). Exciton formation, relaxation, and decay in PCDTBT. *Journal of the American Chemical Society, 132*(49), 17459-17470.

Bao, Q., Liu, X., Braun, S., & Fahlman, M. (2014). Oxygen-and water-based degradation in [6, 6]-phenyl-C61-butyric acid methyl ester (PCBM) films. *Advanced Energy Materials, 4*(6). 1301272- 1301278.

Baranovskii, S., Cordes, H., Hensel, F., & Leising, G. (2000). Charge-carrier transport in disordered organic solids. *Physical Review B, 62*(12), 7934- 7938.

Bekci, D. R., & Erten-Ela, S. (2012). Effect of nanostructured ZnO cathode layer on the photovoltaic performance of inverted bulk heterojunction solar cells. *Renewable Energy, 43*, 378-382.

Bhushan, B. (2012). *Fundamentals of tribology and bridging the gap between the macro-and micro/nanoscales* (Vol. 10): Springer Science & Business Media.

Bin Mohd Yusoff, A. R., Kim, H. P., & Jang, J. (2014). High performance organic photovoltaics with zinc oxide and graphene oxide buffer layers. *Nanoscale, 6*(3), 1537-1544.

Blom, P. W., Mihailetchi, V. D., Koster, L. J. A., & Markov, D. E. (2007). Device physics of polymer: fullerene bulk heterojunction solar cells. *Advanced Materials, 19*(12), 1551-1566.

Blouin, N., Michaud, A., & Leclerc, M. (2007). A low-bandgap poly (2, 7-carbazole) derivative for use in high-performance solar cells. *Advanced Materials, 19*(17), 2295-2300.

Brabec, C. J., Cravino, A., Meissner, D., Sariciftci, N. S., Fromherz, T., Rispens, M. T., & Hummelen, J. C. (2001). Origin of the open circuit voltage of plastic solar cells. *Advanced Functional Materials, 11*(5), 374-380.

Brabec, C. J., Winder, C., Sariciftci, N. S., Hummelen, J. C., Dhanabalan, A., van Hal, P. A., & Janssen, R. A. (2002). A low-bandgap semiconducting polymer for photovoltaic devices and infrared emitting diodes. *Advanced Functional Materials, 12*(10), 709-712.

Bronstein, H., Chen, Z., Ashraf, R. S., Zhang, W., Du, J., Durrant, J. R., . . . & Geerts, Y. (2011). Thieno [3, 2-b] thiophene− diketopyrrolopyrrole-containing polymers for high-performance organic field-effect transistors and organic photovoltaic devices. *Journal of the American Chemical Society, 133*(10), 3272-3275.

Brown, G. F., & Wu, J. (2009). Third generation photovoltaics. *Laser & Photonics Reviews, 3*(4), 394-405.

Bruner, C., Miller, N. C., McGehee, M. D., & Dauskardt, R. H. (2013). Molecular intercalation and cohesion of organic bulk heterojunction photovoltaic devices. *Advanced Functional Materials, 23*(22), 2863-2871.

Bruner, C., Novoa, F., Dupont, S., & Dauskardt, R. (2014). Decohesion kinetics in polymer organic solar cells. *ACS Applied Materials & Interfaces, 6*(23), 21474-21483.

Bulavko, G., & Ishchenko, A. A. (2014). Organic bulk heterojunction photovoltaic structures: design, morphology and properties. *Russian Chemical Reviews, 83*(7), 575.

Bulle-Lieuwma, C., Van Gennip, W., Van Duren, J., Jonkheijm, P., Janssen, R., & Niemantsverdriet, J. (2003). Characterization of polymer solar cells by TOF-SIMS depth profiling. *Applied Surface Science, 203*, 547-550.

Burlingame, Q., Tong, X., Hankett, J., Slootsky, M., Chen, Z., & Forrest, S. R. (2015). Photochemical origins of burn-in degradation in small molecular weight organic photovoltaic cells. *Energy & Environmental Science, 8*(3), 1005-1010.

Cai, W., Gong, X., & Cao, Y. (2010). Polymer solar cells: recent development and possible routes for improvement in the performance. *Solar Energy Materials and Solar Cells, 94*(2), 114-127.

Campos-Delgado, J., Romo-Herrera, J. M., Jia, X., Cullen, D. A., Muramatsu, H., Kim, Y. A., & Okuno, Y. (2008). Bulk production of a new form of sp 2 carbon: crystalline graphene nanoribbons. *Nano Letters, 8*(9), 2773-2778.

Campoy-Quiles, M., Ferenczi, T., Agostinelli, T., Etchegoin, P. G., Kim, Y., Anthopoulos, T. D., & Nelson, J. (2008). Morphology evolution via self-organization and lateral and vertical diffusion in polymer:fullerene solar cell blends. *Nature Materials, 7*(2), 158-164.

Cao, B., He, X., Fetterly, C. R., Olsen, B. C., Luber, E. J., & Buriak, J. M. (2016). Role of interfacial layers in organic solar cells: Energy level pinning versus phase segregation. *ACS Applied Materials & Interfaces, 8*(28), 18238-18248.

Cao, H., He, W., Mao, Y., Lin, X., Ishikawa, K., Dickerson, J. H., & Hess, W. P. (2014). Recent progress in degradation and stabilization of organic solar cells. *Journal of Power Sources, 264*, 168-183.

Chandrasekaran, J., Nithyaprakash, D., Ajjan, K., Maruthamuthu, S., Manoharan, D., & Kumar, S. (2011). Hybrid solar cell based on blending of organic and inorganic materials—An overview. *Renewable and Sustainable Energy Reviews, 15*(2), 1228-1238.

Chang, C.-H., & Chen, S.-A. (2007). Effect of ionization potential change in poly (3, 4-ethylenedioxythiophene): poly (styrenesulfonic acid) on the performance of polymer light emitting diodes due to its reaction with indium tin oxide. *Applied Physics Letters, 91*(10), 103514-103516.

Chang, S. H., Chiang, C.-H., Kao, F.-S., Tien, C.-L., & Wu, C.-G. (2014a). Unraveling the enhanced electrical conductivity of PEDOT:PSS thin films for ITO-free organic photovoltaics. *IEEE Photonics Journal, 6*(4), 1-7.

Chen, C. C., Chang, W. H., Yoshimura, K., Ohya, K., You, J., Gao, J., & Yang, Y. (2014). An efficient triple-junction polymer solar cell having a power conversion efficiency exceeding 11%. *Advanced Materials, 26*(32), 5670-5677.

Chen, C. P., Chen, Y. D., & Chuang, S. C. (2011). High-performance and highly durable inverted organic photovoltaics embedding solution-processable vanadium oxides as an interfacial hole-transporting layer. *Advanced Materials, 23*(33), 3859-3863.

Chen, C. P., Huang, C. Y., & Chuang, S. C. (2015). Highly thermal stable and efficient organic photovoltaic cells with crosslinked networks appending open-cage fullerenes as additives. *Advanced Functional Materials, 25*(2), 207-213.

Chen, L., Tian, S., & Chen, Y. (2014). Enhanced performance for organic bulk heterojunction solar cells by cooperative assembly of ter (ethylene oxide) pendants. *Polymer Chemistry, 5*(15), 4480-4487.

Chen, M.-C., Chiou, Y.-S., Chiu, J.-M., Tedla, A., & Tai, Y. (2013). Marked improvement in the stability of small molecule organic photovoltaics by interfacial modification using self-assembled monolayers to prevent indium diffusion into the active layer. *Journal of Materials Chemistry A, 1*(11), 3680-3687.

Chen, S., Manders, J. R., Tsang, S.-W., & So, F. (2012). Metal oxides for interface engineering in polymer solar cells. *Journal of Materials Chemistry, 22*(46), 24202-24212.

Chen, Z., Deutsch, T. G., Dinh, H. N., Domen, K., Emery, K., Forman, A. J., & Jaramillo, T. F. (2013). Incident photon-to-current efficiency and photocurrent spectroscopy. *Photoelectrochemical Water Splitting* (pp. 87-97): Springer.

Cheng, C.-E., Tsai, C.-W., Lin, T.-W., Pei, Z., Chang, C.-S., & Chien, F. S.-S.(2014). Graphene oxide as hole transport layers for P3HT:PCBM solar cells. In Conference IX: Photovoltaic Technology, Optic.

Cheng, C.-E., Tsai, C.-W., Pei, Z., Lin, T.-W., Chang, C.-S., & Chien, F. S.-S. (2015). UV-treated graphene oxide as anode interfacial layers for P3HT: PCBM solar cells. *Journal of Physics D: Applied Physics, 48*(25), 255103-255110.

Cheng, P., & Zhan, X. (2016). Stability of organic solar cells: Challenges and strategies. *Chemical Society Reviews, 45*(9), 2544-2582.

Cheng, Y.-J., Yang, S.-H., & Hsu, C.-S. (2009). Synthesis of conjugated polymers for organic solar cell applications. *Chemical Reviews, 109*(11), 5868-5923.

Cheng, Y. J., Hsieh, C. H., Li, P. J., & Hsu, C. S. (2011). Morphological stabilization by in situ polymerization of fullerene derivatives leading to efficient, thermally stable organic photovoltaics. *Advanced Functional Materials, 21*(9), 1723-1732.

Cho, S.-P., Yeo, J.-S., Kim, D.-Y., Na, S.-i., & Kim, S.-S. (2015). Brush painted V_2O_5 hole transport layer for efficient and air-stable polymer solar cells. *Solar Energy Materials and Solar Cells, 132*, 196-203.

Cho, S., Seo, J. H., Park, S. H., Beaupré, S., Leclerc, M., & Heeger, A. J. (2010). A thermally stable semiconducting polymer. *Advanced Materials, 22*(11), 1253-1257.

Choi, H., Kim, B., Ko, M. J., Lee, D.-K., Kim, H., Kim, S. H., & Kim, K. (2012). Solution processed WO_3 layer for the replacement of PEDOT:PSS layer in organic photovoltaic cells. *Organic Electronics, 13*(6), 959-968.

Choi, H., Mai, C.-K., Kim, H.-B., Jeong, J., Song, S., Bazan, G. C., & Heeger, A. J. (2015). Conjugated polyelectrolyte hole transport layer for inverted-type perovskite solar cells. *Nature Communications, 6(7358)*,1-6.

Chou, T.-R., Chen, S.-H., Chiang, Y.-T., Lin, Y.-T., & Chao, C.-Y. (2015). Highly conductive PEDOT:PSS film by post-treatment with dimethyl sulfoxide for ITO-free liquid crystal display. *Molecular Crystals and Liquid Crystals, 612*(1), 201-210.

Chueh, C.-C., Li, C.-Z., & Jen, A. K.-Y. (2015). Recent progress and perspective in solution-processed interfacial materials for efficient and stable polymer and organometal perovskite solar cells. *Energy & Environmental Science, 8*(4), 1160-1189.

Chung, J. Y., Lee, J.-H., Beers, K. L., & Stafford, C. M. (2011). Stiffness, strength, and ductility of nanoscale thin films and membranes: A combined wrinkling–cracking methodology. *Nano Letters, 11*(8), 3361-3365.

Clarke, T. M., & Durrant, J. R. (2010). Charge photogeneration in organic solar cells. *Chemical Reviews, 110*(11), 6736-6767.

Conibeer, G. (2007). Third-generation photovoltaics. *Materials Today, 10*(11), 42-50.

Conti, J., Holtberg, P., Doman, L., Smith, K., Sullivan, J., Vincent, K., & Kearney, D. (2011). International energy outlook 2011. *US Energy Information Administration, Technical Report No. DOE/EIA-0484*.

Córcoles, L., Abad, J., Padilla, J., & Urbina, A. (2015). Wavelength influence on the photodegradation of P3HT: PCBM organic solar cells. *Solar Energy Materials and Solar Cells, 141*, 423-428.

Cowan, S. R., Banerji, N., Leong, W. L., & Heeger, A. J. (2012). Charge formation, recombination, and sweep-out dynamics in organic solar cells. *Advanced Functional Materials, 22*(6), 1116-1128.

Crispin, X., Jakobsson, F., Crispin, A., Grim, P., Andersson, P., Volodin, A., & Berggren, M. (2006). The origin of the high conductivity of poly (3, 4-ethylenedioxythiophene)-poly (styrenesulfonate)(PEDOT:PSS) plastic electrodes. *Chemistry of Materials, 18*(18), 4354-4360.

Daems, N., Sheng, X., Vankelecom, I. F., & Pescarmona, P. P. (2014). Metal-free doped carbon materials as electrocatalysts for the oxygen reduction reaction. *Journal of Materials Chemistry A, 2*(12), 4085-4110.

De Jong, M., Van Ijzendoorn, L., & De Voigt, M. (2000). Stability of the interface between indium-tin-oxide and poly (3, 4-ethylenedioxythiophene)/poly (styrenesulfonate) in polymer light-emitting diodes. *Applied Physics Letters, 77*(14), 2255-2257.

De Sio, A., Chakanga, K., Sergeev, O., Von Maydell, K., Parisi, J., & Von Hauff, E. (2012). ITO-free inverted polymer solar cells with ZnO: Al cathodes and stable top anodes. *Solar Energy Materials and Solar Cells, 98*, 52-56.

Dehsari, H. S., Shalamzari, E. K., Gavgani, J. N., Taromi, F. A., & Ghanbary, S. (2014). Efficient preparation of ultralarge graphene oxide using a PEDOT: PSS/GO composite layer as hole transport layer in polymer-based optoelectronic devices. *RSC Advances, 4*(98), 55067-55076.

Deibel, C., & Dyakonov, V. (2010). Polymer-fullerene bulk heterojunction solar cells. *Reports on Progress in Physics, 73*(9), 096401-096439.

Deibel, C., Strobel, T., & Dyakonov, V. (2010). Role of the charge transfer state in organic donor–acceptor solar cells. *Advanced Materials, 22*(37), 4097-4111.

Dementjev, A., De Graaf, A., Van de Sanden, M., Maslakov, K., Naumkin, A., & Serov, A. (2000). X-ray photoelectron spectroscopy reference data for identification of the C 3 N 4 phase in carbon–nitrogen films. *Diamond and Related Materials, 9*(11), 1904-1907.

Dennler, G., Scharber, M. C., & Brabec, C. J. (2009). Polymer-Fullerene bulk-heterojunction solar cells. *Advanced Materials, 21*(13), 1323-1338.

Derue, L., Dautel, O., Tournebize, A., Drees, M., Pan, H., Berthumeyrie, S., Pavageau, B., Cloutet, E., Chambon, S., Hirsch, L. & Rivaton, A. (2014). Thermal stabilisation of polymer–fullerene bulk heterojunction morphology for efficient photovoltaic solar cells. *Advanced Materials, 26*(33), 5831-5838.

Deschler, F., De Sio, A., Von Hauff, E., Kutka, P., Sauermann, T., Egelhaaf, H. J., & Da Como, E. (2012). The effect of ageing on exciton dynamics, charge separation, and recombination in P3HT/PCBM photovoltaic blends. *Advanced Functional Materials, 22*(7), 1461-1469.

Dey, S., Vivo, P., Efimov, A., & Lemmetyinen, H. (2011). Enhanced performance and stability of inverted organic solar cells by using novel zinc-benzothiazole complexes as anode buffer layers. *Journal of Materials Chemistry, 21*(39), 15587-15592.

Dimitrov, S. D., & Durrant, J. R. (2013). Materials design considerations for charge generation in organic solar cells. *Chemistry of Materials, 26*(1), 616-630.

Ding, Z., Hao, Z., Meng, B., Xie, Z., Liu, J., & Dai, L. (2015). Few-layered graphene quantum dots as efficient hole-extraction layer for high-performance polymer solar cells. *Nano Energy, 15*, 186-192.

Dittmer, J. J., Marseglia, E. A., & Friend, R. H. (2000). Electron trapping in dye/polymer blend photovoltaic cells. *Advanced Materials, 12*(17), 1270-1274.

Domínguez, I. F., Topham, P. D., Bussiere, P.-O., Bégué, D., & Rivaton, A. (2015). Unravelling the photodegradation mechanisms of a low bandgap polymer by combining experimental and modelling approaches. *Journal of Physical Chemistry C, 119*, 2166-2176.

Dou, L., You, J., Hong, Z., Xu, Z., Li, G., Street, R. A., & Yang, Y. (2013). 25th anniversary article: A decade of organic/polymeric photovoltaic research. *Advanced Materials, 25*(46), 6642-6671.

Duan, C., Zhong, C., Huang, F., & Cao, Y. (2013). Interface engineering for high performance bulk-heterojunction polymeric solar cells. *Organic Solar Cells* (pp. 43-79): Springer.

Dupont, S. R., Oliver, M., Krebs, F. C., & Dauskardt, R. H. (2012). Interlayer adhesion in roll-to-roll processed flexible inverted polymer solar cells. *Solar Energy Materials and Solar Cells, 97*, 171-175.

Ecker, B., Nolasco, J. C., Pallarés, J., Marsal, L. F., Posdorfer, J., Parisi, J., & von Hauff, E. (2011). Degradation effects related to the hole transport layer in organic solar cells. *Advanced Functional Materials, 21*(14), 2705-2711.

Elkington, D., Cooling, N., Zhou, X., Belcher, W., & Dastoor, P. (2014). Single-step annealing and encapsulation for organic photovoltaics using an exothermically-setting encapsulant material. *Solar Energy Materials and Solar Cells, 124*, 75-78.

Eloi, C. C., Robertson, D. J., Rao, A. M., Zhou, P., Wang, K., & Eklund, P. C. (1993). An investigation of photoassisted diffusion of oxygen in solid C_{60} films using resonant alpha-scattering. *Journal of Materials Research, 8*(12), 3085-3089.

Elumalai, N. K., Saha, A., Vijila, C., Jose, R., Jie, Z., & Ramakrishna, S. (2013). Enhancing the stability of polymer solar cells by improving the conductivity of the nanostructured MoO_3 hole-transport layer. *Physical Chemistry Chemical Physics, 15*(18), 6831-6841.

Elumalai, N. K., & Uddin, A. (2016). Open circuit voltage of organic solar cells: an in-depth review. *Energy & Environmental Science, 9*(2), 391-410.

Endale, T., Sovernigo, E., Radivo, A., Dal Zilio, S., Pozzato, A., Yohannes, T., & Tormen, M. (2014). Investigation of photodegradation in polymer solar cells blended with different fullerenes derivatives. *Solar Energy Materials and Solar Cells, 123*, 150-158.

Espinosa, N., Dam, H. F., Tanenbaum, D. M., Andreasen, J. W., Jørgensen, M., & Krebs, F. C. (2011). Roll-to-roll processing of inverted polymer solar cells using

hydrated vanadium (V) oxide as a PEDOT:PSS replacement. *Materials, 4*(1), 169-182.

Etzold, F., Howard, I. A., Mauer, R., Meister, M., Kim, T.-D., Lee, K.-S., & Laquai, F. (2011). Ultrafast exciton dissociation followed by nongeminate charge recombination in PCDTBT:PCBM photovoltaic blends. *Journal of the American Chemical Society, 133*(24), 9469-9479.

Facchetti, A. (2013). Polymer donor–polymer acceptor (all-polymer) solar cells. *Materials Today, 16*(4), 123-132.

Farah, A. A., Rutledge, S. A., Schaarschmidt, A., Lai, R., Freedman, J. P., & Helmy, A. S. (2012). Conductivity enhancement of poly (3, 4-ethylenedioxythiophene)-poly (styrenesulfonate) films post-spincasting. *Journal of Applied Physics, 112*(11), 113709-113716.

Fechler, N., Fellinger, T.-P., & Antonietti, M. (2013). One-pot synthesis of nitrogen–sulfur-co-doped carbons with tunable composition using a simple isothiocyanate ionic liquid. *Journal of Materials Chemistry A, 1*(45), 14097-14102.

Feng, X. (2015). *Nanocarbons for Advanced Energy Storage* (Vol. 1): John Wiley & Sons.

Ferenczi, T. A., Müller, C., Bradley, D. D., Smith, P., Nelson, J., & Stingelin, N. (2011). Organic semiconductor: insulator polymer ternary blends for photovoltaics. *Advanced Materials, 23*(35), 4093-4097.

Feron, K., Nagle, T. J., Rozanski, L. J., Gong, B. B., & Fell, C. J. (2013). Spatially resolved photocurrent measurements of organic solar cells: tracking water ingress at edges and pinholes. *Solar Energy Materials and Solar Cells, 109*, 169-177.

Fu, C., Zhao, G., Zhang, H., & Li, S. (2013). Evaluation and characterization of reduced graphene oxide nanosheets as anode materials for lithium-ion batteries. *International Journal of Electrochemical Society, 8*, 6269-6280.

Fuge, G. M., Rennick, C. J., Pearce, S. R., May, P. W., & Ashfold, M. N. (2003). Structural characterisation of CN_x thin films deposited by pulsed laser ablation. *Diamond and Related Materials, 12*(3), 1049-1054.

Fung, D. D., & Choy, W. C. (2013). Introduction to organic solar cells: *Organic Solar Cells* (pp. 1-16): Springer.

Ganguly, A., Sharma, S., Papakonstantinou, P., & Hamilton, J. (2011). Probing the thermal deoxygenation of graphene oxide using high-resolution in situ X-ray-based spectroscopies. *The Journal of Physical Chemistry C, 115*(34), 17009-17019.

Gao, F., & Inganäs, O. (2014). Charge generation in polymer–fullerene bulk-heterojunction solar cells. *Physical Chemistry Chemical Physics, 16*(38), 20291-20304.

Gao, L., Zhang, Z. G., Xue, L., Min, J., Zhang, J., Wei, Z., & Li, Y. (2016). All-polymer solar cells based on absorption-complementary polymer donor and acceptor with high power conversion efficiency of 8.27%. *Advanced Materials, 28*(9), 1884–1890

Gao, W. (2015). *Graphene Oxide*: Springer.

Gao, Y., Yip, H. L., Chen, K. S., O'Malley, K. M., Acton, O., Sun, Y., & Jen, A. K. Y. (2011). Surface doping of conjugated polymers by graphene oxide and its application for organic electronic devices. *Advanced Materials, 23*(16), 1903-1908.

Gautier, E., Lorin, A., Nunzi, J. M., Schalchli, A., Benattar, J. J., & Vital, D. (1996). Electrode interface effects on indium–tin–oxide polymer/metal light emitting diodes. *Applied Physics Letters, 69*(8), 1071-1073.

Gershon, T. (2011). Metal oxide applications in organic-based photovoltaics. *Materials Science and Technology, 27*(9), 1357-1371.

Gevorgyan, S. A., Madsen, M. V., Dam, H. F., Jørgensen, M., Fell, C. J., Anderson, K. F., & Elschner, A. (2013). Interlaboratory outdoor stability studies of flexible roll-to-roll coated organic photovoltaic modules: Stability over 10,000 h. *Solar Energy Materials and Solar Cells, 116*, 187-196.

Girotto, C., Voroshazi, E., Cheyns, D., Heremans, P., & Rand, B. P. (2011). Solution-processed MoO_3 thin films as a hole-injection layer for organic solar cells. *ACS Applied Materials & Interfaces, 3*(9), 3244-3247.

Glatthaar, M., Riede, M., Keegan, N., Sylvester-Hvid, K., Zimmermann, B., Niggemann, M., & Gombert, A. (2007). Efficiency limiting factors of organic bulk heterojunction solar cells identified by electrical impedance spectroscopy. *Solar Energy Materials and Solar Cells, 91*(5), 390-393.

Glen, T., Scarratt, N., Yi, H., Iraqi, A., Wang, T., Kingsley, J., & Donald, A. (2015). Grain size dependence of degradation of aluminium/calcium cathodes in organic solar cells following exposure to humid air. *Solar Energy Materials and Solar Cells, 140*, 25-32.

Green, M. A., Emery, K., Hishikawa, Y., Warta, W., & Dunlop, E. D. (2015). Solar cell efficiency tables (Version 45). *Progress in Photovoltaics: Research and Applications, 23*(1), 1-9.

Griffin, J. (2014). *Transition Metal Oxides and Their Use as Hole Extraction Materials in Organic Photovoltaic Devices.* University of Sheffield.

Grossiord, N., Kroon, J. M., Andriessen, R., & Blom, P. W. (2012). Degradation mechanisms in organic photovoltaic devices. *Organic Electronics, 13*(3), 432-456.

Groves, C., & Greenham, N. (2008). Bimolecular recombination in polymer electronic devices. *Physical Review B, 78*(15), 155205-155212.

Guerrero, A., Boix, P. P., Marchesi, L. F., Ripolles-Sanchis, T., Pereira, E. C., & Garcia-Belmonte, G. (2012). Oxygen doping-induced photogeneration loss in P3HT: PCBM solar cells. *Solar Energy Materials and Solar Cells, 100*, 185-191.

Guerrero, A., Heidari, H., Ripolles, T. S., Kovalenko, A., Pfannmöller, M., Bals, S., & Garcia-Belmonte, G. (2015). Shelf life degradation of bulk heterojunction solar cells: Intrinsic evolution of charge transfer complex. *Advanced Energy Materials, 5*(7). 1401997- 1402004

Günes, S., Neugebauer, H., & Sariciftci, N. S. (2007). Conjugated polymer-based organic solar cells. *Chemical Reviews, 107*(4), 1324-1338.

Guo, B., Sun, X. G., Veith, G. M., Bi, Z., Mahurin, S. M., Liao, C., & Dai, S. (2013). Nitrogen-enriched carbons from alkali salts with high coulombic efficiency for energy storage applications. *Advanced Energy Materials, 3*(6), 708-712.

Gupta, D., Mukhopadhyay, S., & Narayan, K. (2010). Fill factor in organic solar cells. *Solar Energy Materials and Solar Cells, 94*(8), 1309-1313.

Hafiz, S. M., Ritikos, R., Whitcher, T. J., Razib, N. M., Bien, D. C. S., Chanlek, N., & Huang, N. M. (2014). A practical carbon dioxide gas sensor using room-temperature hydrogen plasma reduced graphene oxide. *Sensors and Actuators B: Chemical, 193*, 692-700.

Halls, J., Pichler, K., Friend, R., Moratti, S., & Holmes, A. (1996). Exciton diffusion and dissociation in a poly (p-phenylenevinylene)/C60 heterojunction photovoltaic cell. *Applied Physics Letters, 68*(22), 3120-3122.

Halls, J., Walsh, C., Greenham, N., Marseglia, E., Friend, R., Moratti, S., & Holmes, A. (1995). Efficient photodiodes from interpenetrating polymer networks. *Nature, 376*(6540), 498.

Hancox, I., Rochford, L. A., Clare, D., Walker, M., Mudd, J. J., Sullivan, P., & Jones, T. S. (2012). Optimization of a high work function solution processed vanadium oxide hole-extracting layer for small molecule and polymer organic photovoltaic cells. *The Journal of Physical Chemistry C, 117*(1), 49-57.

Haugeneder, A., Neges, M., Kallinger, C., Spirkl, W., Lemmer, U., Feldmann, J., & Müllen, K. (1999). Exciton diffusion and dissociation in conjugated polymer/fullerene blends and heterostructures. *Physical Review B, 59*(23), 15346-15351.

He, D., Du, X., Zhang, W., Xiao, Z., & Ding, L. (2013). Improving the stability of P3HT/$PC_{61}BM$ solar cells by a thermal crosslinker. *Journal of Materials Chemistry A, 1*(14), 4589-4594.

He, J., Wang, Y., He, D., Liu, Z., & Zhuo, Z. (2014). Solution-processable functionalized graphene oxide as an efficient hole transport layer in organic photovoltaics. *Journal of Nanoscience and Nanotechnology, 14*(5), 3588-3591.

He, Z., Wu, H., & Cao, Y. (2014). Recent advances in polymer solar cells: Realization of high device performance by incorporating water/alcohol-soluble conjugated polymers as electrode buffer layer. *Advanced Materials, 26*(7), 1006-1024.

Hintz, H., Egelhaaf, H.-J., Peisert, H., & Chassé, T. (2010). Photo-oxidation and ozonization of poly (3-hexylthiophene) thin films as studied by UV/VIS and photoelectron spectroscopy. *Polymer Degradation and Stability, 95*(5), 818-825.

Hoppe, H., Arnold, N., Sariciftci, N., & Meissner, D. (2003). Modeling the optical absorption within conjugated polymer/fullerene-based bulk-heterojunction organic solar cells. *Solar Energy Materials and Solar Cells, 80*(1), 105-113.

Hoppea, H., & Sariciftci, N. S. (2004). Organic solar cells: An overview. *Journal of Materials Research, 19*(7), 1924-1945.

Hösel, M., Søndergaard, R. R., Jørgensen, M., & Krebs, F. C. (2014). Failure modes and fast repair procedures in high voltage organic solar cell installations. *Advanced Energy Materials, 4*(7), 1301625- 1301631.

Hou, J., & Guo, X. (2013). Active layer materials for organic solar cells. *Organic Solar Cells* (pp. 17-42): Springer.

Hsu, C.-C., Su, H.-W., Hou, C.-H., Shyue, J.-J., & Tsai, F.-Y. (2015). Atomic layer deposition of NiO hole-transporting layers for polymer solar cells. *Nanotechnology, 26*(38), 385201-385206.

Huang, H., & Huang, J. (2014). *Organic and Hybrid Solar Cells*: Springer.

Huang, J.-H., Huang, T.-Y., Wei, H.-Y., Ho, K.-C., & Chu, C.-W. (2012). Wet-milled transition metal oxide nanoparticles as buffer layers for bulk heterojunction solar cells. *RSC Advances, 2*(19), 7487-7491.

Huang, J.-S., Chou, C.-Y., Liu, M.-Y., Tsai, K.-H., Lin, W.-H., & Lin, C.-F. (2009). Solution-processed vanadium oxide as an anode interlayer for inverted polymer solar cells hybridized with ZnO nanorods. *Organic Electronics, 10*(6), 1060-1065.

Huang, J. H., Ibrahem, M. A., & Chu, C. W. (2015). Wet-milled anatase titanium oxide nanoparticles as a buffer layer for air-stable bulk heterojunction solar cells. *Progress in Photovoltaics: Research and Applications, 23*(8), 1017-1024.

Huang, Y., Kramer, E. J., Heeger, A. J., & Bazan, G. C. (2014). Bulk heterojunction solar cells: Morphology and performance relationships. *Chemical Reviews, 114*(14), 7006-7043.

Hummelen, J. C., Knight, B. W., LePeq, F., Wudl, F., Yao, J., & Wilkins, C. L. (1995). Preparation and characterization of fulleroid and methanofullerene derivatives. *The Journal of Organic Chemistry, 60*(3), 532-538.

Irani, R., Rozati, S., & Beke, S. (2013). Structural and optical properties of nanostructural V_2O_5 thin films deposited by spray pyrolysis technique: Effect of the substrate temperature. *Materials Chemistry and Physics, 139*(2), 489-493.

Irwin, M. D., Servaites, J. D., Buchholz, D. B., Leever, B. J., Liu, J., Emery, J. D., & Freeman, A. J. (2011). Structural and electrical functionality of NiO interfacial films in bulk heterojunction organic solar cells. *Chemistry of Materials, 23*(8), 2218-2226.

Jagadamma, L. K., Abdelsamie, M., El Labban, A., Aresu, E., Ndjawa, G. O. N., Anjum, D. H., & Amassian, A. (2014). Efficient inverted bulk-heterojunction solar cells from low-temperature processing of amorphous ZnO buffer layers. *Journal of Materials Chemistry A, 2*(33), 13321-13331.

Jayawardena, K. I., Rhodes, R., Gandhi, K. K., Prabhath, M. R., Dabera, G. D. M., Beliatis, M. J., & Silva, S. R. P. (2013). Solution processed reduced graphene oxide/metal oxide hybrid electron transport layers for highly efficient polymer solar cells. *Journal of Materials Chemistry A, 1*(34), 9922-9927.

Jeon, S. O., & Lee, J. Y. (2012). Improved lifetime in organic solar cells using a bilayer cathode of organic interlayer/Al. *Solar Energy Materials and Solar Cells, 101*, 160-165.

Jeon, Y.-J., Yun, J.-M., Kim, D.-Y., Na, S.-I., & Kim, S.-S. (2014). Moderately reduced graphene oxide as hole transport layer in polymer solar cells via thermal assisted spray process. *Applied Surface Science, 296*, 140-146.

Jeong, H.-K., Lee, Y. P., Lahaye, R. J., Park, M.-H., An, K. H., Kim, I. J., & Lee, Y. H. (2008). Evidence of graphitic AB stacking order of graphite oxides. *Journal of the American Chemical Society, 130*(4), 1362-1366.

Jørgensen, M., Norrman, K., Gevorgyan, S. A., Tromholt, T., Andreasen, B., & Krebs, F. C. (2012). Stability of polymer solar cells. *Advanced Materials, 24*(5), 580-612.

Jørgensen, M., Norrman, K., & Krebs, F. C. (2008). Stability/degradation of polymer solar cells. *Solar Energy Materials and Solar Cells, 92*(7), 686-714.

Julien, C., Pereira-Ramos, J., & Momchilov, A. (2012). *New trends in intercalation compounds for energy storage* (Vol. 61): Springer Science & Business Media.

Jung, J. W., Jo, J. W., & Jo, W. H. (2011). Enhanced performance and air stability of polymer solar cells by formation of a self-assembled buffer layer from fullerene-end-capped poly (ethylene glycol). *Advanced Materials, 23*(15), 1782-1787.

Kang, H., Kim, G., Kim, J., Kwon, S., Kim, H., & Lee, K. (2016). Bulk-heterojunction organic solar cells: Five core technologies for their commercialization. *Advanced Materials, 28*(36), 7821-7861.

Kanwat, A., & Jang, J. (2014). Extremely stable organic photovoltaic incorporated with WO_x doped PEDOT:PSS anode buffer layer. *Journal of Materials Chemistry C, 2*(5), 901-907.

Karam, N. H., King, R. R., Cavicchi, B. T., Krut, D. D., Ermer, J. H., Haddad, M., & Eldredge, J. W. (1999). Development and characterization of high-efficiency Ga

0.5 In 0.5 P/GaAs/Ge dual-and triple-junction solar cells. *IEEE Transactions on Electron Devices, 46*(10), 2116-2125.

Karl, T. R., & Trenberth, K. E. (2003). Modern global climate change. *Science, 302*(5651), 1719-1723.

Katz, E., Gevorgyan, S., Orynbayev, M., & Krebs, F. C. (2006). Out-door testing and long-term stability of plastic solar cells. *The European Physical Journal Applied Physics, 36*(3), 307-311.

Kaune, G., Metwalli, E., Meier, R., Körstgens, V., Schlage, K., Couet, S., Müller-Buschbaum, P. (2011). Growth and morphology of sputtered aluminum thin films on P3HT surfaces. *ACS Applied Materials & Interfaces, 3*(4), 1055-1062.

Kawano, K., & Adachi, C. (2009). Evaluating carrier accumulation in degraded bulk heterojunction organic solar cells by a thermally stimulated current technique. *Advanced Functional Materials, 19*(24), 3934-3940.

Kawano, K., Pacios, R., Poplavskyy, D., Nelson, J., Bradley, D. D., & Durrant, J. R. (2006). Degradation of organic solar cells due to air exposure. *Solar Energy Materials and Solar Cells, 90*(20), 3520-3530.

Ke, J.C., Wang, Y.H., Chen, K.L., & Huang, C.-J. (2015). Effect of open-circuit voltage in organic solar cells based on various electron donor materials by inserting molybdenum trioxide anode buffer layer. *Solar Energy Materials and Solar Cells, 133*, 248-254.

Kesters, J., Verstappen, P., Raymakers, J., Vanormelingen, W., Drijkoningen, J., D'Haen, J., & Maes, W. (2015). Enhanced organic solar cell stability by polymer (PCPDTBT) side chain functionalization. *Chemistry of Materials, 27*(4), 1332-1341.

Kettle, J., Waters, H., Ding, Z., Horie, M., & Smith, G. C. (2015). Chemical changes in PCPDTBT: PCBM solar cells using XPS and TOF-SIMS and use of inverted device structure for improving lifetime performance. *Solar Energy Materials and Solar Cells, 141*, 139-147.

Kettle, J., Waters, H., Horie, M., & Chang, S. (2012). Effect of hole transporting layers on the performance of PCPDTBT: PCBM organic solar cells. *Journal of Physics D: Applied Physics, 45*(12), 125102-12508.

Kim, D. Y. (2014). Zinc Oxide Nanostructures for Flexible and Transparent Electronics. Ph.D. Thesis.

Kim, H. J., Lee, H. H., & Kim, J. J. (2009). Real time investigation of the interface between a P3HT: PCBM layer and an Al electrode during thermal annealing. *Macromolecular Rapid Communications, 30*(14), 1269-1273.

Kim, H. P., bin Mohd Yusoff, A. R., & Jang, J. (2013). Organic solar cells using a reduced graphene oxide anode buffer layer. *Solar Energy Materials and Solar Cells, 110*, 87-93.

Kim, J., Kanwat, A., Kim, H. M., & Jang, J. (2015). Solution processed polymer light emitting diode with vanadium-oxide doped PEDOT: PSS. *Physica Status Solidi (a), 212*(3), 640-645.

Kim, J., Lee, H., Lee, S. J., da Silva, W. J., bin Mohd Yusoff, A. R., & Jang, J. (2015). Graphene oxide grafted polyethylenimine electron transport materials for highly efficient organic devices. *Journal of Materials Chemistry A, 3*(44), 22035-22042.

Kim, J., Lee, S., Nam, S., Lee, H., Kim, H., & Kim, Y. (2012). A pronounced dispersion effect of crystalline silicon nanoparticles on the performance and stability of polymer:fullerene solar cells. *ACS Applied Materials & Interfaces, 4*(10), 5300-5308.

Kim, J. K., Kim, S. J., Park, M. J., Bae, S., Cho, S.-P., Du, Q. G., Hong, B. H. (2015). Surface-engineered graphene quantum dots incorporated into polymer layers for high performance organic photovoltaics. *Scientific Reports, 5(*14276*)*,1-10

Kim, J. K., Park, I., Kim, W., Wang, D. H., Choi, D. G., Choi, Y. S., & Park, J. H. (2014). Enhanced performance and stability of polymer BHJ photovoltaic devices from dry transfer of PEDOT: PSS. *ChemSusChem, 7*(7), 1957-1963.

Kim, M.-S., Kim, B.-G., & Kim, J. (2009). Effective variables to control the fill factor of organic photovoltaic cells. *ACS Applied Materials & Interfaces, 1*(6), 1264-1269.

Kim, T., Kang, J., Yang, S., Sung, S., Kim, Y., & Park, C. (2014). Facile preparation of reduced graphene oxide-based gas barrier films for organic photovoltaic devices. *Energy & Environmental Science, 7*(10), 3403-3411.

Kim, T., Kim, J.H., Kang, T. E., Lee, C., Kang, H., Shin, M., Kim, T.-S. (2015). Flexible, highly efficient all-polymer solar cells. *Nature Communications, 6(*8547*)*, 1-7.

Kim, W., Kim, J. K., Kim, E., Ahn, T. K., Wang, D. H., & Park, J. H. (2015). Conflicted effects of a solvent additive on PTB7:$PC_{71}BM$ bulk heterojunction solar cells. *The Journal of Physical Chemistry C, 119*(11), 5954-5961.

Kololuoma, T., Lu, J., Alem, S., Graddage, N., Movileanu, R., Moisa, S., & Tao, Y. (2015). *Flexo printed sol-gel derived vanadium oxide films as an interfacial hole-transporting layer for organic solar cells.* Paper presented at the SPIE OPTO.

Kong, J., Song, S., Yoo, M., Lee, G. Y., Kwon, O., Park, J. K.., & Suh, H. (2014). Long-term stable polymer solar cells with significantly reduced burn-in loss. *Nature Communications, 5*(5688), 1-8.

Kösemen, A., Tore, N., Parlak, E. A., Kösemen, Z. A., Ulbricht, C., Usluer, O., & San, S. E. (2014). An efficient organic inverted solar cell with AnE-PVstat: PCBM active layer and V_2O_5/Al anode layer. *Solar Energy, 99*, 88-94.

Kraabel, B., Lee, C., McBranch, D., Moses, D., Sariciftci, N., & Heeger, A. (1993). Ultrafast photoinduced electron transfer in conducting polymer—buckminsterfullerene composites. *Chemical Physics Letters, 213*(3), 389-394.

Krebs, F. C. (2006). Encapsulation of polymer photovoltaic prototypes. *Solar Energy Materials and Solar Cells, 90*(20), 3633-3643.

Kumar, A., Devine, R., Mayberry, C., Lei, B., Li, G., & Yang, Y. (2010). Origin of Radiation-Induced Degradation in Polymer Solar Cells. *Advanced Functional Materials, 20*(16), 2729-2736.

Kumar, N. A., Gambarelli, S., Duclairoir, F., Bidan, G., & Dubois, L. (2013). Synthesis of high quality reduced graphene oxide nanosheets free of paramagnetic metallic impurities. *Journal of Materials Chemistry A, 1*(8), 2789-2794.

Kyaw, A., Sun, X., Jiang, C., Lo, G., Zhao, D., & Kwong, D. (2008). An inverted organic solar cell employing a sol-gel derived ZnO electron selective layer and thermal evaporated MoO_3 hole selective layer. *Applied Physics Letters, 93*(22), 221107-221109

Lampande, R., Kim, G. W., Boizot, J., Kim, Y. J., Pode, R., & Kwon, J. H. (2013). A highly efficient transition metal oxide layer for hole extraction and transport in inverted polymer bulk heterojunction solar cells. *Journal of Materials Chemistry A, 1*(23), 6895-6900.

Lan, J.-L., Cherng, S.J., Yang, Y.H., Zhang, Q., Subramaniyan, S., Ohuchi, F. S., & Cao, G. (2014). The effects of Ta_2O_5–ZnO films as cathodic buffer layers in inverted polymer solar cells. *Journal of Materials Chemistry A, 2*(24), 9361-9370.

Lattante, S. (2014). Electron and hole transport layers: Their use in inverted bulk heterojunction polymer solar cells. *Electronics, 3*(1), 132-164.

Lee, C., Kang, H., Lee, W., Kim, T., Kim, K. H., Woo, H. Y., & Kim, B. J. (2015). High-performance all-polymer solar cells via side-chain engineering of the polymer acceptor: The importance of the polymer packing structure and the nanoscale blend morphology. *Advanced Materials, 27*(15), 2466-2471.

Lee, D.Y., Na, S.I., & Kim, S.-S. (2016). Graphene oxide/PEDOT: PSS composite hole transport layer for efficient and stable planar heterojunction perovskite solar cells. *Nanoscale, 8*(3), 1513-1522.

Lee, S.H., Cheong, H. M., Seong, M. J., Liu, P., Tracy, C. E., Mascarenhas, A., & Deb, S. K. (2003). Raman spectroscopic studies of amorphous vanadium oxide thin films. *Solid State Ionics, 165*(1), 111-116.

Lee, S.-H., Seo, J.-W., & Lee, J.-Y. (2015). Stable inverted small molecular organic solar cells using a p-doped optical spacer. *Nanoscale, 7*(1), 157-165.

Lee, S. J., Kim, H. P., bin Mohd Yusoff, A. R., & Jang, J. (2014). Organic photovoltaic with PEDOT: PSS and V_2O_5 mixture as hole transport layer. *Solar Energy Materials and Solar Cells, 120*, 238-243.

Lee, Y. J., Yi, J., Gao, G. F., Koerner, H., Park, K., Wang, J., & Hsu, J. W. (2012). Low-temperature solution-processed molybdenum oxide nanoparticle hole transport layers for organic photovoltaic devices. *Advanced Energy Materials, 2*(10), 1193-1197.

Lenes, M., Koster, L., Mihailetchi, V., & Blom, P. (2006). Thickness dependence of the efficiency of polymer: fullerene bulk heterojunction solar cells. *Applied Physics Letters, 88*(24), 243502-243504.

Li, G., Chu, C., Shrotriya, V., Huang, J., & Yang, Y. (2006). Efficient inverted polymer solar cells. *Applied Physics Letters, 88*(25), 153504-253506.

Li, G., Zhu, R., & Yang, Y. (2012). Polymer solar cells. *Nature Photonics, 6*(3), 153-161.

Li, N., Stubhan, T., Luechinger, N. A., Halim, S. C., Matt, G. J., Ameri, T., & Brabec, C. J. (2012). Inverted structure organic photovoltaic devices employing a low temperature solution processed WO_3 anode buffer layer. *Organic Electronics, 13*(11), 2479-2484.

Li, S.S., Tu, K.H., Lin, C.C., Chen, C.W., & Chhowalla, M. (2010). Solution-processable graphene oxide as an efficient hole transport layer in polymer solar cells. *ACS Nano, 4*(6), 3169-3174.

Li, X., Xie, F., Zhang, S., Hou, J., & Choy, W. C. (2015). MoO_x and V_2O_x as hole and electron transport layers through functionalized intercalation in normal and inverted organic optoelectronic devices. *Light: Science & Applications, 4*(4), 1-7.

Lian, J., Yuan, Y., Peng, E., & Huang, J. (2014). Interfacial layers in organic solar cells. *Organic and Hybrid Solar Cells* (pp. 121-176): Springer.

Lindmayer, J., & Allison, J. (1990). The violet cell: An improved silicon solar cell. *Solar Cells, 29*(2-3), 151-166.

Lioudakis, E., Othonos, A., Alexandrou, I., & Hayashi, Y. (2007). Optical properties of conjugated poly (3-hexylthiophene)/[6, 6]-phenylC61-butyric acid methyl ester composites. *Journal of Applied Physics, 102*(8), 083104-083104.

Liu, C., Yi, C., Wang, K., Yang, Y., Bhatta, R. S., Tsige, M., & Gong, X. (2015). Single-junction polymer solar cells with over 10% efficiency by a novel two-dimensional donor–acceptor conjugated copolymer. *ACS Applied Materials & Interfaces, 7*(8), 4928-4935.

Liu, J., Durstock, M., & Dai, L. (2014). Graphene oxide derivatives as hole-and electron-extraction layers for high-performance polymer solar cells. *Energy & Environmental Science, 7*(4), 1297-1306.

Liu, J., Shi, Y., & Yang, Y. (2001). Solvation-induced morphology effects on the performance of polymer-based photovoltaic devices. *Advanced Functional Materials, 11*(6), 1-5.

Liu, J., Xue, Y., & Dai, L. (2012). Sulfated graphene oxide as a hole-extraction layer in high-performance polymer solar cells. *The Journal of Physical Chemistry Letters, 3*(14), 1928-1933.

Liu, S., Liu, R., Chen, Y., Ho, S., Kim, J. H., & So, F. (2014). Nickel oxide hole injection/transport layers for efficient solution-processed organic light-emitting diodes. *Chemistry of Materials, 26*(15), 4528-4534.

Liu, X., Kim, H., & Guo, L. J. (2013). Optimization of thermally reduced graphene oxide for an efficient hole transport layer in polymer solar cells. *Organic Electronics, 14*(2), 591-598.

Lo, M., Ng, T., Liu, T., Roy, V., Lai, S., Fung, M., & Lee, S. (2010). Limits of open circuit voltage in organic photovoltaic devices. *Applied Physics Letters, 96*(11), 113303.

Loh, K. P., Bao, Q., Eda, G., & Chhowalla, M. (2010). Graphene oxide as a chemically tunable platform for optical applications. *Nature Chemistry, 2*(12), 1015-1024.

Long, X., Wang, N., Ding, Z., Dou, C., Liu, J., & Wang, L. (2016). Low-bandgap polymer electron acceptors based on double B← N bridged bipyridine (BNBP) and diketopyrrolopyrrole (DPP) units for all-polymer solar cells. *Journal of Materials Chemistry C, 4*(42), 9961-9967.

Lu, L., Kelly, M. A., You, W., & Yu, L. (2015). Status and prospects for ternary organic photovoltaics. *Nature Photonics, 9*(8), 491-500.

Lu, L., Zheng, T., Wu, Q., Schneider, A. M., Zhao, D., & Yu, L. (2015). Recent advances in bulk heterojunction polymer solar cells. *Chemical Reviews, 115*(23), 12666-12731.

Ma, H., Yip, H. L., Huang, F., & Jen, A. K. Y. (2010). Interface engineering for organic electronics. *Advanced Functional Materials, 20*(9), 1371-1388.

Madsen, M. V., Tromholt, T., Norrman, K., & Krebs, F. C. (2013). Concentrated light for accelerated photo degradation of polymer materials. *Advanced Energy Materials, 3*(4), 424-427.

Manders, J. R., Tsang, S. W., Hartel, M. J., Lai, T. H., Chen, S., Amb, C. M., & So, F. (2013). Solution-processed nickel oxide hole transport layers in high efficiency polymer photovoltaic cells. *Advanced Functional Materials, 23*(23), 2993-3001.

Mandoc, M., Koster, L., & Blom, P. (2007). Optimum charge carrier mobility in organic solar cells. *Applied Physics Letters, 90*(13), 133504-133506.

Mane, A., Ganbavle, V., Gaikwad, M., Nikam, S., Rajpure, K., & Moholkar, A. (2015). Physicochemical properties of sprayed V_2O_5 thin films: Effect of substrate temperature. *Journal of Analytical and Applied Pyrolysis, 115*, 57-65.

Markov, D., Tanase, C., Blom, P., & Wildeman, J. (2005). Simultaneous enhancement of charge transport and exciton diffusion in poly (p-phenylene vinylene) derivatives. *Physical Review B, 72*(4), 045217-045222.

Mateker, W. R., Sachs-Quintana, I., Burkhard, G. F., Cheacharoen, R., & McGehee, M. D. (2015). Minimal long-term intrinsic degradation observed in a polymer solar cell illuminated in an oxygen-free environment. *Chemistry of Materials, 27*(2), 404-407.

Mattevi, C., Eda, G., Agnoli, S., Miller, S., Mkhoyan, K. A., Celik, O., Chhowalla, M. (2009). Evolution of electrical, chemical, and structural properties of transparent and conducting chemically derived graphene thin films. *Advanced Functional Materials, 19*(16), 2577-2583.

Mayer, A. C., Scully, S. R., Hardin, B. E., Rowell, M. W., & McGehee, M. D. (2007). Polymer-based solar cells. *Materials Today, 10*(11), 28-33.

Mbule, P., Kim, T., Kim, B., Swart, H., & Ntwaeaborwa, O. (2013). Effects of particle morphology of ZnO buffer layer on the performance of organic solar cell devices. *Solar Energy Materials and Solar Cells, 112*, 6-12.

Meyer, J., Zilberberg, K., Riedl, T., & Kahn, A. (2011). Electronic structure of vanadium pentoxide: An efficient hole injector for organic electronic materials. *Journal of Applied Physics, 110*(3), 033710-033714.

Mihailetchi, V., Blom, P., Hummelen, J., & Rispens, M. (2003). Cathode dependence of the open-circuit voltage of polymer:fullerene bulk heterojunction solar cells. *Journal of Applied Physics, 94*(10), 6849-6854.

Mikhnenko, O. V., Kuik, M., Lin, J., van der Kaap, N., Nguyen, T. Q., & Blom, P. W. (2014). Trap-limited exciton diffusion in organic semiconductors. *Advanced Materials, 26*(12), 1912-1917.

Miller, D. R., Wang, J., & Gillan, E. G. (2002). Rapid, facile synthesis of nitrogen-rich carbon nitride powders. *Journal of Materials Chemistry, 12*(8), 2463-2469.

Ming, H. N. (2010). Simple room-temperature preparation of high-yield large-area graphene oxide. *International Journal of Nanomedicine, 6*, 3443-3448.

Mittal, K. L. (2004). *Polymer surface modification: Relevance to adhesion* (Vol. 3): CRC Press.

Morse, G. E., Tournebize, A., Rivaton, A., Chassé, T., Taviot-Gueho, C., Blouin, N., & Tierney, S. (2015). The effect of polymer solubilizing side-chains on solar cell stability. *Physical Chemistry Chemical Physics, 17*(17), 11884-11897.

Motaung, D. E., Malgas, G. F., & Arendse, C. J. (2011). Insights into the stability and thermal degradation of P3HT: C60 blended films for solar cell applications. *Journal of Materials Science, 46*(14), 4942-4952.

Muhammad, F. F., & Sulaiman, K. (2011). Effects of thermal annealing on the optical, spectroscopic, and structural properties of tris (8-hydroxyquinolinate) gallium films grown on quartz substrates. *Materials Chemistry and Physics, 129*(3), 1152-1158.

Mühlbacher, D., Scharber, M., Morana, M., Zhu, Z., Waller, D., Gaudiana, R., & Brabec, C. (2006). High photovoltaic performance of a low-bandgap polymer. *Advanced Materials, 18*(21), 2884-2889.

Murase, S., & Yang, Y. (2012). Solution processed MoO_3 interfacial layer for organic photovoltaics prepared by a facile synthesis method. *Advanced Materials, 24*(18), 2459-2462.

Nam, S., Seo, J., Woo, S., Kim, W. H., Kim, H., Bradley, D. D., & Kim, Y. (2015). Inverted polymer fullerene solar cells exceeding 10% efficiency with poly (2-ethyl-2-oxazoline) nanodots on electron-collecting buffer layers. *Nature Communications,* 6(8929),1-9.

Nardes, A. M., Kemerink, M., De Kok, M., Vinken, E., Maturova, K., & Janssen, R. (2008). Conductivity, work function, and environmental stability of PEDOT:PSS thin films treated with sorbitol. *Organic Electronics, 9*(5), 727-734.

Nelson, J. (2011). Polymer: fullerene bulk heterojunction solar cells. *Materials Today, 14*(10), 462-470.

Nikiforov, M. P., Strzalka, J., Jiang, Z., & Darling, S. B. (2013). Lanthanides: New metallic cathode materials for organic photovoltaic cells. *Physical Chemistry Chemical Physics, 15*(31), 13052-13060.

Norrman, K., Gevorgyan, S. A., & Krebs, F. C. (2008). Water-induced degradation of polymer solar cells studied by H218O labeling. *ACS Applied Materials & Interfaces, 1*(1), 102-112.

Norrman, K., Larsen, N., & Krebs, F. C. (2006). Lifetimes of organic photovoltaics: Combining chemical and physical characterisation techniques to study degradation mechanisms. *Solar Energy Materials and Solar Cells, 90*(17), 2793-2814.

Norrman, K., Madsen, M. V., Gevorgyan, S. A., & Krebs, F. C. (2010). Degradation patterns in water and oxygen of an inverted polymer solar cell. *Journal of the American Chemical Society, 132*(47), 16883-16892.

O'Malley, K. M., Yip, H. L., & Jen, A. K. Y. Metal oxide interlayers for polymer solar cells. *Organic Photovoltaics: Materials, Device Physics, and Manufacturing Technologies* (pp.319-342). John Wiley & Sons.

O'Connor, B., Chan, E. P., Chan, C., Conrad, B. R., Richter, L. J., Kline, R. J., & DeLongchamp, D. M. (2010). Correlations between mechanical and electrical properties of polythiophenes. *ACS Nano, 4*(12), 7538-7544.

Ohkita, H., & Ito, S. (2013). Exciton and charge dynamics in polymer solar cells studied by transient absorption spectroscopy. *Organic Solar Cells* (pp. 103-137): Springer.

Padilla, M., Michl, B., Thaidigsmann, B., Warta, W., & Schubert, M. (2014). Short-circuit current density mapping for solar cells. *Solar Energy Materials and Solar Cells, 120*, 282-288.

Pan, J., Li, P., Cai, L., Hu, Y., & Zhang, Y. (2016). All-solution processed double-decked PEDOT:PSS/V_2O_5 nanowires as buffer layer of high performance polymer photovoltaic cells. *Solar Energy Materials and Solar Cells, 144*, 616-622.

Park, S.-Y., Kim, H.-R., Kang, Y.-J., Kim, D.-H., & Kang, J.-W. (2010). Organic solar cells employing magnetron sputtered p-type nickel oxide thin film as the anode buffer layer. *Solar Energy Materials and Solar Cells, 94*(12), 2332-2336.

Park, S. H., Roy, A., Beaupre, S., Cho, S., Coates, N., Moon, J. S., Heeger, A. J. (2009). Bulk heterojunction solar cells with internal quantum efficiency approaching 100 %. *Nature Photonics, 3*(5), 297-302.

Park, Y., Soon Choi, K., & Young Kim, S. (2012). Graphene oxide/PEDOT: PSS and reduced graphene oxide/PEDOT:PSS hole extraction layers in organic photovoltaic cells. *Physica Status Solidi (a), 209*(7), 1363-1368.

Parnell, A. J., Cadby, A. J., Dunbar, A. D., Roberts, G. L., Plumridge, A., Dalgliesh, R. M.,Jones, R. A. (2016). Physical mechanisms responsible for the water-induced degradation of PC61BM P3HT photovoltaic thin films. *Journal of Polymer Science Part B: Polymer Physics, 54*(2), 141-146.

Peet, J., Kim, J. Y., Coates, N. E., Ma, W. L., Moses, D., Heeger, A. J., & Bazan, G. C. (2007). Efficiency enhancement in low-bandgap polymer solar cells by processing with alkane dithiols. *Nature Materials, 6*(7), 497-500.

Peters, C. H., Sachs-Quintana, I., Kastrop, J. P., Beaupre, S., Leclerc, M., & McGehee, M. D. (2011). High efficiency polymer solar cells with long operating lifetimes. *Advanced Energy Materials, 1*(4), 491-494.

Pivrikas, A., Sariciftci, N. S., Juška, G., & Österbacka, R. (2007). A review of charge transport and recombination in polymer/fullerene organic solar cells. *Progress in Photovoltaics: Research and Applications, 15*(8), 677-696.

Po, R., Carbonera, C., Bernardi, A., & Camaioni, N. (2011). The role of buffer layers in polymer solar cells. *Energy & Environmental Science, 4*(2), 285-310.

Qi, B., & Wang, J. (2012). Open-circuit voltage in organic solar cells. *Journal of Materials Chemistry, 22*(46), 24315-24325.

Qi, B., & Wang, J. (2013). Fill factor in organic solar cells. *Physical Chemistry Chemical Physics, 15*(23), 8972-8982.

Radovic, L. R. (2004). *Chemistry & Physics of Carbon* (Vol. 29): CRC Press.

Rafique, S., Abdullah, S. M., Mahmoud, W. E., Al-Ghamdi, A. A., & Sulaiman, K. (2016). Stability enhancement in organic solar cells by incorporating V_2O_5 nanoparticles in the hole transport layer. *RSC Advances, 6*(55), 50043-50052.

Rafique, S., Abdullah, S. M., Sulaiman, K., & Iwamoto, M. (2017). Layer by layer characterisation of the degradation process in PCDTBT:$PC_{71}BM$ based normal architecture polymer solar cells. *Organic Electronics, 40*, 65-74.

Reddy, Y. A. K., Reddy, A. S., & Reddy, P. S. (2013). Substrate temperature dependent properties of Cu doped NiO films deposited by DC reactive magnetron sputtering. *Journal of Materials Science & Technology*, *29*(7), 647-651.

Reese, M. O., Nardes, A. M., Rupert, B. L., Larsen, R. E., Olson, D. C., Lloyd, M. T., & Kopidakis, N. (2010). Photoinduced degradation of polymer and polymer–fullerene active layers: Experiment and theory. *Advanced Functional Materials, 20*(20), 3476-3483.

Rivaton, A., Chambon, S., Manceau, M., Gardette, J.-L., Lemaître, N., & Guillerez, S. (2010). Light-induced degradation of the active layer of polymer-based solar cells. *Polymer Degradation and Stability, 95*(3), 278-284.

Roesch, R., Eberhardt, K.-R., Engmann, S., Gobsch, G., & Hoppe, H. (2013). Polymer solar cells with enhanced lifetime by improved electrode stability and sealing. *Solar Energy Materials and Solar Cells, 117*, 59-66.

Romero-Gomez, P., Betancur, R., Martinez-Otero, A., Elias, X., Mariano, M., Romero, B., & Martorell, J. (2015). Enhanced stability in semi-transparent PTB7/$PC_{71}BM$ photovoltaic cells. *Solar Energy Materials and Solar Cells, 137*, 44-49.

Roncali, J. (1997). Synthetic principles for bandgap control in linear π-conjugated systems. *Chemical Reviews, 97*(1), 173-206.

Roncali, J. (2007). Molecular engineering of the band gap of π-conjugated systems: Facing technological applications. *Macromolecular Rapid Communications, 28*(17), 1761-1775.

Rosenthal, D., Ruta, M., Schlögl, R., & Kiwi-Minsker, L. (2010). Combined XPS and TPD study of oxygen-functionalized carbon nanofibers grown on sintered metal fibers. *Carbon, 48*(6), 1835-1843.

Ryu, M. S., & Jang, J. (2011). Enhanced efficiency of organic photovoltaic cells using solution-processed metal oxide as an anode buffer layer. *Solar Energy Materials and Solar Cells, 95*(11), 3015-3020.

Sabu, T., Kuruvilla, J., Malhotra, S., Goda, K., & Sreekala, M. (2012). Polymer Composites, Macro-and Microcomposites: ISBN 978-3-527-32624-2.

Şahin, Y., Alem, S., de Bettignies, R., & Nunzi, J.-M. (2005). Development of air stable polymer solar cells using an inverted gold on top anode structure. *Thin Solid Films, 476*(2), 340-343.

Sakamoto, S., Okumura, M., Zhao, Z., & Furukawa, Y. (2005). Raman spectral changes of PEDOT:PSS in polymer light-emitting diodes upon operation. *Chemical Physics Letters, 412*(4), 395-398.

Sapkota, S. B., Spies, A., Zimmermann, B., Dürr, I., & Würfel, U. (2014). Promising long-term stability of encapsulated ITO-free bulk-heterojunction organic solar cells under different aging conditions. *Solar Energy Materials and Solar Cells, 130*, 144-150.

Sariciftci, N., Smilowitz, L., Heeger, A. J., & Wudl, F. (1992). Photoinduced electron transfer from a conducting polymer to buckminsterfullerene. *Science, 258*(5087), 1474-1476.

Sarker, A. K., Kim, J., Wee, B.-H., Song, H.-J., Lee, Y., Hong, J.-D., & Lee, C. (2015). Hydroiodic acid treated PEDOT: PSS thin film as transparent electrode: an approach towards ITO free organic photovoltaics. *RSC Advances, 5*(64), 52019-52025.

Savagatrup, S., Makaram, A. S., Burke, D. J., & Lipomi, D. J. (2014). Mechanical properties of conjugated polymers and polymer-fullerene composites as a function of molecular structure. *Advanced Functional Materials, 24*(8), 1169-1181.

Savagatrup, S., Printz, A. D., O'Connor, T. F., Zaretski, A. V., Rodriquez, D., Sawyer, E. J., & Lipomi, D. J. (2015). Mechanical degradation and stability of organic solar cells: Molecular and microstructural determinants. *Energy & Environmental Science, 8*(1), 55-80.

Schafferhans, J., Baumann, A., Wagenpfahl, A., Deibel, C., & Dyakonov, V. (2010). Oxygen doping of P3HT: PCBM blends: Influence on trap states, charge carrier mobility and solar cell performance. *Organic Electronics, 11*(10), 1693-1700.

Scharber, M. C., Mühlbacher, D., Koppe, M., Denk, P., Waldauf, C., Heeger, A. J., & Brabec, C. J. (2006). Design rules for donors in bulk-heterojunction solar cells—Towards 10% energy-conversion efficiency. *Advanced Materials, 18*(6), 789-794.

Scharber, M. C., & Sariciftci, N. S. (2013). Efficiency of bulk-heterojunction organic solar cells. *Progress in Polymer Science, 38*(12), 1929-1940.

Scheidler, M., Lemmer, U., Kersting, R., Karg, S., Riess, W., Cleve, B.,Göbel, E. (1996). Monte Carlo study of picosecond exciton relaxation and dissociation in poly (phenylenevinylene). *Physical Review B, 54*(8), 5536-5544.

Schilinsky, P., Waldauf, C., & Brabec, C. J. (2002). Recombination and loss analysis in polythiophene based bulk heterojunction photodetectors. *Applied Physics Letters, 81*(20), 3885-3887.

Schulz, P., Cowan, S. R., Guan, Z. L., Garcia, A., Olson, D. C., & Kahn, A. (2014). NiO_X/MoO_3 Bi-layers as efficient hole extraction contacts in organic solar cells. *Advanced Functional Materials, 24*(5), 701-706.

Schweiger, B., Kim, J., Kim, Y. J., & Ulbricht, M. (2015). Electropolymerized molecularly imprinted polypyrrole film for sensing of clofibric acid. *Sensors, 15*(3), 4870-4889.

Seck, M., Vincze, A., Satka, A., Hasko, D., Uherek, F., Tournebize, A., & Chasse, T. (2015). Characterization of the degradation process of Si-PCPDTBT:$PC_{70}BM$ (1: 2) blend layers deposited on ITO/glass substrate. *Solar Energy Materials and Solar Cells, 132*, 210-214.

Seeland, M., Rösch, R., & Hoppe, H. (2011). Luminescence imaging of polymer solar cells: Visualization of progressing degradation. *Journal of Applied Physics, 109*(6), 064513-064517.

Seemann, A., Egelhaaf, H.-J., Brabec, C. J., & Hauch, J. A. (2009). Influence of oxygen on semi-transparent organic solar cells with gas permeable electrodes. *Organic Electronics, 10*(8), 1424-1428.

Seemann, A., Sauermann, T., Lungenschmied, C., Armbruster, O., Bauer, S., Egelhaaf, H.-J., & Hauch, J. (2011). Reversible and irreversible degradation of organic solar cell performance by oxygen. *Solar Energy, 85*(6), 1238-1249.

Seo, H. O., Jeong, M. G., Kim, K. D., Kim, D. H., Kim, Y. D., & Lim, D. C. (2014). Studies of degradation behaviors of poly (3-hexylthiophene) layers by X-ray photoelectron spectroscopy. *Surface and Interface Analysis, 46*(8), 544-549.

Servaites, J. D., Yeganeh, S., Marks, T. J., & Ratner, M. A. (2010). Efficiency enhancement in organic photovoltaic cells: Consequences of optimizing series resistance. *Advanced Functional Materials, 20*(1), 97-104.

Shao, L., Li, J., Liang, X., Xie, T., Meng, S., Jiang, D., & Chen, M. (2016). Novel β-In 2.77 S 4 nanosheet-assembled hierarchical microspheres: Synthesis and high performance for photocatalytic reduction of Cr (vi). *RSC Advances, 6*(22), 18227-18234.

Sharma, A., Andersson, G., & Lewis, D. A. (2011). Role of humidity on indium and tin migration in organic photovoltaic devices. *Physical Chemistry Chemical Physics, 13*(10), 4381-4387.

Sharma, A., Watkins, S. E., Lewis, D. A., & Andersson, G. (2011). Effect of indium and tin contamination on the efficiency and electronic properties of organic bulk hetero-junction solar cells. *Solar Energy Materials and Solar Cells, 95*(12), 3251-3255.

Sharma, S., Jain, K. K., & Sharma, A. (2015). Solar cells: In research and applications—A review. *Materials Sciences and Applications, 6*(12), 1145-1155.

Shivanna, R., Shoaee, S., Dimitrov, S., Kandappa, S. K., Rajaram, S., Durrant, J. R., & Narayan, K. (2014). Charge generation and transport in efficient organic bulk heterojunction solar cells with a perylene acceptor. *Energy & Environmental Science, 7*(1), 435-441.

Shrotriya, V., Li, G., Yao, Y., Chu, C.-W., & Yang, Y. (2006). Transition metal oxides as the buffer layer for polymer photovoltaic cells. *Applied Physics Letters, 88*(7), 073508-073510.

Shuttle, C. G., O'Regan, B., Ballantyne, A. M., Nelson, J., Bradley, D. D., & Durrant, J. R. (2008). Bimolecular recombination losses in polythiophene: Fullerene solar cells. *Physical Review B, 78*(11), 113201-113204.

Siddiki, M. K., Li, J., Galipeau, D., & Qiao, Q. (2010). A review of polymer multijunction solar cells. *Energy & Environmental Science, 3*(7), 867-883.

Sivula, K., Ball, Z. T., Watanabe, N., & Fréchet, J. M. (2006). Amphiphilic diblock copolymer compatibilizers and their effect on the morphology and performance of polythiophene: fullerene solar cells. *Advanced Materials, 18*(2), 206-210.

Smith, C. T., Rhodes, R. W., Beliatis, M. J., Jayawardena, K. I., Rozanski, L. J., Mills, C. A., & Silva, S. R. P. (2014). Graphene oxide hole transport layers for large area, high efficiency organic solar cells. *Applied Physics Letters, 105*(7), 073304-073308.

Some, S., Kim, Y., Hwang, E., Yoo, H., & Lee, H. (2012). Binol salt as a completely removable graphene surfactant. *Chemical Communications, 48*(62), 7732-7734.

Some, S., Kim, Y., Yoon, Y., Yoo, H., Lee, S., Park, Y., & Lee, H. (2013). High-quality reduced graphene oxide by a dual-function chemical reduction and healing process. *Scientific Reports, 3(1929)*, 1-5.

Steim, R., Kogler, F. R., & Brabec, C. J. (2010). Interface materials for organic solar cells. *Journal of Materials Chemistry, 20*(13), 2499-2512.

Steirer, K. X., Chesin, J. P., Widjonarko, N. E., Berry, J. J., Miedaner, A., Ginley, D. S., & Olson, D. C. (2010). Solution deposited NiO thin-films as hole transport layers in organic photovoltaics. *Organic Electronics, 11*(8), 1414-1418.

Stratakis, E., Savva, K., Konios, D., Petridis, C., & Kymakis, E. (2014). Improving the efficiency of organic photovoltaics by tuning the work function of graphene oxide hole transporting layers. *Nanoscale, 6*(12), 6925-6931.

Stratakis, E., Stylianakis, M. M., Koudoumas, E., & Kymakis, E. (2013). Plasmonic organic photovoltaic devices with graphene based buffer layers for stability and efficiency enhancement. *Nanoscale, 5*(10), 4144-4150.

Street, R., Song, K., & Cowan, S. (2011). Influence of series resistance on the photocurrent analysis of organic solar cells. *Organic Electronics, 12*(2), 244-248.

Stubhan, T., Li, N., Luechinger, N. A., Halim, S. C., Matt, G. J., & Brabec, C. J. (2012). High fill factor polymer solar cells incorporating a low temperature solution processed WO3 hole extraction layer. *Advanced Energy Materials, 2*(12), 1433-1438.

Stübinger, T., & Brütting, W. (2001). Exciton diffusion and optical interference in organic donor–acceptor photovoltaic cells. *Journal of Applied Physics, 90*(7), 3632-3641.

Su, Y.-W., Lan, S.-C., & Wei, K.-H. (2012). Organic photovoltaics. *Materials Today, 15*(12), 554-562.

Sun, N., Fang, G., Qin, P., Zheng, Q., Wang, M., Fan, X., & Liu, J. (2010). Efficient flexible organic solar cells with room temperature sputtered and highly conductive NiO as hole-transporting layer. *Journal of Physics D: Applied Physics, 43*(44), 445101-445105.

Sun, S.-S., & Sariciftci, N. S. (2005). *Organic photovoltaics: Mechanisms, materials, and devices*: CRC press.

Synooka, O., Eberhardt, K. R., Singh, C. R., Hermann, F., Ecke, G., Ecker, B., Hoppe, H. (2014). Influence of thermal annealing on PCDTBT:PCBM composition profiles. *Advanced Energy Materials, 4*(5), 1-10.

Tamai, Y., Ohkita, H., Benten, H., & Ito, S. (2015). Exciton diffusion in conjugated polymers: From fundamental understanding to improvement in photovoltaic conversion efficiency. *The Journal of Physical Chemistry Letters, 6*(17), 3417-3428.

Tamai, Y., Ohkita, H., Namatame, M., Marumoto, K., Shimomura, S., Yamanari, T., & Ito, S. (2016). Light-induced degradation mechanism in poly (3-hexylthiophene)/fullerene blend solar cells. *Advanced Energy Materials, 6*(11), 1600171-1600177.

Tan, Z. A., Li, L., Cui, C., Ding, Y., Xu, Q., Li, S., Li, Y. (2012). Solution-processed tungsten oxide as an effective anode buffer layer for high-performance polymer solar cells. *The Journal of Physical Chemistry C, 116*(35), 18626-18632.

Tanenbaum, D. M., Dam, H. F., Rösch, R., Jørgensen, M., Hoppe, H., & Krebs, F. C. (2012). Edge sealing for low cost stability enhancement of roll-to-roll processed flexible polymer solar cell modules. *Solar Energy Materials and Solar Cells, 97*, 157-163.

Tang, C. W. (1986). Two-layer organic photovoltaic cell. *Applied Physics Letters, 48*(2), 183-185.

Tavakkoli, M., Ajeian, R., Badrabadi, M. N., Ardestani, S. S., Feiz, S. M. H., & Nasab, K. E. (2011). Progress in stability of organic solar cells exposed to air. *Solar Energy Materials and Solar Cells, 95*(7), 1964-1969.

Teng, C., Lu, X., Zhu, Y., Wan, M., & Jiang, L. (2013). Polymer in situ embedding for highly flexible, stretchable and water stable PEDOT:PSS composite conductors. *RSC Advances, 3*(20), 7219-7223.

Terán-Escobar, G., Pampel, J., Caicedo, J. M., & Lira-Cantú, M. (2013). Low-temperature, solution-processed, layered V_2O_5 hydrate as the hole-transport layer for stable organic solar cells. *Energy & Environmental Science, 6*(10), 3088-3098.

Tipnis, R., Bernkopf, J., Jia, S., Krieg, J., Li, S., Storch, M., & Laird, D. (2009). Large-area organic photovoltaic module—fabrication and performance. *Solar Energy Materials and Solar Cells, 93*(4), 442-446.

Tokito, S., Noda, K., & Taga, Y. (1996). Metal oxides as a hole-injecting layer for an organic electroluminescent device. *Journal of Physics D: Applied Physics, 29*(11), 2750–2753.

Tournebize, A., Bussière, P. O., Wong-Wah-Chung, P., Thérias, S., Rivaton, A., Gardette, J. L., & Leclerc, M. (2013). Impact of UV-visible light on the morphological and photochemical behavior of a low-bandgap poly (2, 7-Carbazole) derivative for use in high-performance solar cells. *Advanced Energy Materials, 3*(4), 478-487.

Tournebize, A., Rivaton, A., Peisert, H., & Chassé, T. (2015). The crucial role of confined residual additives on the photostability of P3HT: PCBM active layers. *The Journal of Physical Chemistry C, 119*(17), 9142-9148.

Tromholt, T., Madsen, M. V., Carlé, J. E., Helgesen, M., & Krebs, F. C. (2012). Photochemical stability of conjugated polymers, electron acceptors and blends for polymer solar cells resolved in terms of film thickness and absorbance. *Journal of Materials Chemistry, 22*(15), 7592-7601.

Troshin, P., Lyubovskaya, R., & Razumov, V. (2008). Organic solar cells: Structure, materials, critical characteristics, and outlook. *Nanotechnologies in Russia, 3*(5-6), 242-271.

Trost, S., Becker, T., Zilberberg, K., Behrendt, A., Polywka, A., Heiderhoff, R., & Riedl, T. (2015). Plasmonically sensitized metal-oxide electron extraction layers for organic solar cells. *Scientific Reports, 5*(7765),1-9.

Trukhanov, V. A., Bruevich, V. V., & Paraschuk, D. Y. (2015). Fill factor in organic solar cells can exceed the Shockley-Queisser limit. *Scientific reports,* 5(11478),1-10.

Udum, Y., Denk, P., Adam, G., Apaydin, D. H., Nevosad, A., Teichert, C., & Scharber, M. C. (2014). Inverted bulk-heterojunction solar cell with cross-linked hole-blocking layer. *Organic Electronics, 15*(5), 997-1001.

Varnamkhasti, M. G., Fallah, H. R., Mostajaboddavati, M., Ghasemi, R., & Hassanzadeh, A. (2012). Comparison of metal oxides as anode buffer layer for small molecule organic photovoltaic cells. *Solar Energy Materials and Solar Cells, 98*, 379-384.

Vitoratos, E., Sakkopoulos, S., Dalas, E., Paliatsas, N., Karageorgopoulos, D., Petraki, F., & Choulis, S. (2009). Thermal degradation mechanisms of PEDOT:PSS. *Organic Electronics, 10*(1), 61-66.

Voroshazi, E., Verreet, B., Buri, A., Müller, R., Di Nuzzo, D., & Heremans, P. (2011). Influence of cathode oxidation via the hole extraction layer in polymer: fullerene solar cells. *Organic Electronics, 12*(5), 736-744.

Wachs, I. E., & Routray, K. (2012). Catalysis science of bulk mixed oxides. *ACS Catalysis, 2*(6), 1235-1246.

Wakizaka, D., Fushimi, T., Ohkita, H., & Ito, S. (2004). Hole transport in conducting ultrathin films of PEDOT/PSS prepared by layer-by-layer deposition technique. *Polymer, 45*(25), 8561-8565.

Wang, D. H., Kim, J. K., Seo, J. H., Park, I., Hong, B. H., Park, J. H., & Heeger, A. J. (2013). Transferable graphene oxide by stamping nanotechnology: Electron-transport layer for efficient bulk-heterojunction solar cells. *Angewandte Chemie International Edition, 52*(10), 2874-2880.

Wang, D. H., Kim, J. K., Seo, J. H., Park, O. O., & Park, J. H. (2012). Stability comparison: A PCDTBT/PC 71 BM bulk-heterojunction versus a P3HT/PC 71 BM bulk-heterojunction. *Solar Energy Materials and Solar Cells, 101*, 249-255.

Wang, H.Q., Li, N., Guldal, N. S., & Brabec, C. J. (2012). Nanocrystal V_2O_5 thin film as hole-extraction layer in normal architecture organic solar cells. *Organic Electronics, 13*(12), 3014-3021.

Wang, K.C., Jeng, J.Y., Shen, P.S., Chang, Y.C., Diau, E. W.G., Tsai, C.H., & Chen, P. (2014). p-type mesoscopic nickel oxide/organometallic perovskite heterojunction solar cells. *Scientific Reports*, 4(4756),1-8.

Wang, M., Tang, Q., An, J., Xie, F., Chen, J., Zheng, S., Xu, J. (2010). Performance and stability improvement of P3HT: PCBM-based solar cells by thermally evaporated chromium oxide (CrO_x) interfacial layer. *ACS Applied Materials & Interfaces, 2*, 2699-2702.

Wang, M., Zhu, L., Zhou, M., Jiang, C., & Li, Q. (2016). High efficiency organic bulk-heterojunction solar cells applying a new system of co-additives. *Materials Letters, 166*, 227-230.

Wang, P., Liu, Z.-G., Chen, X., Meng, F.-L., Liu, J.-H., & Huang, X.-J. (2013). UV irradiation synthesis of an Au–graphene nanocomposite with enhanced electrochemical sensing properties. *Journal of Materials Chemistry A, 1*(32), 9189-9195.

Wang, X., Egelhaaf, H. J., Mack, H. G., Azimi, H., Brabec, C. J., Meixner, A. J., & Zhang, D. (2014). Morphology related photodegradation of low-band-gap polymer blends. *Advanced Energy Materials, 4*(17), 1400497-1400508.

Wang, Z., Dong, Y., Li, H., Zhao, Z., Wu, H. B., Hao, C., & Lou, X. W. D. (2014). Enhancing lithium–sulphur battery performance by strongly binding the discharge products on amino-functionalized reduced graphene oxide. *Nature Communications*, 5(5002),1-8.

Warren, W., Kanicki, J., Rong, F., Poindexter, E., & McWhorter, P. (1992). Charge trapping centers in N-rich silicon nitride thin films. *Applied Physics Letters, 61*(2), 216-218.

Widmer, J., Tietze, M., Leo, K., & Riede, M. (2013). Open-circuit voltage and effective gap of organic solar cells. *Advanced Functional Materials, 23*(46), 5814-5821.

Wong, K. W., Yip, H., Luo, Y., Wong, K., Lau, W., Low, K., & Chang, C. (2002). Blocking reactions between indium-tin oxide and poly (3, 4-ethylene dioxythiophene): poly (styrene sulphonate) with a self-assembly monolayer. *Applied Physics Letters, 80*(15), 2788-2790.

Wright, M., & Uddin, A. (2012). Organic—inorganic hybrid solar cells: A comparative review. *Solar Energy Materials and Solar Cells, 107*, 87-111.

Xie, F., Choy, W. C., Wang, C., Li, X., Zhang, S., & Hou, J. (2013). Low-temperature solution-processed hydrogen molybdenum and vanadium bronzes for an efficient hole-transport layer in organic electronics. *Advanced Materials, 25*(14), 2051-2055.

Yamanari, T., Ogo, H., Taima, T., Sakai, J., Tsukamoto, J., & Yoshida, Y. (2010). *Photo-degradation and its recovery by thermal annealing in polymer-based organic solar cells.* Paper presented at the Photovoltaic Specialists Conference (PVSC), 2010 35th IEEE.

Yang, D., Zhou, L., Chen, L., Zhao, B., Zhang, J., & Li, C. (2012). Chemically modified graphene oxides as a hole transport layer in organic solar cells. *Chemical Communications, 48*(65), 8078-8080.

Yang, H., Gong, C., Guai, G. H., & Li, C. M. (2012). Organic solar cells employing electrodeposited nickel oxide nanostructures as the anode buffer layer. *Solar Energy Materials and Solar Cells, 101*, 256-261.

Yeh, N., & Yeh, P. (2013). Organic solar cells: Their developments and potentials. *Renewable and Sustainable Energy Reviews, 21*, 421-431.

Yeom, H. R., Heo, J., Kim, G.-H., Ko, S.-J., Song, S., Jo, Y., & Kim, J. Y. (2015). Optimal top electrodes for inverted polymer solar cells. *Physical Chemistry Chemical Physics, 17*(3), 2152-2159.

Yin, Z., Wei, J., & Zheng, Q. (2016). Interfacial materials for organic solar cells: Recent advances and perspectives. *Advanced Science*. John Wiley & Sons.

Yu, D., Nagelli, E., Naik, R., & Dai, L. (2011). Asymmetrically functionalized graphene for photodependent diode rectifying behavior. *Angewandte Chemie International Edition, 50*(29), 6575-6578.

Yu, D., Yang, Y., Durstock, M., Baek, J.-B., & Dai, L. (2010). Soluble P3HT-grafted graphene for efficient bilayer− heterojunction photovoltaic devices. *ACS Nano, 4*(10), 5633-5640.

Yu, G., Gao, J., Hummelen, J. C., Wudl, F., & Heeger, A. J. (1995). Polymer photovoltiac cells: Enhanced efficiencies via a network of internal donor-acceptor heterojunctions. *Science, 270*(5243), 1789-1791.

Yu, G., & Heeger, A. J. (1995). Charge separation and photovoltaic conversion in polymer composites with internal donor/acceptor heterojunctions. *Journal of Applied Physics, 78*(7), 4510-4515.

Yu, J. C., Jang, J. I., Lee, B. R., Lee, G.-W., Han, J. T., & Song, M. H. (2014). Highly efficient polymer-based optoelectronic devices using PEDOT: PSS and a GO composite layer as a hole transport layer. *ACS Applied Materials & Interfaces, 6*(3), 2067-2073.

Yun, J. M., Yeo, J. S., Kim, J., Jeong, H. G., Kim, D. Y., Noh, Y. J., & Na, S. I. (2011). Solution-processable reduced graphene oxide as a novel alternative to PEDOT: PSS hole transport layers for highly efficient and stable polymer solar cells. *Advanced Materials, 23*(42), 4923-4928.

Zawacka, N. K., Andersen, T. R., Andreasen, J. W., Rossander, L. H., Dam, H. F., Jørgensen, M., & Krebs, F. C. (2014). The influence of additives on the morphology and stability of roll-to-roll processed polymer solar cells studied through ex situ and in situ X-ray scattering. *Journal of Materials Chemistry A, 2*(43), 18644-18654.

Zeng, H., Zhu, X., Liang, Y., & Guo, X. (2015). Interfacial layer engineering for performance enhancement in polymer solar cells. *Polymers, 7*(2), 333-372.

Zhang, H., Hines, D., & Akins, D. L. (2014). Synthesis of a nanocomposite composed of reduced graphene oxide and gold nanoparticles. *Dalton Transactions, 43*(6), 2670-2675.

Zhang, Y., Bovill, E., Kingsley, J., Buckley, A. R., Yi, H., Iraqi, A., & Lidzey, D. G. (2016). PCDTBT based solar cells: One year of operation under real-world conditions. *Scientific Reports,* 6(21632),1-8.

Zhao, Z., Teki, R., Koratkar, N., Efstathiadis, H., & Haldar, P. (2010). Metal oxide buffer layer for improving performance of polymer solar cells. *Applied Surface Science, 256*(20), 6053-6056.

Zhao, Z., Wu, Q., Xia, F., Chen, X., Liu, Y., Zhang, W., & Yang, S. (2015). Improving the conductivity of PEDOT:PSS hole Transport layer in polymer solar cells via copper (II) bromide salt doping. *ACS Applied Materials & Interfaces, 7*(3), 1439-1448.

Zhou, L., Yang, D., Yu, W., Zhang, J., & Li, C. (2015). An efficient polymer solar cell using graphene oxide interface assembled via layer-by-layer deposition. *Organic Electronics, 23*, 110-115.

Zhou, N., Dudnik, A. S., Li, T. I., Manley, E. F., Aldrich, T. J., Guo, P., & Chang, R. P. (2016). All-polymer solar cell performance pptimized via systematic molecular weight tuning of both donor and acceptor polymers. *Journal of the American Chemical Society, 138*(4), 1240-1251.

Zhou, Q., Hou, Q., Zheng, L., Deng, X., Yu, G., & Cao, Y. (2004). Fluorene-based low band-gap copolymers for high performance photovoltaic devices. *Applied Physics Letters, 84*(10), 1653-1655.

Zhou, Y., Eck, M., & Krüger, M. (2010). Bulk-heterojunction hybrid solar cells based on colloidal nanocrystals and conjugated polymers. *Energy & Environmental Science, 3*(12), 1851-1864.

Zilberberg, K., Trost, S., Meyer, J., Kahn, A., Behrendt, A., Lützenkirchen-Hecht, D., & Riedl, T. (2011). Inverted organic solar cells with sol–gel processed high work-function vanadium oxide hole-extraction layers. *Advanced Functional Materials, 21*(24), 4776-4783.

Zilberberg, K., Trost, S., Schmidt, H., & Riedl, T. (2011). Solution processed vanadium pentoxide as charge extraction layer for organic solar cells. *Advanced Energy Materials, 1*(3), 377-381.

Zweibel, K. (2010). Should solar photovoltaics be deployed sooner because of long operating life at low, predictable cost? *Energy Policy, 38*(11), 7519-7530.

LIST OF PUBLICATIONS AND PAPERS PRESENTED

Alhummiany, Rafique, and Sulaiman. (2017). XPS analysis of improved operational stability of organic solar cells using V_2O_5 and PEDOT:PSS composite layer: Effect of varied atmospheric conditions. *The Journal of Physical Chemistry C*, *121*(14), 7649-7658.

Rafique, Abdullah, Sulaiman and et al. (2016). Polymer bulk heterojunction organic solar cells with graphene oxide hole transport layer: Effect of varied concentration on photovoltaic performance. *The Journal of Physical Chemistry C*, *121*(1), 140-146.

Rafique, Abdullah, Sulaiman and et al. Stability enhancement in organic solar cells by incorporating V_2O_5 nanoparticles in the hole transport layer. *RSC Advances*, *6*(55), 50043-50052.

Rafique, Abdullah, Sulaiman and et al. (2017). Significantly improved photovoltaic performance in polymer bulk heterojunction solar cells with graphene oxide/PEDOT:PSS double decked hole transport layer. *Scientific Reports*, *7*(39555), 1-10.

Rafique, Abdullah, Sulaiman and et al. (2017). Layer by layer characterisation of the degradation process in PCDTBT:PC_{71}BM based normal architecture polymer solar cells. *Organic Electronics*, *40*, 65-74.